Universidade de Aveiro Departamento de Engenharia Cerâmico e do Vidro
2007

Jie Gao

Filmes Finos de $(Ba_xSr_{1-x})TiO_3$ para Aplicações na Microelectrónica

Sol-Gel $(Ba_xSr_{1-x})TiO_3$ Thin Films for Microelectronic Applications

Universidade de Aveiro Departamento de Engenharia Cerâmico e do Vidro
2007

Jie Gao

Sol-Gel $(Ba_xSr_{1-x})TiO_3$ Thin Films for Microelectronic Applications

Dissertação apresentada à Universidade de Aveiro para cumprimento dos requisitos necessários à obtenção do grau de Mestre em Ciências dos Materiais, realizada sob a orientação científica da Professora Dra. Paula Maria Vilarinho, Professora Associada na Universidade de Aveiro, Departamento de Engenharia Cerâmica e do Vidro e Drª Aiying Wu, Investigadora Auxiliar do Centro de Investigação em Materiais Cerâmicos e Compósitos (CICECO) da Universidade de Aveiro.
A dissertation presented to the University of Aveiro in partial fulfilment of the requirements for the awarding of the master degree in Material Science Engineering carried out under the supervision of of Professor Dr. Paula Maria Vilarinho, Associate Professor at the University of Aveiro, Department of Ceramics and Glass Engineering, and Dr. Aiying Wu, Auxiliary Researcher at Research Center for Ceramic and Composite Materials (CICECO) of the University of Aveiro.

Financial Support from Erasmus
Mundus programme.

o júri

presidente

Prof. Dr. Vitor Brás de Sequeira Amaral
Associate professor from the University of Aveiro, Portugal

Prof. Dr. Angus I. Kingon
Full professor from North Carolina State University, USA

Prof. Dr. Paula Maria Lousada Silveirinha Vilarinho
Associate professor from the University of Aveiro, Portugal

Dr. Aiying Wu
Auxiliary researcher from CICECO, the University of Aveiro, Portugal

Acknowledgements

I would like to express my sincere gratitude to all those who gave me the possibility to complete this thesis.

First of all, I want to thank my supervisors: Prof. Dr. Paula Vilarinho and Dr. Aiying Wu. They are always willing to listen, discuss and give advice throughout the work. The encouragements and guidance from them are always appreciated. I would also give many thanks to the supervisor Prof. Dr. Gerold Schneider of Technique University of Hamburg-Harberg (TUHH) in Germany and his colleagues, especially Mr. Ralf-Peter Herber and Mr. Dieter Schmidt, who trained me in the very beginning how to use Atomic Force Microscopy with great patient.

Thanks to Prof. Dr. Ian Reaney, from the Sheffield University, UK, for his TEM characterization, to Engª Marta Ferro, Engº Augusto Luis Barros Lopes, Engª Conceição Costa, Engª Celia Miranda, Engº Jorge Corker, the technicians of the department of Ceramics and Glass Engineering, for their help in utilization of equipments.

Thanks to the financial support of Erasmus Mundus programme; thanks to the coordinators of European Master of Material Science (EMMS): Prof. Dr. Vitor Amaral, Prof. Dr. Ana Barros, Prof. Dr. Elisabete Costa and Prof. Dr. Hans Wittich; thanks to the international office of the UA and TUHH. Their valuable help made my study and life abroad comfortable and easy.

Last, but not least, I would like to give my special thanks to my family: my husband, Zhi Fu, whose patient love enabled me to complete this work; my parents, Dean Gao and Rong Zhang, for their endless support.

Keywords

Barium Strontium Titanate, BST, thin films, sol-gel, nanometric particles, electric properties, microelectronic applications

summary

Dielectric, piezoelectric and ferroelectric thin films have been in the past years significantly studied because of their technological interest in a wide range of applications in the microelectronics industry.

Among the several ferroelectric materials, compositions within the solid solution between the ferroelectric $BaTiO_3$ and the quantum paraelectric $SrTiO_3$ $(Ba_{1-x}Sr_x)TiO_3$ (BST), possess high dielectric constant and relatively low loss over a wide frequency range (till >1 GHz), low-leakage current density, a large electric field dielectric tunability and a composition dependent Curie temperature. These properties make BST thin films attractive for high density dynamic random access memories (DRAMs), and low cost agile microwave circuits, such as phase shifters, tunable filters, tunable matching network and high tuning frequency range voltage controlled oscillators. Moreover BST is a lead free perovskite making it an ideal material from the environmental point of view.

These applications require the growth of high quality BST thin films, in addition to fundamental understanding of their structural and dielectric properties, which often diverge from those in equivalent bulk material. The high temperatures required for the crystallization of the perovskite BST films are not compatible with Si based large scale integrated circuits. SiO_2 and/or metal silicides formation occurs when BST is deposited on silicon at temperatures above 700ºC. An underlying silicide layer reduces materials high dielectric permittivity, since silicide has lower permittivity than the perovskite oxide, reducing the film effective capacitance. At these high temperatures recrystallization of the electrode layer beneath the film (e.g. platinum layer) may occur, which can lead to hillock formation and electrical shorting of BST films. Moreover, thermal stresses generated at high temperatures might affect the long-term reliability of the device. Hence the improvement and optimization of the processing conditions of BST thin films as well as the development of low temperature processes for the fabrication of BST films are still a key aspect from the technologic point of view. Additionally, a low annealing temperature is also essential when metallic or glass substrates are required.

The present master thesis addresses the investigation on the preparation of BST thin films by sol gel at temperatures lower than 700ºC.

Sol-gel derived $(Ba_{0.8}Sr_{0.2})TiO_3$ thin films with improved dielectric properties were prepared at 600˚C, on $Pt/TiO_2/SiO_2/Si$ substrate through the use of diphasic precursor sols. BST nanometric powders were dispersed in the amorphous BST precursor sol to prepare the diphasic precursor sol and $(Ba_{0.8}Sr_{0.2})TiO_3$ thin films without and with 1 mol%, 5 mol% and 10 mol% $(Ba_{0.8}Sr_{0.2})TiO_3$ seeds were fabricated. The role of seeds was investigated and analyzed on the crystalline phase evolution, microstructure development and electrical properties of BST thin films. The improvement on the characteristics of seeded BST films when compared with unseeded films was highlighted by a

comprehensive structural, microstructural and electric characterization of the films.

It was shown that using perovskite BST nanopowders as seeds results in the crystallization of a single perovskite phase in BST films either at lower temperatures or at shorter annealing time when compared with the preparation of identical films without seeds. The presence of nano sized BST seeds in the film precursor sol lowers the barrier for BST nucleation and results in a high density of small crystallites in the film. XRD analysis showed that the temperature at which the perovskite phase is formed (or identified) was decreased from 650ºC to 550ºC when BST seeds were used in the precursor sols and the temperature at which the pure perovskite phase is obtained was decreased from 700ºC to 600ºC. The seeded BST films exhibit enhanced crystllization kinetics and the overall activation energy for the perovskite crystllization was reduced from 189 kJ/mol for the unseeded film to 86 kJ/mol for 1 mol% seeded BST film and to 80 kJ/mol for 5 mol% seeded film.

Scanning electron microscopy (SEM), atomic force microscopy (AFM), transmission electron microscopy (TEM) were employed to characterize the influence of seeds on the crystallinity, structure, microstructure, morphology and interface between BST thin films and the substrate. Both SEM and AFM surface morphology results showed that the grains of seeded films were smaller, more homogeneously distributed than unseeded ones. The surface roughness of BST films measured by AFM was decreased by the presence of BST nano seeds. TEM analysis clearly revealed that the crystallinity of BST films was enhanced with the presence of BST seeds under the same annealing conditions.

The dielectric properties of BST thin films, including permittivity, loss tangent, tunability of the dielectric constant were evaluated and discussed as a function of seeds content. The dielectric constant of unseeded films annealed at 600ºC for 30 hours in oxygen were improved by the addition of 5 mol% seeds from ~300 to 400 at 1kHz, respectively. Simultaneously, the dissipation factors were decreased by the presence of 5 mol% seeds from ~0.1 to 0.07 at 1 kHz, from 0.07 to 0.01 at 1 MHz, respectively. The presence of 5 mol% seeds improved the tunability of BST films and an increment from 52% to 65% at 6 V was observed for unseeded and 5 mol% seeded BST thin films annealed at 600ºC for 30 hours in oxygen.

The leakage current density of BST films with 5 mol% seeds heat treated at 600ºC for 30 hours in oxygen is 0.95×10^{-7} A/cm^2 up to the applied voltage of 2.33 V (97 kV/cm), which was improved when compared with 0.88×10^{-7} A/cm^2 up to 2.02 V (84 kV/cm) measured for BST films without seeds. The value of the leakage current of both unseeded and 5 mol% seeded films meet the requirements for G-Byte DRAMs.

Identically to the rest of the electrical properties, the polarization versus electric field (P-E) hysteresis was improved by the introduction of seeds. The remnant polarization Pr of BST films with 5 mol% seeds was 3.55 μC/cm^2 with a coercive field of 75 kV/cm, which was considerably enhanced when compared with 1.8 μC/cm^2 for BST films without seeds with a coercive field of 50 kV/cm.

Corroborating the above results, piezo force microscopy (PFM) of BST seeded and non seeded thin films demonstrated the improved ferroelectric properties of BST films prepared with nanometric seeds.

Palavras-chave

Titânio estrôncio e Bário, Filmes Finos, BST, Sol-Gel, Partículas Nanométricas, Sementes, Aplicações Microeletrônicas

resumo

Filmes finos dieléctricos, piezoeléctricos e ferroeléctricos têm sido muito estudados no passado recente, por causa do interesse tecnológico relacionado com a gama alargada de aplicações destes materiais na indústria microelectrónica.

De entre os vários materiais ferroeléctricos, as composições pertencentes à solução sólida composta pelo ferroeléctrico $BaTiO_3$ e o quantum paraléctrico $SrTiO_3$, $(Ba_{1-x}Sr_x)TiO_3$ (BST), possuem constantes dieléctricas elevadas e baixas perdas dieléctricas até frequência elevadas (>1 GHz), baixas densidade de correntes de fuga, elevada sintonabilidade da permitividade dieléctrica com o campo eléctrico e temperatura de Curie dependente da composição. Estas propriedades tornam os filmes finos de BST atractivos para dispositivos de memórias dinâmicas de acesso aleatório DRAMs, e de circuitos sintonizáveis às frequências das microondas (phase shifters, tunable filters, tunable matching network and high tuning frequency range voltage controlled oscillators). Por outro lado BST é um material livre de chumbo o que o torna ideal do ponto de vista ambiental para estas aplicações.

As aplicações acima mencionadas requerem o fabrico de filmes finos de BST de elevada qualidade, juntamente com o entendimento das relações entre a sua estrutura e propriedades, que muitas vezes divergem das propriedades apresentadas pelos materiais equivalentes na forma de monolitos.

As elevadas temperaturas necessárias para a cristalização de fase de perovesquite em filmes finos de BST não é compatível com a integração em larga escala em circuitos à base de silício. A formação de SiO_2 e ou silicietos metálicos ocorre quando BST é depositado sobre silício a temperaturas elevadas acima de 700ºC. Camadas subjacentes de silicietos reduzem a elevada permitividade dieléctrica relativa do material, já que estes silicietos têm permitividade dieléctrica relativa inferior à do óxido perovesquítico. A estas temperaturas elevadas pode ocorrer a recristalização do eléctrodo colocado sob o filme (por exemplo platina), o que origina o aparecimento de curto circuitos nos filmes de BST. Mais ainda, as tensões térmicas geradas às temperaturas elevadas podem afectar a longo prazo o desempenho e a fiabilidade do dispositivo.

Assim o melhoramento e optimização das condições de fabrico de filmes finos de BST, bem como o desenvolvimento de metodologias de processamento destes filmes a temperaturas mais baixas continua a ser um aspecto chave do ponto de vista tecnológico e de comercialização destes materiais. Acrescente-se que um processamento a baixas temperaturas é ainda essencial quando é necessária a utilização de substratos metálicos ou de vidro.

A presente tese descreve a investigação conduzida na preparação de filmes finos de BST por sol gel a temperaturas inferiores a 700ºC.

Filmes finos de $(Ba_{0.8}Sr_{0.2})TiO_3$ (BST80/20) com propriedades melhoradas foram preparados por sol gel a 600˚C, sobre substratos de $Pt/TiO_2/SiO_2/Si$, através da utilização de soles precursores difásicos. Partículas nanométricas de BST foram dispersas em soles precursores de BST e filmes finos de BST80/20 sem e com 1 mol%, 5 mol% and 10 mol% de sementes de BST foram fabricados. O papel das sementes foi investigado e analisado na formação de fases, desenvolvimento microestrutural e propriedades dieléctricas dos filmes de BST. O estudo sistemático da estrutura, microestrutura e propriedades evidenciou as melhorias das características dos filmes de BST sementados.

Foi mostrado que a utilização de partículas nanométricas de BST como sementes resulta na cristalização da fase pura de perovesquite nos filmes de BST ou a temperaturas mais baixas ou para tempos mais curtos. A presença de nanopartículas de BST nos soles precursores dos filmes baixa a barreira enérgica para a nucleação da fase de perovesquite de BST e origina no filme uma densidade elevada de pequenas cristalites. As análise de difracção de raios X mostraram que a temperatura à qual a fase de perovesquite se forma decresceu de 650ºC para 550ºC quando se utilizam sementes de BST nos soles precursores e que a temperatura à qual a fase pura de perovesquite é obtida decresceu de 700ºC para 600ºC. Os filmes sementados de BST exibem uma cinética de cristalização optimizada e a energia de activação para a cristalização da fase de perovesquite foi reduzida de 189 kJ/mol para os filmes não sementados para 86 kJ/mol e 80 kJ/mol para os filmes sementados com 1 mol% e 5 mol% de sementes, respectivamente.

Para caracterizar a influência das sementes na estrutura, grau de cristalinidade, microestrutura, morfologia e interface filme / substrato foram utilizadas as técnicas de microscopia electrónica de varrimento (SEM), microscopia de força atómica (AFM) e microscopia electrónica de transmissão (TEM). Os resultados da morfologia da superfície dos filmes obtidos quer por SEM quer por AFM mostraram que os grãos dos filmes sementados são claramente menores e apresentam uma distribuição mais homogénea, relativamente aos filmes não sementados. A rugosidade da superfície dos filmes quantificada por AFM decresceu por adição das sementes. As análises de TEM revelaram que a cristalinidade dos filmes sementados é superior relativamente aos filmes não sementados, para filmes preparados em idênticas condições.

As propriedades dieléctricas dos filmes finos de BST, que incluem a permitividade dieléctrica relativa, a perda dieléctrica, a sintonabilidade da permitividade dieléctrica foram avaliadas e analisadas em função do teor de

sementes. A permitividade dieléctrica relativa de filmes não sementados e tratados termicamente a 600ºC durante 30 horas em oxigénio variou de ~300 para 400 a 1 kHz, pela adição de 5 mol% de sementes. Simultaneamente a perda dieléctrica decresceu para os filmes com 5 mol% de sementes de ~0.1 para 0.07 a 1 kHz e de 0.07 para 0.01 a 1 MHz. A presença de sementes melhorou a sintonabilidade dos filmes de BST, verificando-se um incremento de 52% para 65% a 6 V para os filmes sementados com 5 mol% de sementes em relação aos filmes não sementados ambos tratados termicamente a 600ºC por 30 horas em oxigénio.

A densidade de corrente de fuga variou de 0.88×10^{-7} A/cm^2 até uma voltagem aplicada de 2.02 V (84 kV/cm) para os filmes de BST não sementados e tratados termicamente a 600ºC durante 30 horas em oxigénio, para 0.95×10^{-7} A/cm^2 até uma voltagem aplicada de 2.33 V (97 kV/cm) para filmes de BST com 5 mol% de sementes preparados nas mesmas condições. Os valores de densidade de corrente de fuga dos filmes sementados cumprem os requisitos estipulados por exemplo para as memórias dinâmicas de acesso aleatório (DRAM) de capacidade da ordem de G-Bytes.

De forma idêntica à restante caracterização eléctrica, a presença de sementes em filmes de BST melhorou sua a resposta histerética da variação da polarização com o campo (P-E). Foram determinados valores de polarização remanescente de 3.55 μC/cm^2 com campos coercivos de 75 kV/cm para filmes com 5mol% de sementes, valores estes consideravelmente superiores aos valores determinados para filmes não sementados de 1.8 μC/cm^2 e 50 kV/cm para a polarização remanescente e o campo coercivo, respectivamente.

Suportando os resultados anteriores, a microscopia de força piezoeléctrica (PFM) demonstrou igualmente a melhoria das propriedades ferroléctricas dos filmes de BST preparados com sementes.

TABLE OF CONTENTS

List of Symbols

A	area of a capacitor
C	capacitance value
C	Curie constant
d	thickness of a capacitor
d_{ij}	piezoelectric coefficient or strain constant (relates a field along the i axis to the strain in the j direction)
D_S	dielectric breakdown strength or dielectric strength
E	electric filed
Ea	activation energy
Ec	coercive electric field
E_{crit}	electric breakdown
Gbit	gigabit
J	leakage current density
n	tunability
n_r	relative tunability
P	polarization
Pr	remnant polarization
Ps	saturated polarization
Q	quality factor
R	gas constant
r_A	ionic radius of A cation in ABO_3 perovskite
r_B	ionic radius of B cation in ABO_3 perovskite
r_O	ionic radius of oxygen anion in ABO_3 perovskite
t	dielectric thickness
tanδ	dielectric loss tangent
Tc	curie temperature
U_{br}	breakdown voltage
x	strain
ε_o	vacuum permittivity
ε_r	relative permittivity or dielectric constant
εr'	the real part of the dielectric constant
εr''	the imaginary part of the dielectric constant
ε_s	static permittivity
σ	stress
τ	relaxation time
χ	electric susceptibility

List of Abbreviations

AC	alternating current
AFM	Atomic Force Microscopy
BST	barium strontium titanate, $(Ba_xSr_{1-x})TiO_3$
BT	barium titanate, $BaTiO_3$
CMOS	complementary metal-oxide-semiconductor
CSD	chemical solution deposition
CVD	chemical vapor deposition
DRAM	dynamic random access memory
ED	electron diffraction
EDS	energy dispersive spectroscopy
$\overline{G}$	average grain size
ITO	indium titanium oxide
LPCVD	low pressure chemical vapor deposition
LSCVD	liquid source chemical vapor deposition
MIM	metal-insulator-metal
MOCVD	metal organic chemical vapor deposition
MOD	metal organic deposition
MW	microwave
PFM	Piezo Force Microscopy
PLD	pulsed laser deposition
PLZT	lead lanthanum zirconate titanate
PMN	lead magnesium niobate
PVD	physical vapor deposition
PZT	lead zirconate titanate
RF	radio frequency
RMS	root mean square
RTA	rapid thermal annealing
SEM	Scanning Electron Microscopy
TEM	Transmission Electron Microscope
XRD	X-ray diffraction

List of Figures

Figure 3.22. Topography (a-1) and (b-1), out of plane PFM signal (a-2) and simultaneous cross-sections of topography and PFM taken on unseeded BST thin films annealed at 750ºC for 1 hour; topography (b-1), out of plane PFM signal (b-2) and simultaneous cross-sections of topography and PFM taken on 5 mol% seeded BST thin films annealed at 750ºC for 1 hour.

Figure 3.23. Room-temperature leakage current density of unseeded and 5 mol% seeded BST thin films annealed at 600ºC for 30 hours in oxygen as a function of applied external voltage.

List of Tables

Chapter 1 Introduction

1.1 Introduction to ferroelectric thin films

Nowadays, everybody, even for those who do not aware of it, is recognizing the so-called *Information Technology*. For example, there has been a huge demanding on memory with higher density, communication systems which are more convenient for users such as 3G wireless phones and Bluetooth. These systems include a number of high density capacitances, tuned circuits working in radio frequency (RF) and microwave (MW).

Recently, ferroelectrics are studied and utilized as essential components in these applications due to their specific dielectric, ferroelectric, piezoelectric, pyroelectric properties [1]. For instance, ferroelectric thin films have now been used for several years in RF devices and in Non-volatile memories. Ferroelectric films based components are also being developed for tunable microwave circuits [2].

1.1.1 Fundamental properties of ferroelectrics

1.1.1.1 Dielectric properties

When an electric field E is applied to an ideal insulator there is no long-range charge transport, as in a conductor, only a short-range dislocation of the positive and negative charge center which causes the appearance of electric dipole moments in the

material. The material is called a *dielectric*. The effect of the electrical field can be twofold:

1. The electric field *induces* electrical dipoles and aligns them in the field direction. In other words, the material does not contain electric dipoles without the electric field.
2. The electric field aligns electrical dipoles that are *already present* in the material. In other words, the material contains spontaneous electric dipoles even without a field. In this case the dipoles are randomly oriented and for zero filed the net polarization is null.

The total effect of an electric field on a dielectric material is called *polarization* ($\mu C/cm^2$). Several polarization mechanisms were identified: atomic, ionic, dipolar and space charge; being each related to the nature of the charged entities, which suffer charge displacement, or to the nature of the displacement [3].

Dielectrics are insulators with high dielectric permittivity. Dielectric permittivity or dielectric constant is defined as the capacity of a material to store electrical charge and it gives rise to the simplest practical application of a dielectric material – a capacitor. Nonetheless, the various polarization responses of the dielectric under an electric field are being increasingly used in micro and nanoelectronic devices. In general, a capacitor consists of two metal plates insulated from each other by a dielectric. The capacitance of a capacitor depends on its shape, size and relative permittivity, ε_r of the medium between the plates, as:

$$C = \varepsilon_r A / d \tag{1.1}$$

where C stands for the capacitance of the material, A for the area of the capacitive cell and d for its thickness.

The relative dielectric permittivity is often the quantity used to quantify the response of an insulator material to the applied electric field is defined as:

$$\varepsilon_r = \varepsilon_o / \varepsilon_s \tag{1.2}$$

where ε_s stands for static permittivity of the material, and ε_0 for the vacuum permittivity. The relative permittivity of a medium is related to its electric susceptibility, χ by:

$$\varepsilon_r = 1 + \chi \tag{1.3}$$

Reorientation of the dipoles in response to an electric field is characterized by a **relaxation time**, **τ**. As shown in figure 1.1, when an alternating electric current (AC) is applied, the relaxation time varies for each of the various contributions to the polarization: the response is fastest for the electronic polarization, which will disappear when the frequency is larger than 10^{16} Hz; slows down for ionic polarization when the frequency is smaller than 10^{13} Hz; still slows down for dipolar polarization that disappear at 10^{10} Hz; and is quite slow for space charge polarization that not exist when the frequency is higher than 10^3 Hz.

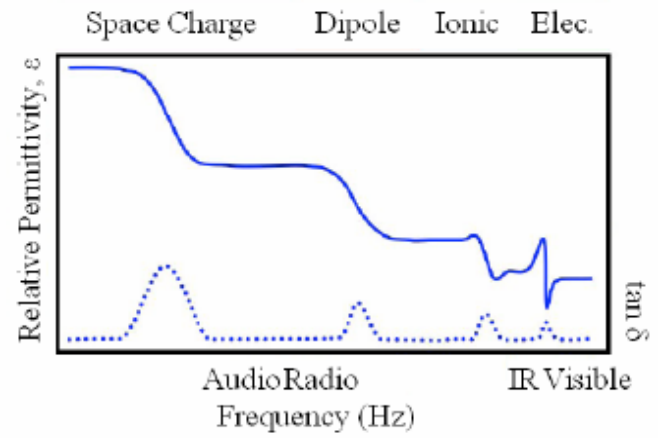

Figure 1.1. Theoretical frequency dispersion for a dielectric showing all possible polarization mechanisms and the expected frequencies for their relaxation [4].

When the relaxation time is much faster than the frequency of the applied electric field, polarization occurs instantaneously; when the relaxation time is much slower than frequency of the applied electric field, no polarization occurs; when the relaxation time and the frequency of the applied field are similar, a phase lag occurs and energy is

absorbed. This is called the loss of a *dielectric* and it is normally quantified by the dissipation factor tanδ as:

$$\tan\delta = \varepsilon_r'' / \varepsilon_r' \quad (1.4)$$

where ε_r' is the real part of the dielectric constant and ε_r'' is the imaginary part of the dielectric constant. The parameter tanδ is a measure of the energy dissipated per cycle and the energy stored in the dielectric and a quality factor Q defined as:

$$Q = 1 / \tan\delta \quad (1.5)$$

which represents an important design parameter for practical applications.

1.1.1.2 Piezoelectric property

If a mechanical stress provokes the development of a polarization, these materials are called *piezoelectric*. The word piezo is Greek and means "push". The effect known as piezoelectricity was discovered by brothers Pierre and Jacques Curie in 1880. Piezoelectricity is defined as a change in electric polarization with a change in applied stress, which is a direct piezoelectric effect. Of the 32 crystal classes, 21 lack a center of symmetry and all of these classes support direct piezoelectricity except for point group 432. The converse piezoelectric effect is the change of strain or stress in a material due to an applied electric field. Both of these effects are illustrated in figure 1.2 as cartoons [5].

In a *piezoelectric* the relationship between the applied deformation and the induced polarization is linear and reversible. The relationships between the strain x, stress σ, electric field strength E, and electric polarization P in a *piezoelectric* material are:

$$P = d\sigma \text{ (direct effect)}, \quad (1.6)$$

$$X = dE \text{ (converse effect)}, \quad (1.7)$$

where d stands for the piezoelectric coefficient or strain constant (d_{ij} relates a field along the i axis to the strain in the j direction). The d_{33} coefficient is the most commonly cited of these coefficients and it is the corresponding coefficient for both strain and field along the polar axis.

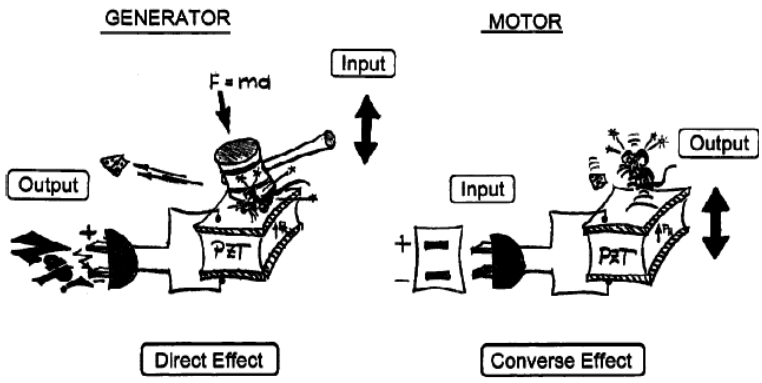

Figure 1.2. Piezoelectric effects in ferroelectric ceramics [5].

1.1.1.3 Ferroelectric property

The phenomenon of ferroelectricity was discovered by J. Valasek in 1921 when he found that polarization of potassium sodium tartrate could be reversed by an externally applied electric field [6]. Valasek named this phenomenon as ferroelectric behavior due to the similarities with the ferromagnetic properties of iron, which were previously understood. A group of compounds showing ferroelectric properties, most of which did not contain iron, were discovered by the 1950s. The name ferroelectricity became indelibly attached to these materials.

Ferroelectrics are materials which show spontaneous electric polarization and whose direction of spontaneous polarization can be reversed by an electric field. In ferroelectrics the relationship between the applied field and the polarization is described by a hysteresis loop (figure 1.3). The application of a low electric filed to a non-polarized ferroelectric provokes a linear and reversible increase of the polarization as the field

increases. The slope of this variation corresponds to the initial dielectric permittivity of the material. As the field increases, the further increase of the polarization is non-linear and, for high field values, the variation of P with E is small and approaches to a saturation value. The polarization value extrapolated for zero field (E=0) gives a saturation polarization Ps. When the external field is removed, the polarization does not fall to zero, keeping a remnant value designated as remnant polarization Pr. To cancel this value, a field in the opposite direction and of magnitude Ec should be applied. This field Ec required to reduce the polarization to zero is called the coercive field. Further increasing of the field in the negative direction will cause the switching of the polarization. Reversing the field direction once again will complete the hysteresis cycle.

The hysteretic behavior of ferroelectrics is related to their domain structure. The regions of the ferroelectrics where the dipoles are aligned in the same direction are called *domains*. The several existing domains are separated by interfaces called *domain walls*, which typically have the dimensions of 1 to 2 lattice spacing. The domains are randomly oriented prior to the application of the electric field and at E=0 the macroscopic polarization is null. For a low applied electric field (region of linear relationship between P and E) the field is not large enough to switch any domain, therefore the ferroelectric will behave as a linear dielectric. As the applied electric field increases, the domains begin to align parallel to the applied filed and the polarization will increase rapidly until all domains are aligned in the field direction. Eventually, for a high applied field, the sample will only be a mono domain. When the field strength decreases, the polarization will generally decrease but not return to zero. When the field is reduced to zero many of the domains will remain aligned in the applied field direction and the ferroelectric will exhibit a remnant polarization Pr. The process of switching all the domains under a single orientation is called *poling*. The remnant polarization Pr in a ferroelectric cannot be removed until the applied field in the opposite (negative) direction reaches the value of the coercive field Ec. Further increasing of the field in the negative direction will cause a complete alignment of the dipoles in this direction. Reversing the field direction once again will complete the hysteresis cycle.

A ferroelectric material undergoes a *phase transition* from the *ferroelectric* to the *paraelectric* state at a temperature called Tc (Curie temperature) as described in figure 1.4. Below the Curie temperature, the material exhibits *ferroelectricity* due to the appearance of the spontaneous polarization and to the mutual interaction between the dipoles which causes a significant increase of the local field. Above Curie temperature, with the loss of the polar structure, the material does not exhibit spontaneous polarization and it is termed *paraelectric* [7]. The phase transition from the ferroelectric to the paraelectric is reversible.

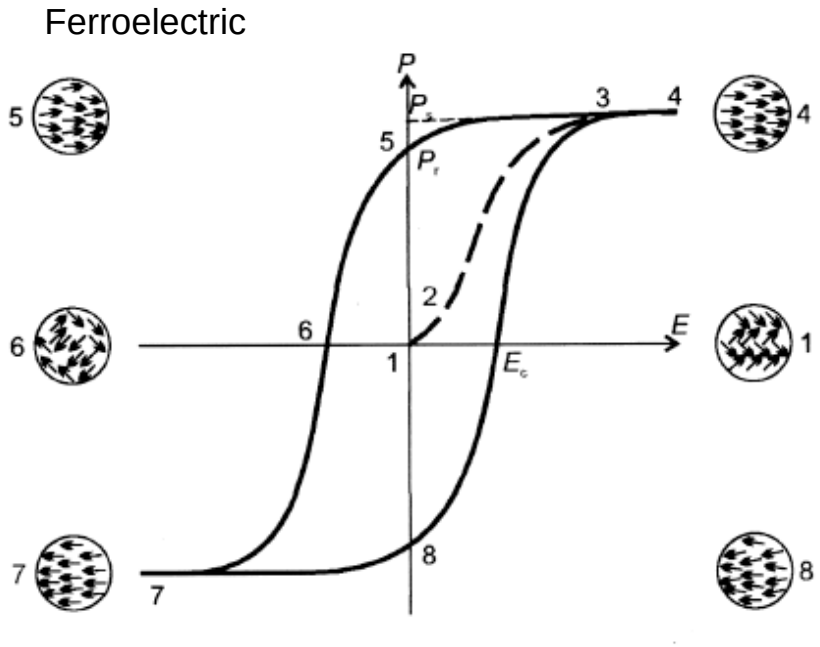

Figure 1.3. A typical ferroelectric hysterisis loop of a ferroelectric material below its Curie temperature [3].

As can be seen in figure 1.4, the relative dielectric constant increases as the temperature approaches the Curie point. In this region the dielectric constant is most sensitive to the magnitude of the applied electric field. Above Tc, permittivity decreases with temperature and often exhibits a Curie-Weiss behavior:

$$\varepsilon_r(T)=C/(T-T_c) \tag{1.8}$$

where C stands for Curie constant. In the paraelectric regime, the spontaneous polarization is zero but permittivity remains high (figure 1.5). Therefore, ferroelectric materials exhibit a memory effect via the hysteretic behavior, which is not present in the paraelectric phase. Hence, the ferroelectric phase is necessary for non-volatile memory applications, whereas the paraelectric phase is preferred for Dynamic Random Access Memories (DRAM) applications.

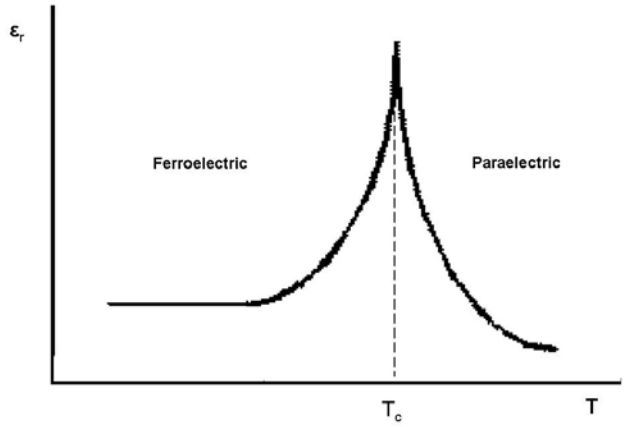

Figure 1.4. The change in permittivity at a ferroelectric-paraelectric phase transition [8].

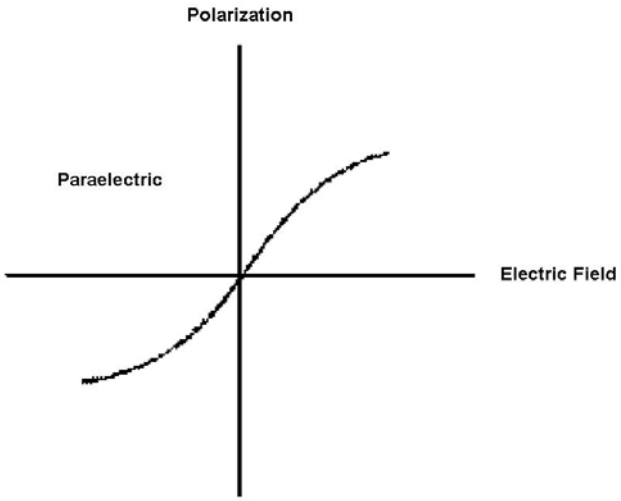

Figure 1.5. The polarization behavior of a ferroelectric material above its Curie temperature [8].

1.1.1.4 Electric breakdown, breakdown strength, leakage current and conduction mechanisms

If the voltage applied to a capacitor is increased, eventually a big bang accompanied with the release of smoke will be produced - the dielectric material inside the capacitor will have experienced "electric breakdown", as demonstrated in figure 1.6. The $\boldsymbol{E_{crit}}$ in figure 1.6 is also called dielectric breakdown strength (D_S) or dielectric strength of the material, which is a measure of the quality of the dielectric material. It is defined as the maximum electric field that the dielectric can withstand without breakdown, under given conditions. It is usually measured in V/cm and can be expressed as [9]

$$\text{dielectric breakdown strength} = Ds = U_{br}/t \tag{1.9}$$

where U_{br} stands for the breakdown voltage (V) of the capacitor and t for the dielectric thickness (cm).

Knowledge of the dielectric strength is very important for the design of thin-film capacitors because it determines the voltage at which destructive breakdown of the dielectric will occur. As a result the working voltage is taken as half of the breakdown voltage.

Unfortunately, $\boldsymbol{E_{crit}}$ is not a well defined material property, it depends on many parameters, the most notable (besides the basic material itself) being production process, thickness, temperature, internal structure (defects and the like), age, environment where it is used (especially humidity) and time it experienced field stress.

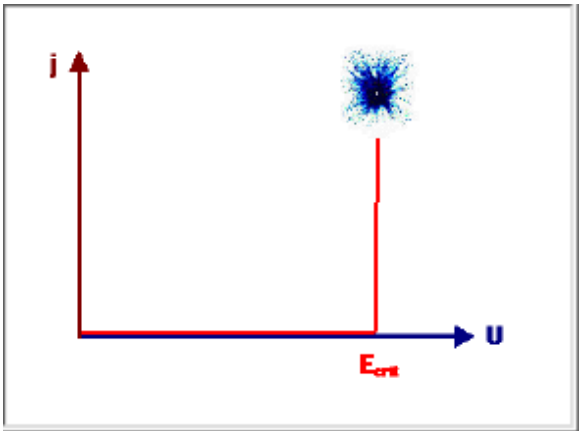

Figure 1.6. The DC current vs. field strength characteristics of a dielectric, where E_{crit} is the critical value of the field strength. After reaching E_{crit} a sudden flow of current may, within very short time (10^{-8} s), destroy the dielectric [10].

Leakage current is the uncontrolled current flowing across regions of semiconductor structure /device in which no current should be flowing. It is becoming an increasingly important fraction of the total power dissipation of integrated circuits [11]. It is an important parameter in thin film technology since it determines the performance of the device in use and its reliability.

As reported in specialized literature the following are the main *conduction mechanisms* for the thin films [12]:

(1) **Fowler-Nordheim Tunneling**: also called field emission. In quantum mechanics tunneling effect are electrons tunnelled through the potential barrier in the presence of a high electric field even if the total particle energy is less than the barrier height.

(2) **Thermionic emission across Schottky barriers**: defines as the process where electrons are emitted across Schottky barrier. The driving force for this process is the thermal energy, which provides a non-zero density of carriers at energies larger than the Schottky barrier.

(3) **Poole-Frenkel emission**: in this mechanism the trapped electrons generated by defect or impurity in the material can escape by thermal emission, and the current flows due to

electrons "jumping" from trap (without the presence of an electric field) to trap (in the presence of an electric field).

Leakage current is a very intricate phenomenon and in thin oxide films it becomes particular complex. The leakage current in some of the useful ferroelectric thin films have been frequently related to the quality of the film that includes aspects such as, density, cracks, defects, stress / strain, interface charges.

1.1.2 Ferroelectric materials

There are more than 500 ferroelectric compounds excluding solid - solutions [13]. However, the way to choose an optimum material is an application - dependent problem. Therefore, for most demanding applications only oxides are usually considered. A number of review papers and textbooks have appeared regarding the basic physical properties, structure, fabrication methods and applications of ferroelectric materials [2, 3, 5, 14, 15]. Currently, oxides based on the perovskite crystal structures are the most widely utilized and studied ferroelectrics [16].

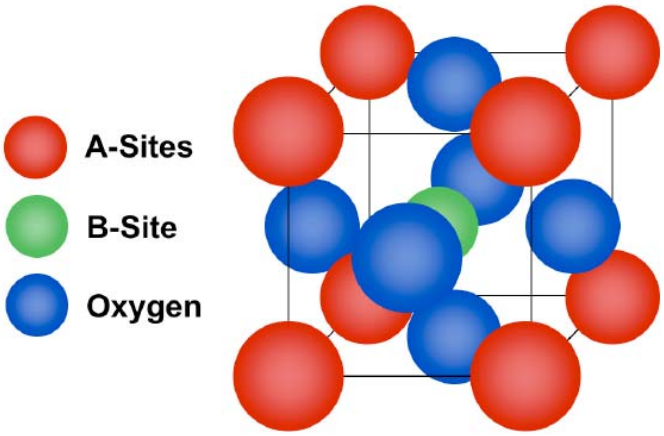

Figure 1.7. Unit cell of ABO_3 type perovskite structured material [17].

Most ferroelectrics, such as Barium Titanate ($BaTiO_3$), Lead Titanate ($PbTiO_3$), Lead Zirconate Titanate (PZT), Lead Lanthanum Zirconate Titanate (PLZT), Lead Magnesium Niobate (PMN), Potassium Niobate ($KNbO_3$), Potassium Sodium Niobate ($K_xNa_{1-x}NbO_3$), and Potassium Tantalate Niobate ($K(Ta_xNb_{1-x})O_3$), are of the perovskite crystal structure. An ideal perovskite structure with a general chemical formula ABO_3 is

depicted in figure 1.7, where A-site cations located at the corners of a cubic unit cell, a B-site cation in the center, and oxygen anions on the six faces [18].

Using geometry and knowledge of crystal chemistry, Goldschmidt defined a tolerance factor for the perovskite structure as [19]:

$$t = \frac{r_A + r_O}{\sqrt{2}(r_B + r_O)} \tag{1.10}$$

where r_A, r_B and r_O stands for the ionic radii of A, B and Oxygen ions, respectively. It was concluded that the perovskite structure would be formed if the limits of the tolerance factor, t, would be between 0.88 and 1.09 [20].

1.2 Literature review of Barium Strontium Titanate (BST) thin films

1.2.1 BST thin films for application in Giga - byte DRAMs

$(Ba_{1-x}Sr_x)TiO_3$, often referred to as BST, is a complete solid solution of ferroelectric $BaTiO_3$ (Tc~120 °C) and quantum paraelectric $SrTiO_3$ (Tc ~ -250 °C). Aside from the composition of x=1, BST thin film is a ferroelectric material with a Curie temperature that decreases almost linearly with increasing x from 120ºC to around room temperature (shown in figure 1.8). The linear drop of Tc is ca. 3.4ºC per mol%. This variation permits to use BST either in the ferroelectric or in the paraelectric state depending upon the temperature and the application type. For instance, 30 mol% Sr would shift the Tc down to room temperature. As a consequence, $(Ba_{0.7}Sr_{0.3})TiO_3$ is paraelectric at the operating temperature range (0-70ºC ambient and 0-100ºC on chips) required for DRAM to avoid fatigue phenomena by ferroelectric domain switching, achieving simultaneously maximum permittivity around this operating temperature required for high capacitance storage [21].

Ferroelectric materials have received much attention from the DRAM industry in the last few decades and are being challenged to produce memory cell small enough to realize Giga - byte cell density [22].

In the actual “shrink technology” to decrease the size of microelectronics devices and at the same time to improve this performance, one of the most critical challenges will be the high memory cell capacitance, which is the crucial parameter determining the sensing signal voltage, sensing speed, data retention times and endurance against the soft error event [22]. In the existing capacitor technologies, the way to increase the capacitance is simply by decreasing the thickness (t) or increasing the area (A) of the

capacitor. However, the reduction of the thickness of the traditionally used SiO_2 dielectrics is already at the limit [23]. Further reduction in the thickness will result in direct charge tunneling through the SiO_2 dielectric [24]. Moreover, increasing capacitor area using complex geometries and decreasing SiO_2 dielectric thickness have only been sufficient for 16 and 256 Mega - byte memory cell generation, higher memory cells required for the coming high capacity DRAM generation needs high permittivity materials. BST is promising for DRAM due to its high dielectric constant, low leakage current, low temperature coefficient of electrical properties, small dielectric loss, environment friendly advantage (lead free), lack of fatigue or aging problems, fabrication compatibility with device progress and tailored Curie temperature [22].

The basic parameters for applying capacitor thin films on DRAMs are dielectric constant, leakage current density and reliability. The targets for ideal G-byte era DRAM capacitors include the followings: (i) SiO_2 equivalent thickness <0.2 nm for Gbit; (ii) leakage current density$<1\times10^{-7}$ A cm^{-2} at 1.6 V; (iii) life time 10 years at 85ºC and 1.6 V; (iv) stability 1015 cycles at >100 MHz; and (v) general compatibility to semiconductor processing [21].

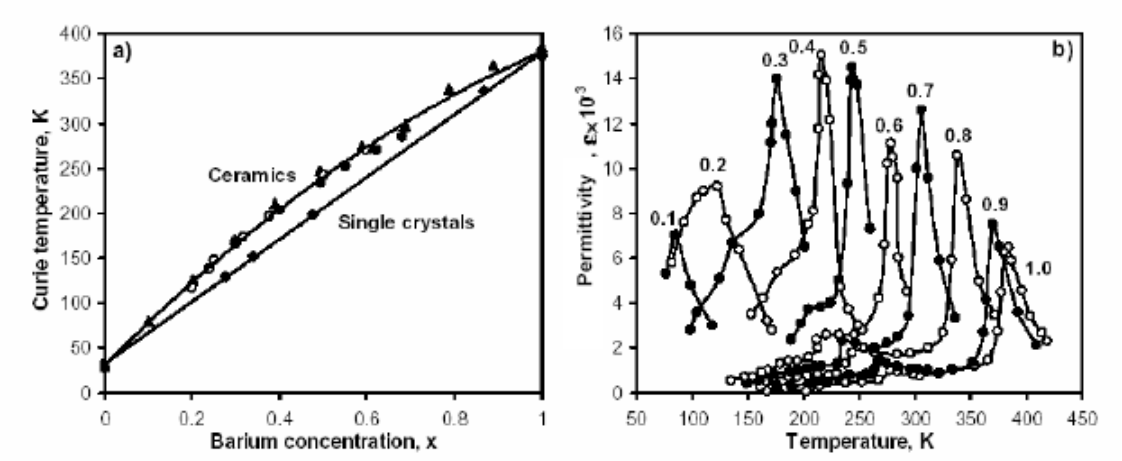

Figure 1.8. (a) Curie temperature of BST ceramics and single-crystal materials as a function of barium concentration x [25], and (b) temperature dependence of the permittivity values of BST ceramic materials for different barium concentrations [26].

1.2.2 BST thin films for application in microwave tunable devices

Besides its interest as DRAMs dielectrics BST has been studied for application in microwave devices since the early 1960s [27]. It is well known for its high tunability, or variation of the relative dielectric permittivity as a function of the applied electric field, resulting in a change of phase velocity in the microwave devices, which allows tuning in real time for a particular application. Besides, BST offers relatively low loss at microwave frequencies, high breakdown voltage and fast tuning speed. As a result, BST has been now considered as one of the most promising material for tunable microwave devices applications [28-30].

Different microwave devices have been developed and studied based on these valuable properties. Examples include tunable resonators, phase-shifters, variable-power dividers and voltage-controlled oscillators [31-37]. Such components have a wide range of applications in telecommunication and radar systems for both military and commercial services.

The dependence of the relative permittivity (ε_r) on the applied bias electric field (E) is commonly described by *tunability*, n, and is defined as the ratio of permittivity with zero applied electric field to that measured with an applied electric field, E:

$$n = \frac{\varepsilon_r(o)}{\varepsilon_r(E)} \tag{1.11}$$

Another way to define tunability is given below:

$$n_r = \frac{\varepsilon_r(o) - \varepsilon_r(E)}{\varepsilon_r(o)} = 1 - \frac{1}{n} \tag{1.12}$$

where $\varepsilon_r(0)$ and $\varepsilon_r(E)$ represent the dielectric constant value at zero applied electric field and the maximum applied electric field, respectively.

Tunability of 10-60% at 4V μm^{-1}, low dissipation factor (0.001) and suitable relative permittivity (100-1000) are commonly required for tunable microwave devices.

Recently research on BST system has been focused on ways to improve the dielectric tunability and reduce the dielectric loss of BST capacitors for the above mentioned applications.

1.2.3 Processing of BST thin films

The properties of BST thin films markedly depend on the growth method, composition, stoichiometry, microstructure (grain size and size distribution), film thickness, characteristics of electrode, and homogeneity of the film [22].

The two main fabrication techniques used for the preparation of thin films, including BST thin films, are the physical vapor deposition (PVD) [38, 39] and the chemical deposition, which comprise chemical vapor deposition (CVD) [40-42] and chemical solution deposition (CSD) methods [43, 44]. Table 1.1 shows the comparison of the properties of BST films prepared by these various methods.

Table 1.1. Comparison of electrical data from BST samples prepared by various deposition techniques (PLD- Pulsed Laser Deposition, LSCVD – Liquid Source Chemical Vapour Deposition, MOD- Metal Organic Deposition).

Deposition techniques	Processing temperature	Composition	Film Thickness (nm)	Dielectric constant	Loss tangent	Leakage current density (A/cm^2)	References
PLD	700ºC	$(Ba_{0.6}Sr_{0.4})TiO_3$	200	350 (at 100 kHz)	0.07 (at 100 kHz)	-	[38]
Sputtering	600ºC	$(Ba_{0.6}Sr_{0.4})TiO_3$	220	682 (at 100 kHz)	0.015 (at 100 kHz)	3.0×10^{-8} at 455 kV/cm	[39]
LSCVD	750ºC	$(Ba_{0.7}Sr_{0.3})TiO_3$	150	390 (at 100kHz)	0.06 (at 100 kHz)	3.2×10^{-6} at 135 kV/cm	[40]
MOD	750ºC	$(Ba_{0.7}Sr_{0.3})TiO_3$	300	563 (at 100 kHz)	0.02 (at 100 kHz)	1.0×10^{-6} at 100 kV/cm	[42]
Sol-Gel	700ºC	$(Ba_{0.8}Sr_{0.2})TiO_3$	400	830 (at 1 kHz)	0.05 (at 1 kHz)	8.0×10^{-7} at 225 kV/cm	[43]
Sol-Gel	750ºC	$(Ba_{0.8}Sr_{0.2})TiO_3$	300	400 (at 10 kHz)	0.014 (at 10 kHz)	1×10^{-6} at 335 kV/cm	[44]

In PVD, atoms from a source (target) are transferred in a continuous and controlled manner under a vacuum atmosphere (> 10^{-5} Torr) to the substrate, in which the

nucleation and growth of the film occurs atomistically. Depending on how the particles (atoms or ions) are removed from the target, the following PVD techniques are considered: RF sputtering, ion beam sputtering, electron beam evaporation and laser ablation [45]. Pulsed laser deposition (PLD) [38] and RF sputtering [39] have been used for BST thin films fabrication. PVD methods are well suited for epitaxial growth, allow precise control of the film thickness and produce BST thin films with low leakage current, but are inappropriate for mass production; the rates of deposition are slow, the costs associated with the equipment are particular high, the control of stoichiometry of the BST thin films is difficult and high temperature (700 ~ 800ºC) is needed for post-deposition crystallization [38].

On the other hand, chemical deposition methods permit higher deposition rates, good stoichiometry control and large area production of defect-free films and at the same time the equipment related costs are lower when compared with the PVD methods.

Chemical vapour deposition (CVD) is a generic name for a group of processes that involve depositing a solid material from a gaseous phase (in which chemical reactions may occur) and is similar in some respect to physical vapor deposition (PVD). The group of CVD techniques includes low - pressure chemical vapor deposition (LPCVD), liquid source chemical vapor deposition (LSCVD), metal organic chemical vapor deposition (MOCVD) and metal organic deposition (MOD). In conventional CVD, films are deposited by surface reaction of the substrate with the gaseous species. The advantages of CVD include a high deposition rate, uniform deposition over large areas and satisfactory step coverage. However, CVD of BST films is restricted by a low vapor pressure of source materials and deterioration during storage [22].

Chemical solution deposition (CSD) refers to a wet chemical method for the fabrication of thin films and includes various solution preparation and processing techniques. The most well known and widely used solution process is the sol-gel route.

CSD methods, especially sol-gel processing, have been increasingly used for the preparation of BST films. Sol-gel processing is a liquid processing method in which

molecular level reactions take place. “Sol” means an assembly of colloids (very small particles with size from few nm to 1000 nm) suspended in a liquid solution. In this suspension, the dispersed phase is so small that gravitational forces are negligible and interactions are dominated by short-range force, e.g., Van der Waals attractions and surface charges. These colloidal particle suspensions exhibit Brownian motions. [46] “Gel” means an assembly of the network formed by molecules when the sol becomes solid [47].

Preparation of metal oxides by the sol gel route occurs via the three basic stages: 1) partial hydrolysis of metal alkoxides to form reactive monomers (or polymers); 2) the polycondensation of the monomers to form colloid oligomers (sol formation); 3) additional hydrolysis to promote polymerization and cross linking that leads to the formation of a 3–dimensional polymeric network (gel formation). [47]

In the *sol gel* process, the precursors (starting compounds) for preparation of a colloid consist of a metal or a metalloid atom surrounded by various ligands that might be inorganic (such as any metal nitrides or hydroxides) or organic (such as acetates or metal organic alkoxides). Alkoxides are the class of precursors most widely used in sol gel technology, because they react promptly with water and the reaction is called *hydrolysis*. [46]. The chemical reaction of monomer formation (partial hydrolysis) occurs according the reaction:

$$M(OR)_n + H_2O \rightarrow (RO)_{n-1}\,MOH + ROH \qquad (1.13)$$

in which M stands for the metal cation (e.g. Ti, Zr, Pb, Ba, among others) and R = $(C_xH_{2x+1})^-$. The link together of hydrolyzed or partially hydrolyzed molecules constitutes the *condensation* reaction that by definition liberates small molecules, such as water or alcohol. The reaction of sol formation (polycondensation) is as the following:

$$2(RO)_{n-1}MOH \rightarrow (RO)_{n-1}–O–\,M(OR)_{n-2}\,OH + ROH \qquad (1.14)$$

If this reaction continues and large metal containing molecules are formed the process is called *polymerization* and a gel is formed and the gelation (cross–linking) occurs according to the following reaction

$$(RO)_{n-1}–O–M(OR)_{n-2}\,OH \rightarrow (RO)_{n-1}–O\text{-}M[(OR)_{n-2}]_nOH + ROH \qquad (1.15)$$

During the polymerization and cross linking process the viscosity of the sol steadily increases until the sol-gel transition point. At this point the viscosity increases suddenly and the gelation occurs [47]. By elimination of the interstitial liquid by drying or other dehydration methods the cross linking increases and finally a solid is formed. Most of the gels are amorphous but easily crystallize when heated [46].

Sol-gel methodology used to prepare films of metal oxides entails three steps: (i) the preparation of the solution (sol), (ii) the deposition of the solution onto the substrate by dip- or spin-coating, followed by a drying step to evaporate the solvents and consolidate the film into an amorphous gel and (iii) finally the subsequent thermal treatment of the deposited layer to remove the organics and to achieve crystallization of the desired phase and densification of the coating.

The increasing interest in the fabrication of BST films by sol-gel is related to its unique advantages. It is a non-vacuum process with high deposition rates. The dissolution of the precursors in solvents implies a mixing of the precursor species at a molecular level, guaranteeing a high degree of chemical homogeneity and the control of the stoichiometry of BST films is fairly easy. The use of chemical precursors of extremely high purity provides films of greater purity than some of the other film deposition routes. Adjusting the concentration and viscosity of the precursor sol produces films of various thicknesses. Additionally, the fabrication of large area films free of defects is possible by sol-gel with low equipment related costs. However, the probability to create cracks is high; the deposition on deep trenched surface and the processing of epitaxially grown films is difficult by this method. The occurrence of cracks can be avoided by the use of additives in the precursor sol and by the control and optimization of the pyrolysis [43, 44].

It is well known that the choice of the fabrication technique is dictated by several factors that include the properties requirements as well as by cost related aspects, and compatibility with previous or subsequent fabrication techniques. Currently for many capacitor applications, cost is the driving factor because thin-film devices often are competing against low-cost discrete devices. In this case, sol-gel techniques are preferred because they offer a relatively simple, low-cost approach to fabricate thin films that is compatible with commercial processing equipment and techniques such as spin coating and photolithography.

In the fabrication of BST thin films by sol-gel the following three steps are involved:

1. Preparation of the Sol:

The sol is prepared by dissolving the precursors in a suitable solvent. This is one of the most important steps in the process, since the sol should be homogeneous, stable (without any precipitates) and possess the required rheological properties (viscosity and surface tension) needed for a good spin or dip coating processing and adhesion of the solution onto the substrate.

In the preparation of multioxides films, such as BST, the choice of the precursor compounds and solvents plays a major role. It is necessary to guarantee that all the constituents are homogeneously mixed and that the hydrolysis and condensation reactions do not occur partially, but instead occur simultaneously. In this way the high level of molecular homogeneity attained in the homogeneous precursor solution is retained in the gel and, consequently, the final stoichiometry will be guaranteed.

The mostly utilized raw materials in BST sol gel thin film fabrication includes barium acetate $Ba(CH_3COO)_2$, strontium acetate $Sr(CH_3COO)_2$, strontium acetate hemihidrated $Sr(CH_3COO)_2 \cdot 1/2H_2O$, tetraethoxytitanium $Ti(OC_2H_5)_4$ and tetrabutoxytitanium $Ti(OC_4H_9)_4$ [43,48,49]. Acetic acid and 2-methoxy ethanol (2-MOE) are the most frequently employed solvents. Acetic acid is expected to form chelates with ionic metals in solution and 2-MOE have a strong affinity with metal atoms in the

complex alkoxide. The chelation is known to reduce the hydrolysis rate of the complex alkoxides. Additionally, 2-MOE can improve the wettability and uniformity of films [50]. However, to avoid the use of the teratogenic MOE solvent, which makes large-scale or industrial use unappealing, modifications of the process have been carried out that include the employment of propionic acid and 1-butanol, which yield excellent films and are not teratogenic [51] and diols as substitutes for the former MOE [52]. In a diol route, also termed as dihydroxy alcohol route, the dihydroxy alcohol is used as the solvent to modify the metal alkoxides. Acting as bridging-chelating ligands diols originate large oligomers/polymers species that allow to achieve a high homogeneity at a molecular level in multicomponent systems, crucial to attain the required compositional stoichiometry of the final material [49]. M. B. Gonzalez et al reported the influence of the solvent on the sol structure and microstructure development and dielectric properties of $Ba_xSr_{1-x}TiO_3$ (BST, x=0.5) thin films. It was found that the films prepared with ethylene glycol show better dielectric properties compared with films prepared from propylene glycol precursors [49]. Films prepared with ethylene glycol show higher values of the dielectric permittivity (~40% higher) and lower values of dielectric losses when compared with films prepared from propylene glycol precursors. The dielectric permittivitty is 459 and 302 at 1 kHz for films prepared with ethylene glycol and 1,2-propanediol, respectively, and annealed at 800 °C [49].

Ethylene glycols were also found a necessary component of the solution to increase stability and to decrease the crystallization temperature of the BST thin films [53]. Moreover glycols were reported as an effective additive to reduce cracks of BST films [54].

2. Deposition and Gel Formation:

After getting the ideal solution the following step involves the deposition of thin layers of the stable sol onto the substrate by such common processes as spinning, dipping or spraying. The final microstructure of the film depends on the size and extent of branching (or aggregation) of the solution species prior to the film deposition and the

relative rates of condensation and evaporation during film deposition. Control of these factors enables to tailor the final microstructure and film properties [46].

Spin coating is a common procedure used to produce thin layers on flat substrates [55]. An excess of the solution is dripped on the top of the substrate. The substrate is then rotated at high speed to spread the fluid all over the substrate by centrifugal forces. This rotation continues until the fluid is spinned off the edges of the substrate and the required thickness is reached. Spin-coating method presents clear advantages related to the rapid processing, easy operation and the use of small amounts of liquid for large areas. However substrate size and shape limits the application of spin coating.

The device used for spin coating is called a spin coater, which is very popular in microlithography and the semiconductor. Spin coater generally consist of a high speed motor with a vacuum plate attached on the top, as shown in figure 1.9.

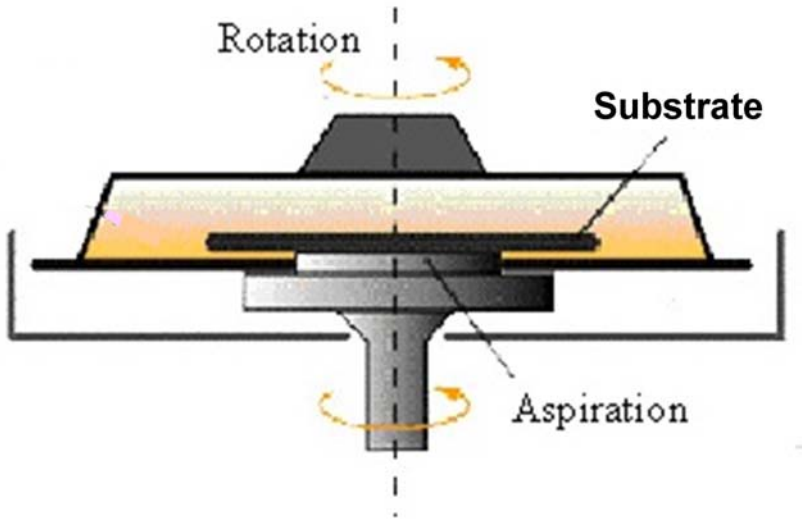

Figure 1.9. A schematic representation of a spin coater [55].

Dip coating refers to the immersing of a substrate into a tank containing coating material, removing the piece from the tank, and allowing it to drain. The coated piece can

then be dried by force-drying or baking. The dip coating process can be, generally, separated into 3 stages:

- Immersion: the substrate is immersed in the solution of the coating material at a constant speed preferably judder free;
- Dwell time: the substrate remains fully immersed and motionless to allow for the coating material to apply itself to the substrate ;
- Withdrawal: the substrate is withdrawn, again at a constant speed to avoid any judders. The faster the substrate is withdrawn from the tank the thicker the coating material that will be applied to the substrate.

Fluid sol transforms to a semi-rigid solid as a result of the polymerization of different species present in the sol. The gel formation is determined by the rate of hydrolysis, condensation or polymerization. After spin-coating or dip-coating procedure film consolidations occurs resulting in a solid gel. The process of consolidation usually involves drying and heat treatment, in which the organic evaporation and burning occurs. This heat treatment (thermolysis and pyrolysis) may occur in air, reducing or oxidizing atmospheres. The first heat treatment occurs between 200 and 400ºC usually on a hot place. During this treatment a large portion of the organics is released and the films shrink around 30%. A second heat treatment at higher temperatures ranging from 500 to 700ºC removes the rest of the organics and hydro-carbon species. This process is repeated after the deposition of each layer or a group of layers. Sometimes a final heat treatment at higher temperatures follows up.

3. Crystallization:

The thin films obtained after deposition are amorphous and need to be heat treated to crystallize. This step constitutes the final processing stage.

It is well known that the dielectric properties and tunability of BST thin films depend on film composition and morphology. On the other hand crystallization and final morphology of the film depend on several parameters, being the most relevant the

deposition method, underlying substrate, film composition and previous thermal treatment history [56].

Due to film growth mechanisms of vacuum deposition techniques, such as PLD and RF (radio frequency) magnetron sputtering, among others, are the most adequate to prepare orientated films and, consequently, epitaxial or textured grown BST films are relatively easy to be obtained through these methods [57-59]. However with CSD techniques it is difficult to grow textured films; the nucleation events are equally probable throughout the bulk of the film as in the film-substrate interface, and nucleation through the bulk of film results in a polycrystalline film. If preferred orientation of BST films is required, the nucleation events must be limited to the film-substrate interface, which is hard to control by CSD methods, especially at low temperature on $Pt/TiO_2/SiO_2/Si$ substrate.

However due to the anisotropic dielectric properties of BST films, studies have been carried out on the fabrication of orientated or textured BST films in order to maximize the dielectric response [60]. A range of methods to obtain textured BST films, such as the control of heat treatment conditions [61], the insertion of seed layers (or intermediate layers) [62-63] and/or the choice of different bottom electrodes [64], have been reported. Most of the works covered the preparation of textured BST films by vacuum techniques. Only a few works reported the use of solution deposition to prepare highly orientated BST films [61-62]. The use of buffer layers to reduce the lattice mismatch and promote epitaxy has been shown to improve both the crystallinity and dielectric properties of BST films. Recently it was reported that the use of a (BST80/20) sol gel seed layer of optimised thickness the perovskite phase nucleation and growth of BST80/20 films was restricted to the bottom interface and as a result (h00) preferred oriented BST thin films on $Pt/Ti/SiO_2/Si$ with a dielectric constant of 830 at 1 KHz were prepared by sol gel at 700°C [43].

The choice of the substrate material is device driven. Silicon is the most commonly used substrate in device applications and conventional ferroelectric devices are ordinarily deposited on $Pt/TiO_2/SiO_2/Si$ substrates. The films deposited on these

substrates are generally polycrystalline and the existence of the grain boundaries is responsible for the degradation of the dielectric properties. The lattice mismatch between the perovskite ferroelectric films and Si substrate makes the epitaxial growth difficult. The use of buffer layers to reduce the lattice mismatch and promote epitaxy has been shown to improve both the crystallinity and dielectric properties of BST films on Si [65].

Composition can also have a strong influence on film morphology. The appearance of a transient (111) Pt_xPb phase during the crystallization of sol gel PZT films on $Pt/TiO_2/SiO_2/Si$ favours the growth of the film along the 111 direction [66]. Rapid thermal annealing (RTA), involving the rapid crystallization of the film by heating at a very fast rate (150ºC /min), holding for short periods of time at the required annealing temperature, and cooling very rapidly, inhibits the unwanted reactions and crystallization of unwanted phases. The RTA is very effective for the processing of ferroelectric thin films.

1.2.4 Objective of the thesis

As discussed above the crystallization temperature of post-deposition heat treatment is a key parameter in the preparation of ferroelectric films. It ensures phase purity and controls of interdiffusion between the film and underlayers, which have a direct impact on the final properties of the films.

The choice of suitable electrode is also a very important factor for a reliable device operation. The interactions between the electrode and thin film can degrade the device performance. This problem can be overcome by selecting a conducting electrode material which offers chemical and mechanical stability. Platinum (Pt) has been considered as the most desirable metal electrode since it is chemically stable in an oxidizing environment and maintains its conducting properties under thermal processing. However, the formation of Pt hilloks at the high temperature of thin films thermal cycling may lead to bad adhesion and short-circuits in the devices [30, 67]. Therefore, the annealing temperature of thin films should be as low as possible to avoid the hillocks.

Additionally the current trend of microelectronics industry towards the development of miniaturized, mobility, flexible devices with high levels of integration at low cost and with enhanced performance have been the driving force for the utilization of alternative substrates, namely flexible metallic substrates. If metals as Cu or Ni will be considered the annealing temperature of the capacitor will be a decisive factor.

According to the literature, during the crystallization of the chemical solution deposition method derived BST thin film [68-69], an intermediate phase termed oxycarbonate, with a chemical formula of $(Ba,Sr)_2Ti_2O_5CO_3$, is formed at around 550-650ºC disappearing at higher temperatures. Since the phase purity is crucial to insure the good electrical properties of BST thin films [70], typical temperatures for the formation

of the perovskite phase in BST films varies between 700 and 800ºC [43, 54,71-72]. At lower treatment temperatures, a mixture of both phases remains in the film and porous films are produced, both of which contribute to a minimized electric response. At higher thermal treatment (700-800ºC) although the pure perovskite phase will be obtained, the electrode recrystallization may occur with the associated degradation mentioned above [30. 49]. Moreover, heat treatments above 750ºC often result in the inter-diffusion among the film, electrode and silicon layers [73-74]. It should be also mentioned that thermal stresses generated at high temperatures might affect the long-term reliability of the device [75].

In order to avoid these problems, the temperature of the preparation process of BST thin films should be as low as possible. At low temperatures, interdiffusion between different layers, undesired chemical reactions and thermal degradation of the underlying circuit are minimized. Additionally, a low annealing temperature is also essential when metallic, glass or polymeric substrates are required.

A common way to decrease the sintering temperature of BST ceramic materials is to add some sintering aids, but the appearance of second phases generally depresses the ferroelectric character of BST [76-77]. Huang et al [69] found that the perovskite formation temperature of the sol-gel derived $(Ba_{2/3}Sr_{1/3})Ti_{1+x}O_3$ powders could be reduced by using excess TiO_2 acting as nucleation sites for the perovskite phase formation. However, few efforts have been undertaken to lower the perovskite crystallization temperature in sol-gel derived BST thin films.

Halder's group reported an aminoalkoxide chemical solution deposition route to prepare BST 70/30 thin films at relatively low annealing temperature, where barium diaminoethoxide $[Ba(OCH_2CH_2NH_2)_2]$ and strontium diaminoethoxide $[Sr(OCH_2CH_2NH_2)_2]$ precursors were prepared under dry nitrogen by the dissolution of the pure Ba and Sr metal in excess 2-aminoethanol $[NH_2CH_2CH_2OH]$. The onset of the crystallization temperature occurring at 600ºC, and dielectric constant value around 310 of the films prepared at 650ºC were reported by this group. [78]

Xu et al reported a sol-gel/hydrothermal process at a low processing temperature of 100-200ºC [79]. The BST gel films were fabricated by a conventional sol-gel process, and hydrothermal treatment of gel films was performed to prepare BST thin films. However, the pyrochlore phase was detected at this annealing temperature, which is deleterious for the performance of BST thin films. The room temperature dielectric constant less than 20 and dissipation factor more than 0.6 were obtained in this work, which are not sufficient for the application. The control of the stoichiometry of these films is particularly difficult.

It is known that the nucleation is a rate-limiting step for perovskite phase formation. Therefore, any process that enhances the nucleation process is likely to decrease the transformation temperature. Based on this theory, Kwok et al [80] developed a seeding process to lower the transformation temperature of lead zirconate titanate (PZT) thin films by using a very thin $PbTiO_3$ seeding layer, which has a low effective activation energy for perovskite formation and was used to provide nucleation sites needed for the low temperature perovskite formation. The perovskite crystallization temperature of PZT thin films was lowered by as much as 100ºC.

On the other hand Wu et al [81-82] have succeeded in decreasing the crystallization temperature of PZT thin films by employing nano sized perovskite lead zirconate titanate (PZT) and barium titanate (BT) powders as seeds to fabricate PZT films by sol-gel. The authors named this process as a diphasic precursor sol gel method. According to their reaction kinetics studies on the PZT perovskite phase transformation from intermediate phase to pure perovskite phase is a nucleation controlled process, where the nucleation of the perovskite phase is considered as the rate-controlling step of the reaction. Thus, the kinetics of this reaction can be improved if the number of nucleation sites is increased. The authors found that addition of seeds decreases the crystallization temperature, allows to obtain uniform and dense microstructures and improved the ferroelectric characteristics markedly [83-84].

Similar approach was recently used by Kobayashi et al [85] to prepare $Ba_{0.5}Sr_{0.5}TiO_3$ thin films containing nano crystalline seeds of BST on indium titanium

oxide (ITO) substrate. BST perovskite phase crystallization initiated at 525ºC when 17 mol% seeds were present; the complete crystallization occured at 600ºC with 17 mol% seeds. Although pure perovskite phase was obtained for seeded films annealed at 600ºC they exhibited a relative low dielectric constant of 303 at 1 KHz, and the dielectric loss of the film were 0.15 at 1 KHz.

Though the Kobayashi group has prepared seeded BST thin films at 600ºC, the influence of seeds on the microstructure, electrical properties were not studied. No leakage current and tunablity behavior were reported. The mechanism of the low-temperature sintering were not investigated either. To improve the electric properties of sol-gel derived BST films, the crystallization kinetics, microstructure evolution of low temperature processing films needs to be studied in detail and systematically.

The aim of this work is:

i) to synthesize monophasic, dense, homogeneous BST thin films with enhanced dielectric properties at a low annealing temperature (600 º C) using nano sized BST perovskite powders as seeds, which will be dispersed in sol stock solution prior to film deposition and with optimized dielectric and ferroelectric response;
ii) to systematically study and to quantify the influence of seeds on the phase evolution, microstructure and electrical properties of BST thin films.

1.2.5 References

[1] M. Goel, Recent Developments in Electroceramics: MEMS Applications for Energy and Environment, Ceramics International, **30**(2004) 1147

[2] N. Setter, D. Damjanovic, L. Eng, G. Fox, S. Gevorgian, S. Hong, A. Kingon, H. Kohlstedt, N. Y. Park, G. B. Stephenson, I. Stolitchnov, A. K. Taganstev, D. V. Taylor, T. Yamada, S. Streiffer, Ferroelectric Thin Films: Review of Materials, Properties, and Applications, Journal of Applied Physics, **100**(2006) 051606

[3] Paula M. Vilarinho, Functional Materials: Properties, Processing and Applications, in Scanning Probe Microscopy: Characterization, Nanofabrication and Device Application of Functional Materials, edited by P. M. Vilarinho, Y. Rosenwaks, A. Kingon, Kluwer Academic Publishers, 2005, pages 3 - 33

[4] B. J. Laughlin, Sputtered $(Ba_x,Sr_{1-x})TiO_3$, BST, Thin Films on Flexible Copper Foils for Use as a Non-Linear Dielectric, Ph.D Thesis of North Carolina State University, 2006

[5] G. H. Haertling, Ferroelectric Ceramics: History and Technology, Journal of the American Ceramic Society, **82**(1999), 797

[6] J. Valasek, Piezo-Electric and Allied Phenomena in Rochelle Salt, Physics Review, **17**(1921) 475

[7] M. E. Lines, A. M. Glass, Principles and Applications of Ferroelectrics and Related Materials, Oxford: Clarendon Press, 1977, 71

[8] C. Basceri, Electrical and Dielectric Properties of $(Ba,Sr)TiO_3$ Thin Film Capacitors for Ultra-High Density Dynamic Random Access Memories, Ph.D Thesis of North Carolina State University, 1997

[9] B. Tareev, Physics of Dielectric Material, Mir Publishing, Moscow, 1975, 175

[10] www.tf.uni-kiel.de

[11] R. M. Rao, J. L. Burns, R. B. Brown, Circuit Techniques for Gate and Sub-Threshold Leakage Minimization in Future CMOS Technologies, European Solid-State Circuits Conference (ESSCIRC 2003) 313

[12] www.colorado.edu

[13] Landolt-Bornstein, Ferro- and Antiferroelctric Substances, Springer, 1975

[14] O. Auciello, J. F. Scott, R. Ramesh, The Physics of Ferroelectric Memories, Physics Today, **51**(1998) 22

[15] A. I. Kingon, S. K. Streiffer, Ferroelectric Films and Devices, Current Opinion in Solid State and Materials Science, **4**(1999) 39

[16] B. Jaffe, W. R. Cook, H. Jaffe, Piezoelectric Ceramics, Academic Press, London, 1971

[17] M. D. Losego, The Chemical Solution Deposition of Lead Zirconate Titanate (PZT) Thin Films Directly on Copper Surfaces, Master Thesis of North Carolina State University, USA, 2005

[18] M. T. Weller, Inorganic Materials, Oxford Science, 1994

[19] V. M. Goldschmidt, Construction of Crystals, Zeitschrift fur Technische Physik **8**(1927) 251

[20] T. R. Shrout, A. Halliyal, Preparation of Lead-Based Ferroelectric Relaxor for Capacitors, American Ceramic Society Bulletin, **6**6(1987) 704

[21] T. Y. Tseng, IEDMS C2-5 (1996) 89

[22] S. Ezhilvalavan, T. Y. Tseng, Progress in the Development of (Ba,Sr)TiO_3 (BST) Thin Films for Gigabit Era DRAMs, Materials Chemistry and Physics, **65**(2000), 227

[23] A. I. Kingon, J. P. Maria, S. K. Streiffer, Alternative Dielectrics to Silicon Dioxide for Memory and Logic Devices, Nature, **406**(2000) 1032

[24] S.-H. Lo, D. A. Buchanan, Y. Taur, W. Wang, Quantum-Mechanical Modeling of Electron Tunneling Current from the Inversion Layer of Untra-Thin-Oxide nMOSFETs. IEEE Electron Device Letters, **18**(1997) 209

[25] O. G. Vendik, S. P. Zubko, Ferroelectric Phase Transition and Maximum Dielectric Permittivity of Displacement Type Ferroelectrics ($Ba_xSr_{1-x}TiO_3$), Journal of Applied Physics, **88**(2000) 5343

[26] G. A. Smolensky, V. A. Isupov, Zhurnal Tekhnicheskoi Fiziki, **24**(1954) 1375

[27] G Rupprecht, P. O. Bell, Microwave Losses in Strontium Titanate above the Phase Transition, Physics Review, **125**(1962) 1915

[28] K. H. Ahn, S. S. Kim, S. Bai, Thickness Dependence of Leakage Current Behavior in Epitaxial (Ba,Sr)TiO_3 Film Capacitors, Journal of Applied Physics, **93**(2003) 1725

[29] Y. Liu, A. S. Nagra, E. G. Erker, P. Periaswamy, T. R. Taylor, J. Speck, R. A. York, $BaSrTiO_3$ Interdigitated Capacitors for Distributed Phase Shifter Applications, IEEE Microw Guided Wave Letters, **10**(2000) 448

[30] A. Kumar, S. G. Manavalan, Characterization of Barium Strontium Titanate Films for Tunable Microwave and DRAM Applications, Surface & Coatings Technology, **198**(2005) 406

[31] A. A. Semenov, S. F. Karmanenko, B. A. Kalinikos, A. N. Slavin, G. Srinivasan, J. V. Mantese, Ferrite/Ferroelectric Layered Structures for Magnetic and Electric Field Tunable Microwave Devices, Integrated Ferroelectrics, **77**(2006) 199

[32] J. Nath, D. Ghosh, J.-P. Maria, A. I. Kingon, W. Fathelbab, P. D. Franzon, M. B. Steer, An Electronically Tunable Microstrip Bandpass Filter Using Thin-Film Barium-Strantium-Titanate (BST) Varactors, IEEE Transactions on Microwave Theory and Techniques, **53**(2005) 2707

[33] A. Tombak, J.-P. Maria, F. T. Ayguavives, Z. Jin, G. T. Stauf, A. I. Kingon, A. Mortazawi, Voltage-Controlled RF Filters Employing Thin-Film Barium-Strontium-Titanate Tunable Capacitors, IEEE Transactions on Microwave Theory and Techniques, **51**(2003) 462

[34] A. Mahmud, T. S. Kalkur, A. Jamil, N. Cramer, Design, Modeling and Characterization of an Active Phase Shifter Using a Ferroelectric Capacitor, Integrated Ferroelectrics, **81**(2006) 197

[35] P. M. Suherman, T. J. Jackson, Y. Y. Tse, M. J. Lancaster, Temperature Dependent Dielectric Properties of Coplanar Phase Shifters Fabricated from $Ba_{0.5}Sr_{0.5}TiO_3$ Thin Films, Ferroelectrics, **335**(2006) 69

[36] S. J. Lee, H. C. Ryu, S. E. Moon, M. H. Kwak, Y. T. Kim, K. Y. Kang, X-band Ferroelectric Phase Shifter Using Voltage-Tunable (Ba,Sr)TiO_3 Varactors, Journal of the Korean Physical Society, **48**(2006) 1286

[37] A. Jamil, T. S. Kaukui, N. Cramer, Voltage-Controlled Oscillator Design Using Ferroelectric Varactors, Integrated Ferroelectrics, **81**(2006) 157

[38] D. M. Potrepka, S. Hirsch, M. W. Cole, W. D. Nothwang, S. Zhong, S. P. Alpay, Effect of Strain on Tunability in $Ba_{0.6}Sr_{0.4}TiO_3$ Thin Films on Pt-Si Substrate, Journal of Applied Physics, **99**(2006) 014108

[39] Y. Wang, B. Liu, F. Wei, Z. Yang, J. Du, Fabrication and Electrical Properties of (111) Textured $(Ba_{0.6}Sr_{0.4})TiO_3$ Film on Platinized Si Substrate, Applied Physics Letters, **90**(2007) 042905

[40] H. J. Chung, J. H. Kim, W. S. Moon, S. B. Park, S. C. Hwang, M. Y. Lee, S. I. Woo, Preparation of BST Thin Films on Pt Electrode on Si Wafer with Down-Flow LSMCVD Reactor, Integrated Ferroelectrics, **12**(1996) 185

[41] S. Regnery, Y. Ding, P. Ehrhart, C. L. Jia, K. Szot, R. Thomas, R. Waser, Metal-Organic Chemical-Vapor Deposition of $(Ba,Sr)TiO_3$: Nucleation and Growth on Pt-(111), Journal of Applied Physics, **98**(2005) 084904

[42] S. Yamamichi, P.-Y. Lesaicherre, H. Yamaguchi, K. Takemura, S. Sone, H. Yabuta, K. Sato, T. Tamura, K. Nakajima, S. Ohnishi, K. Tokashiki, Y. Hayashi, Y. Kato, Y. Miyasaka, M. Yoshida, H. Ono, A Stacked Capacitor Technology with ECR Plasma MOCVD $(Ba,Sr)TiO_3$ and RuO_2/Ru/TiN/TiSix Storage Nodes for Gb-Scale DRAMs, IEEE Transactions on Electron Devices, **44**(1997) 1076

[43] Z. Fu, A. Wu, P. Vilarinho, Effect of Seed Layer Thickness on Texture and Electrical Properties of Sol-Gel Derived $(Ba_{0.8}Sr_{0.2})TiO_3$ Thin Films, Chemistry of Materials, **18**(2006) 3343

[44] J.-G. Cheng, X.-J. Meng, J. Tang, S.-L. Lou, J.-H. Chu, Fabrication and Electrical Properties of Sol-Gel-Derived $Ba_{0.8}Sr_{0.2}TiO_3$ Ferroelectric Films from a 0.05-M Spin-on Solution, Applied Physics: A, **70**(2000) 411

[45] M. Ohring, The Materials Science of Thin Films, Elsevier Science & Technology Books, 2001

[46] C. J. Brinker, G. W. Scherer, Sol-Gel Science: the Physics and Chemistry of Sol-Gel Processing, Academic processing, 1990

[47] Y. Xu, Ferroelectric Thin Films Fabricated by Sol – Gel Technique, Proceedings of Sixth International IEEE Conference on Solid-State and Integrated-Circuit Technology, **1**(2001) 696

[48] J. G. Cheng, X. J. Meng, B. Li, J. Tang, S. L. Guo, J. H. Chu, Ferroelectricity in Sol-Gel Derived $Ba_{0.8}Sr_{0.2}TiO_3$ Thin Films Using a Highly Diluted Precursor Solution, Applied Physics Letters, **75**(1999) 2132

[49] M. B. Gonzalez, A. Wu, P. M. Vilarinho, Influence of Solvents on the Microstructure and Dielectric Properties of $Ba_{0.5}Sr_{0.5}TiO_3$ Thin Films Prepared by a Diol-Based Sol-Gel Process, Chemistry of Mateials, **18**(2006) 1737

[50] N. V. Giridharan, R. Varatharajan, R. Jayavel, P. Ramasamy, Fabrication and Characterization of $(Ba,Sr)TiO_3$ Thin Films by Sol-Gel Technique Through Organic Precursor Route, Materials Chemistry and Physics, **65**(2000) 261

[51] S. Hoffmann, R. Waser, Control of the Morphology of CSD-Prepared $(Ba,Sr)TiO_3$ Thin Films, Journal of the European Ceramic Society, **19**(1999) 1339

[52] M. L. Calzada, R. Sirera, F. Carmona, B. Jiménez, Investigations of a Diol-Based Process for the Preparation of Lead Titanate Materials, Journal of the American Ceramic Society, **78**(1995) 1802

[53] D. Tahan, A. Safari, L. C. Klein, Sol-Gel Preparation of Barium Strontium Titanate Thin Films, Proceedings of the Ninth IEEE International Symposium on Applications of Ferroelectrics, 1995, 427

[54] J. K. Kim, S. S. Kim, W. J. Kim, J. K. Chung, I.-S. Kim, J.-S. Song, Structural and Electrical Properties of $(Ba_xSr_{1-x})TiO_3$ Thin Films Prepared by a Sol-Gel Method, Integrated Ferroelectrics, **80**(2006) 423

[55] D. W. Schubert, T. Dunkel, Spin Coating from a Molecular Point of View: Its Concentration Regimes, Influence of Molar Mass and Distribution, Materials Research Innovations, **7**(2003) 314

[56] R. W. Schwartz, P. G. Clem, J. A. Voigt, E. R. Byhoff, M. V. Stry, T. J. Headley, N. A. Missert, Control of Microstructure and Orientation in Solution-Deposited $BaTiO_3$ and $SrTiO_3$ Thin Films, Journal of the American Ceramic Society, **82**(1999) 2359

[57] S. B. Majumder, M. Jain, A. Martinez, R. S. Katiyar, Sol–gel Derived Grain Oriented Barium Strontium Titanate Thin Films for Phase Shifter Applications, Jouranl of Applied Physics, **90**(2001) 896

[58] T. M. Shaw, Z. Suo, M. Huang, E. Liniger, R. B. Laibowitz, J. D. Baniecki, The Effect of Stress on the Dielectric Properties of Barium Strontium Titanate Thin Films, Applied Physics Letters, **75**(1999) 2129

[59] J. C. Shin, J. Ark, C. S. Hwang, H. J. Kim, Dielectric and Electrical Properties of Sputter Grown (Ba,Sr)TiO_3 Thin Films, Journal of Applied Physics, **86**(1999) 506

[60] S. E. Moon, E.-K. Kim, M-H. Kwark, H-C. Ryu, Y-T. Kim, K-Y. Kang, S-J. Lee, W-J. Kim, Orientation Dependent Microwave Dielectric Properties of Ferroelectric $Ba_{1-x}Sr_xTiO_3$ thin films, Applied Physics Letters, **83**(2003) 2166

[61] C. S. Hwang, S. H. Joo, Variations of the Leakage Current Density and the Dielectric Constant of Pt/(Ba,Sr)TiO_3/Pt Capacitors by Annealing under a N_2 Atmosphere, Journal of Applied Physics, **85**(1999) 2431

[62] B. H. Park, E. J. Peterson, Q. X. Jia, Effects of Very Thin Strain Layers on Dielectric Properties of Epitaxial $Ba_{0.6}Sr_{0.4}TiO_3$ Films, Applied Physics Letters, **78**(2001), 533

[63] T. Yamada, P. Muralt, V. O. Sherman, C. S. Sandu. N. Setter, Epitaxial Growth of $Ba_{0.3}Sr_{0.7}TiO_3$ Thin Films on Al_2O_3 (0001) Using Ultrathin TiN Layer as a Sacrificial Template, Applied Physics Letters, **90**(2007) 142911

[64] S. B. Majumder, M. Jain, A. Martinez, R. S. Katiyar, Sol–Gel Derived Grain Oriented Barium Strontium Titanate Thin Films for Phase Shifter Applications, Journal of Applied Physics, **90**(2001) 896

[65] I. D. Kim, H. L. Tuller, H. S. Kim, J. S. Park, High Tunability (Ba,Sr)TiO_3 Thin Films Grown on Atomic Layer Deposited TiO_2 and Ta_2O_5 Buffer Layers, Applied Physics Letters, **85**(2004) 4705

[66] A. Wu, P. M. Vilarinho, I. M. M. Salvado, J. L. Baptista, Z. Zhou, I. M. Reaney, A. R. Ramos, M. F. Silva, Effect of Lead Zirconate Titanate Seeds on Pt_xPb Formation During the Pyrolysis of Lead Zirconate Titanate Thin Films, Journal of the American Ceramic Society, **85**(2002) 641

[67] P. D. Hren, H. N. Al-Shareef, S. H. Rou, A. I. Kingon, P. Buaud, E. A. Irene, Hillock Formation in Pt Films, Proceedings of Materials Research Society, 1992

[68] S.-Y. Chen, H.-W. Wang, L.-C. Huang, Role of an Intermediate Phase $(Ba,Sr)_2Ti_2O_5CO_3$ in Doped $(Ba_{0.7}Sr_{0.3})TiO_3$ Thin Films, Materials Chemistry and Physics, **7**(2002) 632

[69] H. Huang, W. Qiu, O. K. Tan, W. Zhu, L. M. Zhou, Effect of Excess TiO_2 on the Phase Evolution and Densification of Sol-Gel Derived (Ba,Sr)TiO_3 powders, Journal of Electroceramics, **16**(2006) 337

[70] J. X. Liao, C. R. Yang, Z. Tian, H. G. Yang, L. Jin, The Influence of Post-Annealing on the Chemical Structures and Dielectric Properties of the Surface Layer of $Ba_{0.6}Sr_{0.4}TiO_3$ films, Journal of Physics D: Applied Physics, **39**(2006) 2473

[71] S. C. Roy, G. L. Sharma, M. C. Bhatnagar, R. Manchanda, V. R. Balakrishnan, S. B. Samanta, Dependence of Dc and Ac Conduction on the Pre-Sintering Temperature in Sol-Gel Derived $Ba_{0.5}Sr_{0.5}TiO_3$ Thin Films, Materials Chemistry and Physics, **100**(2006) 404

[72] S. Jiang, H. Zhang, R. Lin, S. Liu, Electrical Properties of BST Thin Films Fabricated by a Modified Sol-Gel Processing, Integrated Ferroelectrics, **70**(2005) 1

[73] H. Yu, M. Lin, C. Hui, A. Xu, W. Shao, Effect of Bottom Electrodes on The Dielectric Properties of Barium Strontium Titanate Thin Films, Thin Solid Films, **493**(2005) 20

[74] H.-Y. Tian, W.-G. Luo, X.-H. Pu, P.-S. Qiu, X.-Y. He, A.-L. Ding, Synthesis and Characteristics of Strontium-Barium Titanate Graded Thin Films at Low Temperature Using a Sol-Gel Technique, Solid State Communications, **117**(2001) 315

[75] J. Park, C. S. Hwang, D. Y. Yang, Optimization of the Annealing Process for the (Ba,Sr)TiO_3 Thin Films Grown by Low-Temperature (420° C) Metalorganic Chemical Vapor Deposition, Journal of Materials Research, **16**(2001), 1363

[76] M. Valant, D. Suvorov, Low Temperature Sintering of ($Ba_{0.6}Sr_{0.4}$)TiO_3, Journal of the American Ceramic Society, **87**(2004) 1222

[77] T. Hu, H. Jantunen, A. Unsimaki, S. Leppavuori, $Ba_{0.7}Sr_{0.3}TiO_3$ Powders with B_2O_3 Additive Prepared by the Sol-Gel Method for use as Microwave Material, Materials Science in Semiconductor Processing, **5**(2002) 215

[78] S. Halder, T. Schneller, R. Waser, Crystallization Temperature Limit of (Ba,Sr)TiO_3 Thin Films Prepared by a Non Oxocarbonate Phase Forming CSD Route, Journal of Sol-Gel Science and Technology, **33**(2005) 299

[79] J. Xu, J. Zhai, X. Yao, Growth and Characterization of $Ba_xSr_{1-x}TiO_3$ Thin films Derived by a Low-Temperature Process, **6**(2006) 2197

[80] C. K. Kwok, S. B. Desu, Low Temperature Perovskite Formation of Lead Zirconate Titanate Thin Films by a Seeding Process, Materials Research Society, **8**(1993) 339

[81] A. Wu, P. M. Vilarinho, I. M. Miranda. Salvado, J. L. Baptista, Seeding Studies in PZT Thin Films, Materials Research Bulletin, **33**(1998) 59

[82] A. Wu, P. M. Vilarinho, I. M. Miranda. Salvado, J. L. Baptista, Processing and Seeding Effects on Crystallization of PZT Thin Films from Sol-Gel Method, Journal of the European Ceramic Society, **17**(1997) 1443

[83] C. K. Kwok, S. B. Deau, Formation Kinetics of $PbZr_xTi_{1-x}O_3$ thin films, Journal Materials Research, **9**(1994) 1728

[84] K. Higuchi, K. Miyazawa, T. Sakuma, K. Suzuki, Microstructure Characterization of Sol-Gel Derived PZT Films, Journal of Materials Science, **29**(1994) 436

[85] Y. Kobayashi, Y. IIzuka, T. Tanase, M. Konno, Low-Temperature Synthesis of Single-Phase Barium Strontium Titanate Thin Film With a nm-Seeding Technique and Its Dielectric Properties, Journal of Sol-Gel Science and Technology, **33**(2005) 315

Chapter 2 Experimental procedures

The following section describes the experimental procedure conducted to fabricate $(Ba_{0.8}Sr_{0.2})TiO_3$ (BST80/20) thin films on $Pt/TiO_2/SiO_2/Si$ substrates, through the use of diphasic precursor sol gel method and to characterize the obtained films.

BST80/20 nanometric particles were firstly prepared by sol-gel and then dispersed in BST80/20 sols previously prepared.

BST80/20 thin films with 0 mol%, 1 mol%, 5 mol%, and 10 mol% were prepared by spin coating the respective diphasic precursor sols onto the platinized Si substrates.

For the characterization of unseeded and seeded BST films different characterization tools were utilized. The structure, phase content and microstructure of the films was analyzed by X-ray Diffraction (XRD), Atomic Force Microscopy (AFM), Scanning Electron Microscopy (SEM) and Transmission Electron Microscopy (TEM). Commercial Impedance Analyzers were used to measure dielectric permittivity and dielectric losses as a function of frequency and capacitance versus electric field behaviour. The ferroelectric hysteresis P-E loops were traced by a commercial ferroelectric tester. Piezoresponse force microscopy (PFM) was used for the imaging of the local ferroelectric domain structure.

2.1 Preparation and characterization of nanosized BST powders to be used as seeds

Various methods have been utilized to synthesis stoichiometric and fine BST powders, including solid-state reaction [1], sol-gel [2], spray pyrolysis [3-4], precipitation [5, 6] and polymeric precursor methods (also called Pechini process) [7], among others.

Solid-state reaction between $BaCO_3$, $SrCO_3$ and TiO_2 at high temperature (~1100ºC) constitutes the conventional method to synthesis BST. In spite of its low cost, this method produces normally coarse and agglomerated powders with a large and inhomogeneous particle size distribution. In order to reduce the particle size, a milling step is usually required, limiting the purity control of the powders obtained through solid-state reaction.

Precipitation of a solute from a homogeneous supersaturated solution (where the concentration exceeds the saturation limit) is a well-known process in industrial chemistry for obtaining crystalline particles [8]. The synthesis of BST powders by precipitation is based on a supersaturated solution in which an exchange reaction between the stoichiometric solutions containing Ti ions and a precursor containing stoichiometric quantities of Ba and Sr ions is induced by the control of pH and temperature. To reestablish the equilibrium conditions a solid is formed out of the solute phase and precipitates. Precipitation is a fairly simple and low cost powder processing technique in which the precipitated BST powders possess a high degree of chemical purity. In addition, the particle morphology and size distribution can be controlled, at least to some extent, by controlling the processing parameters, namely, pH, temperature, order of reagents addition, stirring and washing conditions, etc. Disadvantages of the method includes: (1) limitations related to cation solubility product to guarantee a homogeneous and stoichiometric precipitation (specially in complex oxides such as BST) [7], (ii) the need of post precipitation washing for separation of the supernatant, drying and heat treatment to crystallize the powders in the required crystallographic phase. The drying and calcination often lead to the formation of agglomerates and aggregates [9].

Polymeric precursor method is based on the fact that certain inorganic polymers, obtained commonly through the hydrolysis of cations in salts, controlled hydrolysis of metal-organics and the overall sol-gel reaction, can serve as precursor materials for oxide powders [8]. Highly reactive BST powders can be obtained after eliminating the organic part at 300ºC. This process permits good control of the product stoichiometry. The disadvantage of this method is the possible formation of stable carbonate phases during the decomposition of the organic material [7].

Sol-gel provides an alternative methodology for powder preparation. As described before (section 1.2.3), sol-gel method generally involves the use of metal alkoxides, which undergo hydrolysis and condensation polymerization reactions to produce the gels [10]. The bulk gels are used as solid precursors for the powder preparation [8]. Sol-gel method allows to obtain powders with very high chemical purity, chemical homogeneity at a molecular, controlled size and shape, enhanced reactivity and low processing temperature [10] which constitutes the added value of this methodology over the others. Thus, sol gel processing was utilized in this work for the preparation of BST nanometric powders.

The starting materials used for the synthesis of $(Ba_{0.8}Sr_{0.2})TiO_3$ powders were barium hydroxide-8·H_2O (>96%, M&B), strontium hydroxide-8·H_2O (>98%, Riedel-de Haën), tetraisopropyl orthotitanate (>98%, Merck) and deionized water. The $(Ba_xSr_{1-x})TiO_3$ powders were synthesized by the procedure described in the flow chart of figure 2.1. Aqueous solutions of strontium and barium hydroxides were prepared in hot deionized water and then, tetraisopropyl orthotitanate was added in a N_2 atmosphere. Suspensions were stirred at 400 rpm for 2 hours at 95ºC. Powders were washed with deionized water until the pH value of the washing solution reaches 7. Finally, the products were overnight dried in an oven at 100ºC.

The chemical reactions that occurred can be written as follows:

$$0.2Sr(OH)_2 + 0.8Ba(OH)_2 + Ti(OC_3H_7)_4 + H_2O \rightarrow Ba_{0.8}Sr_{0.2}TiO_3 + 4C_3H_7OH \quad (2.1)$$

In order to avoid particle agglomerates the obtained powders were dispersed in ethanol (MERCK, 99.95%) and centrifuged with a speed of 3000 rpm for 8 minutes in an ultracentrifuge (Beckman, L8-30M). The supernatant suspension was then selected and concentrated in an oven at 50ºC during 12h. The obtained powders were used as nano particles (BST seeds) in this work.

The phase analysis of the powders was carried out using X-ray diffraction (XRD) with a Rigaku (D/Max-C series) X-ray diffactometer, having Cu-Kα radiation (λ=0.15064 nm). Morphology studies were conducted by Scanning Electron Microscopy

(SEM, Hitachi, S-4100). The particle size distribution was determined using a Particle Size Analyzer (Coulter LS 230).

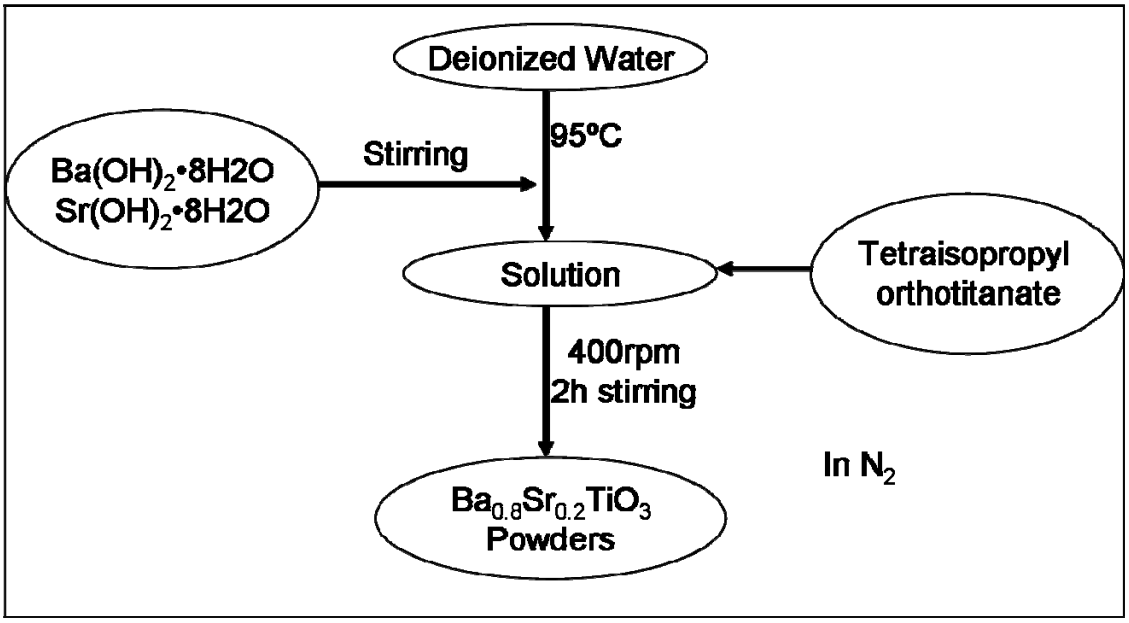

Figure 2.1. Flowchart of the preparation of $(Ba_{0.8}Sr_{0.2})TiO_3$ powders by sol-gel method.

2.2 Preparation and characterization of BST thin films by a modified sol-gel method

2.2.1 Solution preparation

Solution without seeds:

The raw materials used for the preparation of the solutions were barium acetate ($Ba(CH_3COO)_2$, Merck, 99%), strontium acetate ($Sr(CH_3COO)_2 \cdot ½H_2O$, ABCR, 98%) and tetrabutyl titanate ($Ti(OC_4H_9)_4$, Merck, >98%). Acetylacetone ($C_5H_8O_2$, Merck, >99.5%) was used as stabilizer for Ti alkoxide. Glacial acetic acid (CH_3COOH, Merck, >99.8%) and ethylene glycol ($HOCH_2CH_2OH$, Merck,>99.5%) were used as solvents. Barium acetate and strontium acetate powders were dissolved in acetic acid with a molar ratio of 8:2. Since barium acetate and strontium acetate were only partially dissolved in glacial acetic acid at room temperature, the mixture was heated in a hot plate at 80ºC for 2 hours and stirred at a constant speed. Meanwhile $Ti(OC_4H_9)_4$ was stabilized with a mixture of ethylene glycol and acetylacetone and then was added into $Ba(CH_3COO)_2/Sr(CH_3COO)_2$ solution with a molar ratio of 1:1 under constant stirring. The concentration of Ba and Sr was adjusted to 0.2 mol/l by adding glacial acetic acid to the mixture and stirred for 4 hours. The resulting solution was yellow and transparent.

Solution with seeds:

The preparation procedure of BST nano-sized powders was described in section 2.1. The BST nano particles were dispersed in ethanol and used as seeds. The seeded diphasic BST sols were prepared by mixing 1, 5 and 10 mol% (atomic mol %) BST seeds to the BST precursor sol, therefore the concentrations of seeds in the seeded precursor sols were 1 mol%, 5 mol% or 10 mol% (atomic mol %) of BST in the sol. An ultrasonic bath (Branson, Model 1510E-DTH, USA) was used to disperse the nano-particles.

2.2.2 BST thin film deposition

Platinized silicon substrates, $Pt/TiO_2/SiO_2/Si$, are one of the most currently used in the fabrication of microelectronic devices. The platinum layer is used as the bottom electrode in the integration of ferroelectric films in complementary metal-oxide-semiconductor (CMOS) technology because of its good stability in high temperature and oxidizing environments, its high electric conductivity, and its low leakage current. Therefore, commercially available platinized silicon $Pt/TiO_2/SiO_2/Si$ (INOSTEK) were employed as substrates in the present work.

Using the previously prepared BST solution and suspensions thin layers of BST were deposited on $Pt/TiO_2/SiO_2/Si$ substrates by spin-coating, using a Chemat Technology, KW-4A spin coater. Prior to the deposition, the substrates were cleaned with ethanol and dried. Seeded precursor solutions were ultrasonicated for 20 minutes in order to disperse the seeds particles homogeneously within the sol. The spinning speed was fixed to 3000 rpm. Subsequently the as-deposit films were heated on a hot plate in air at 250ºC for 5 min to evaporate the solvents and pyrolyzed at 350ºC for 15 min to burn the residual organics. This step was repeated after each spinning to ensure complete removal of volatile species between each layer. The desired thickness of the films was achieved after consecutive coatings. The films were then annealed at 600ºC, 650ºC, 700ºC and 750ºC for different periods of time (from 10 to 240 minutes) in air, in a preheated furnace in order to maintain a relatively high rate of temperature rise. This approach was termed as a quasi-rapid-thermal annealing process by Cole et al [11]. Some films were annealed at 500ºC, 550ºC and 600ºC for 30 hours in oxygen to investigate the influence of the annealing atmosphere on the film quality and seeds effect.

2.2.3 BST thin film characterization

The phase evolution analysis of BST thin films was carried out by X-ray diffraction with a Rigaku (D/Max-C series) X-ray diffactometer, using Cu-Kα radiation (λ=0.15064 nm).

Film thickness, surface morphology and microstructure were analyzed by scanning electronic microscopy (SEM) (Hitachi, S-4100) coupled with energy dispersive spectroscopy (EDS). Films specimens were mounted on aluminium stubs using epoxy glue. Carbon paint was applied to the specimen to provide a conductive path to the stub, and an evaporated carbon surface coating was deposited to prevent sample charging inside the microscope. These samples were investigated by SEM using an operation voltage of 25 kV.

The bulk film and interfaces between film and substrate were evaluated by TEM using a Hitachi Model H9000-NA TEM equipped with an energy dispersive X-ray (EDS) detector. For the preparation of TEM cross section samples, two pieces of a sample (less than 3 mm in length) were glued with film surfaces inward using M-band 610 glue. The curing treatment was carried in an oven at 100ºC for 2 hours. The resulting sample was ground using a fine grade silicon carbide paper until a thickness of around 15 μm was achieved. A copper grid was glued onto the sample. The sample was then ion-beam thinned in both sides with an incidence angle of 22º at the beginning of the milling and of 12º at the final of the milling step.

Surface morphology of BST thin films was also studied by Atomic Force Microscopy (AFM) using a commercial AFM equipment (Multimode, Nanoscope IIIA, Digital Instruments) in taping mode.

Using the obtained SEM and AFM topography images the average grain size ($\overline{G}$) was calculated by the lineal intercept technique with the equation [12]

$$\overline{G} = 1.5\frac{\sum L}{N} \tag{2.2}$$

where $\overline{G}$ stands for average grain size, L stands for linear grain intercept distance, N stands for the number of grains intercepted per unit test length. The grain intercept distance L is the value of chord length generated by intersections of grains and straight test lines of all possible different orientations and locations in the specimen.

For the evaluation of the electrical properties, metal-insulator-metal (MIM) capacitors with Pt/BST/Au structures were fabricated. The Au top circular electrodes with a diameter of 600 μm were sputtered on the film surface using a shadow mask. Then BST films with top electrode were post-annealed at 300ºC for 30 min in order to improve the interface between the metal and the films. The dielectric constant and loss tangent were evaluated with an impedance bridge (HP 4284A) over a frequency range of 100 Hz to 1 MHz at room temperature. The oscillation level of the applied voltage was set to 200 mV. The polarization behaviour of BST thin films was measured by recording the ferroelectric hysteresis loops using an AixACT TF analyzer. The current-voltage characteristics of MIM devices were measured using a KEITHLEY 617 programmable electrometer. The direct current (DC) electric field dependence of the capacitance at room temperature (25ºC) was measured to evaluate the tunability of BST thin films. The measurements were conducted by applying a small alternating current (AC) signal of 0.2 V amplitude and 100 kHz frequency (HP4284 impedance analyzer) while the DC bias was swept from negative voltage to positive voltage.

Local ferroelectric domains of unseeded and seeded films were analysed via the so-called piezoresponse force microscopy (PFM), which is based on the detection of local piezoelectric deformation of a ferroelectric sample induced by an external electric field [13]. In piezoelectric samples this external electric field causes thickness changes and therefore vibrations of the surface which lead to oscillations of the cantilever that can be read out with a lock-in amplifier as shown in figure 2.2 [14]. The different orientations of

the polar axis of adjacent domains lead to a domain contrast in PFM measurements, i. e., the domains are displayed as bright and dark areas in PFM images. In this work, a modified commercial atomic force microscope (Multimode, Nanoscope IIIA, Digital Instruments) was employed in these experiments. A conductive Pt coated Si tip-cantilever (NT-MDT) system was used for the application of external voltages and for vibration detection. BST films were excited by an external ac voltage (5 V, 50 kHz) applied between the PFM tip and the bottom electrode, and the deflection signal from the cantilever was detected by a lock-in amplifier. A topographic image of the film surface was taken simultaneously with the domain image. In the piezoelectric image, domains with opposite polarities exhibit different contrast.

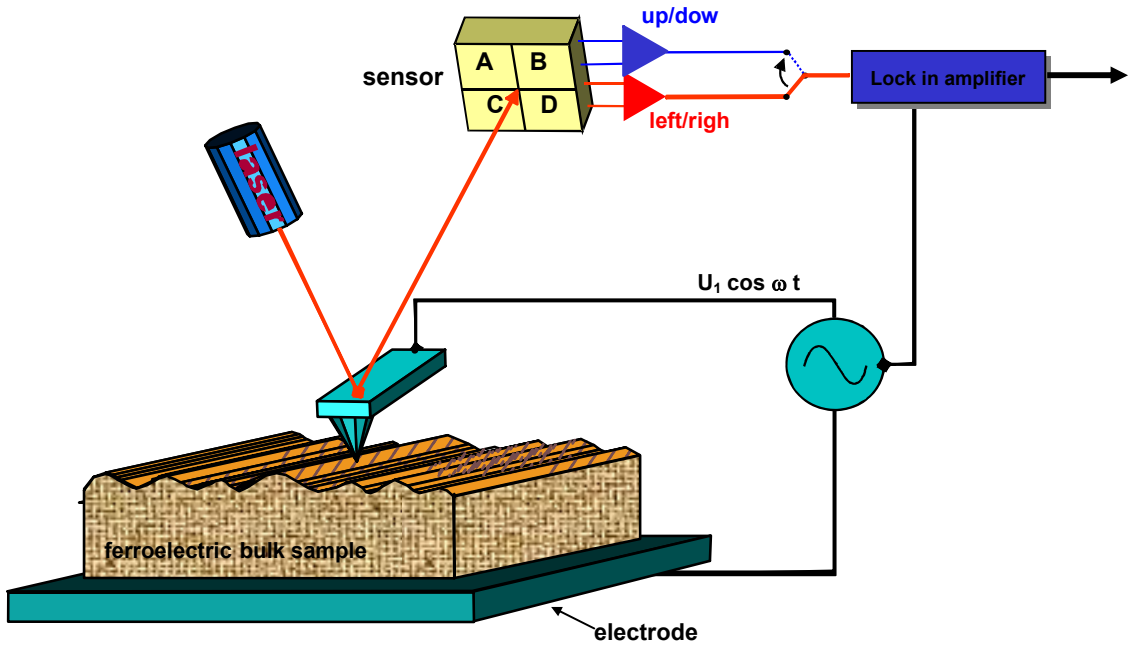

Figure 2.2. A typical PFM setup [14].

2.3 References

[1] S. Kongtaweelert, D. C. Sinclair, S. Panichphant, Phase and Morphology Investigation of $Ba_xSr_{1-x}TiO_3$ (x=0.6, 0.7 and 0.8) Powders, Current Applied Physics, **6**(2006) 474

[2] T. Hu, H. Jantunen, A. Uusimäki, S. Leppävuori, BST Powder with Sol-Gel Process in Tape Casting and Firing, Journal of the European Ceramic Society, **24**(2004) 1111

[3] G. Branković , Z. Branković , M. S. Góes, C. O. Paiva-Santos, M. Cilense, J. A. Varela, E. Longo, Barium Strontium Titanate Powders Prepared by Spray Pyrolysis, Materials Science and Engineering B, **122**(2005) 140

[4] Y. Itoh, K. Okuyama, Preparation of Agglomerate-Free and Highly Crystalline $(Ba_{0.5},Sr_{0.5})TiO_3$ Nanoparticles by Sol-Assisted Spray Pyrolysis, Journal of the Ceramic Society of Japan, **111**(2003) 815

[5] Y. B. Khollam, H. S. Potdar, S. B. Deshpande, A. B. Gaikwad, Synthesis of Star Shaped $(Ba_{1-x}Sr_x)TiO_3$ (BST) Powders, Materials Chemistry and Physics, **97**(2006) 295

[6] I. P. Selvam, V. Kumar, Synthesis of Nanopowders of $(Ba_{1-x}Sr_x)TiO_3$, Materials Letters, **56**(2002) 1089

[7] A. Reis, A. Z. Simões, M. Cilense, M. A. Zaghete, J. A. Varela, Barium Strontium Titanate Powder Obtained by Polymeric Precursor Method, Materials Characterization, **50**(2003) 217

[8] D. Ganguli, M. Chatterjee, Ceramics Powder Preparation: a Handbook, Kluwar Academic Publishers, London, 1997

[9] A. R. Terry, Fundamentals of Ceramic Powder Processing and Synthesis, Academic Press, 1996

[10] C. J. Brinker, G. W. Scherer, Sol-Gel Science: the Physics and Chemistry of Sol-Gel Processing, Academic processing, 1990

[11] M. W. Cole, W. D. Nothwang, C. Hubbard, E. Ngo, M. Ervin, Low Dielectric Loss and Enhanced Tunability of $(Ba_{0.6}Sr_{0.4})TiO_3$ Based Thin Films via Material Compositional Design and Optimized Film Processing Methods, Journal of Applied Physics, **93**(2003) 9218

[12] E. E. Underwood, Quantitative Stereology, Addison-Wesley, 1970, 23-39

[13] A. Gruverman, S. B. Kalinin, Piezoresponse Force Microscopy and Recent Advances in Nanoscale Studies of Ferroelectrics, Journal of Materials Science, **41**(2006) 107

[14] www.tu-harberg.de

Chapter 3 Results and discussions

In this chapter, the characterization of the perovskite nanometric BST particles prepared by sol gel is presented and the ideal morphological characteristics for the role of seeds are identified. The fabrication of BST films through the diphasic sol gel precursors method is outlined and the improvements on the characteristics of seeded BST films when compared with unseeded films are highlighted by a comprehensive structural, microstructural and electric characterization of the films. X-ray Diffraction analysis, Scanning Electron Microscopy (SEM), Transmission Electron Microscopy (TEM) and Atomic Force Microscopy (AFM) of the deposited films were performed and the results are presented in this chapter. From a systematic study of the phase formation process the activation energy for the crystallization of the perovskite phase was calculated for unseeded and seeded films. The dielectric and ferroelectric response of unseeded and seeded BST films were recorded and the results are also reported and discussed in this chapter. Microstructure, grain size, surface roughness and phase content of BST thin films play a key role on the electrical properties of high dielectric thin film capacitors. Bearing this in mind the relations between the structure / microstructure and properties for the BST films prepared using the diphasic precursor sol gel are established and the role of nanometric particles in the fabrication of BST thin films by sol gel is identified.

3.1 Characterization of nanosized BST particles prepared by sol-gel method

The XRD pattern of sol-gel derived BST particles is shown in Figure 3.1. A single perovskite $(Ba_{0.8}Sr_{0.2})TiO_3$ was obtained. The SEM picture of the obtained $(Ba_{0.8}Sr_{0.2})TiO_3$ powders is shown in figure 3.2. The particles are very fine with particle size distributed between 50 nm and 70 nm. From the morphological point of view the powders are a mixture of spherical and cubic shaped grains.

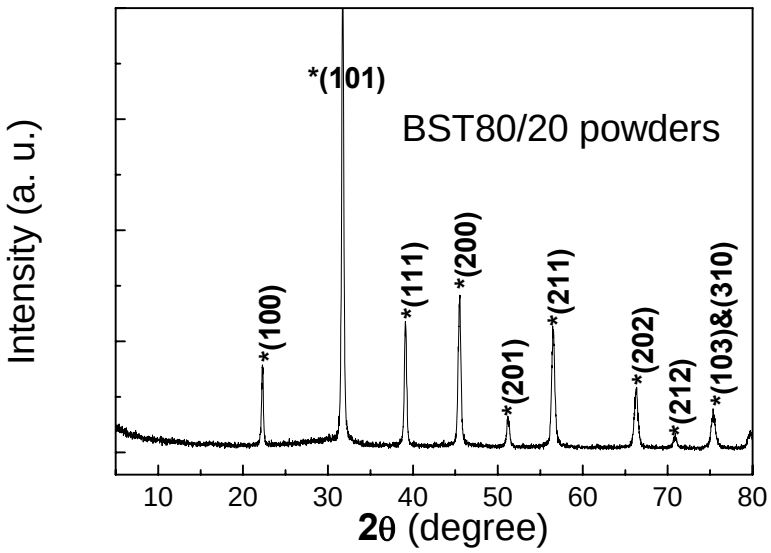

Figure 3.1. XRD patterns of $(Ba_{0.8}Sr_{0.2})TiO_3$ powders obtained by sol-gel method.

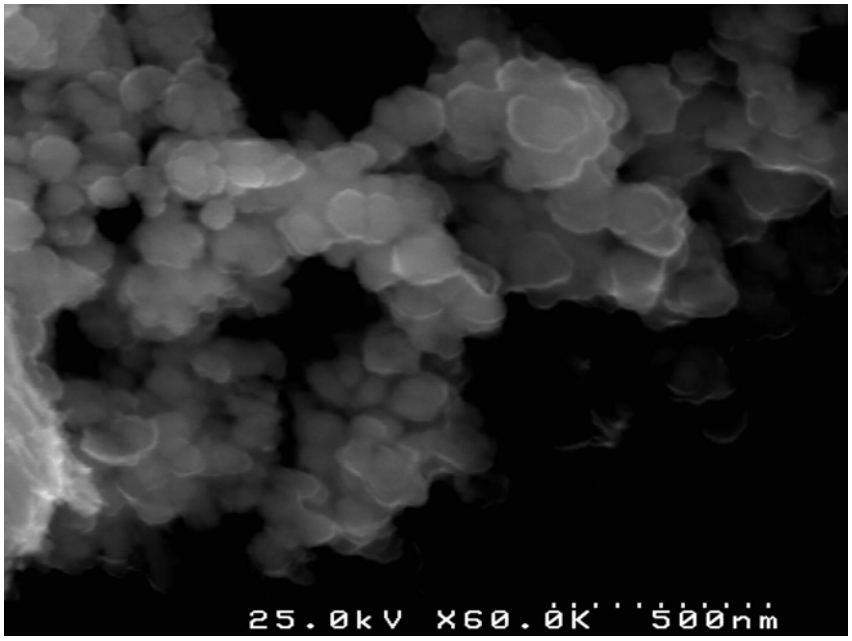

Figure 3.2. SEM photograph of $Ba_{0.8}Sr_{0.2}TiO_3$ powders obtained by sol-gel.

Figure 3.3 (a) shows the particle size distribution of the BST powders. Three peaks, located at ~ 53 nm, 214 nm and 496 nm, are observed in this distribution. The peak located at circa 53 nm corresponds to the individual particle size, as corroborated by the SEM analysis. The cumulative size distribution clearly indicates that 72% of the powders particle size is lower than 70 nm. The peaks at 214 nm and 496 nm indicate some degree of agglomeration of the obtained powders before the centrifuge treatment.

The particle size distribution of the selected supernatant suspension, after the centrifugation at 3000 rpm for 8 minutes, is illustrated in figure 3.3 (b). A fine and narrow particle size distribution with a mean particle size of 114 nm was obtained, which is larger than the individual particle size of 53 nm owning to the soft agglomeration after the centrifuge treatment. The peaks located at 214 nm and 496 nm caused by the agglomeration disappeared. In order to break the soft agglomeration observed in the powders obtained after the centrifugation step, the supernatant was agitated in an ultrasonic bath for 20 min, before the preparation of seeded precursor sols.

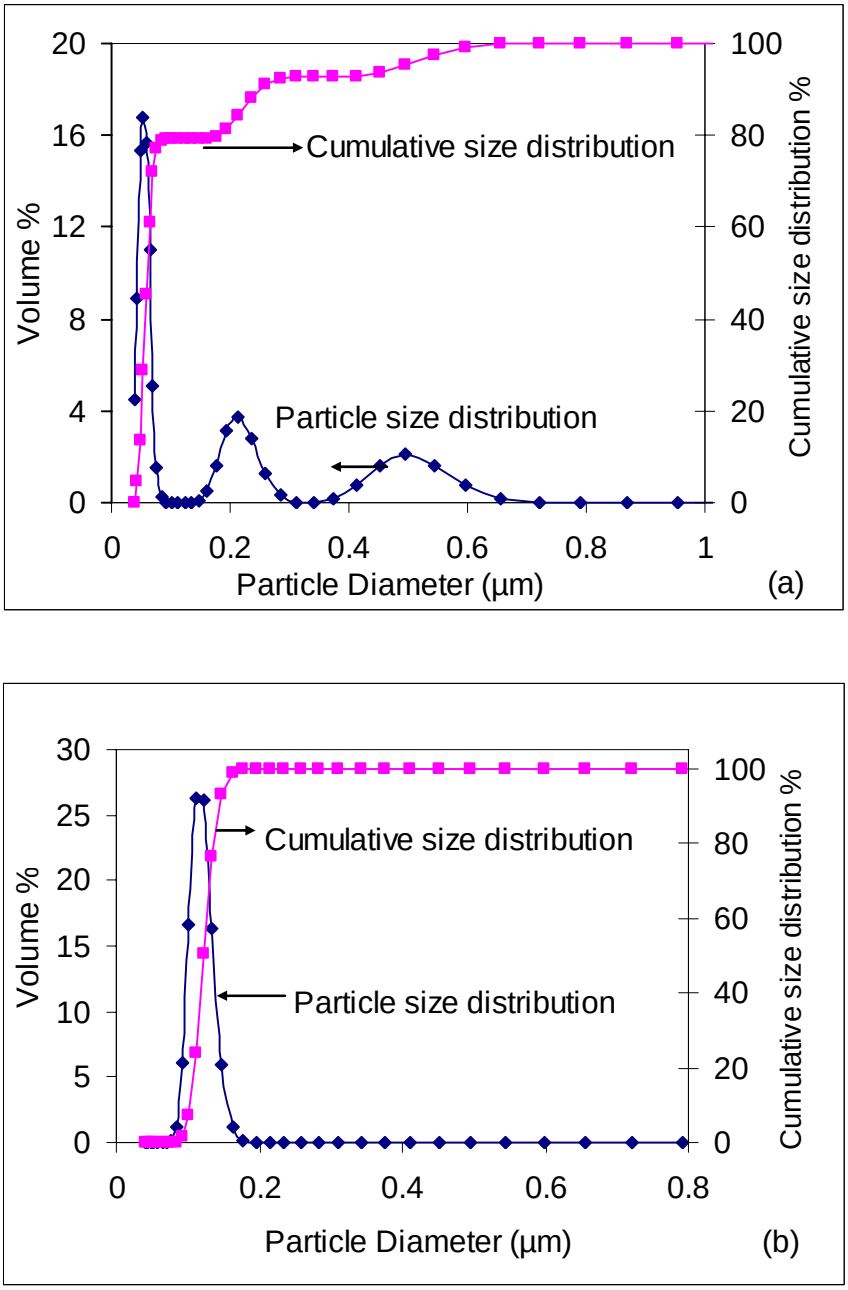

Figure 3.3. Particle size distributions of the sol-gel derived powders (a) as obtained, (b) after centrifuge treatment.

3.2 Phase evolution in BST thin films

XRD patterns in figure 3.4 illustrate the phase evolution of BST films derived from precursors without seeds, with 1 mol% and 5 mol% of seeds.

XRD patterns of unseeded BST films annealed at various temperatures for 1 hour in air are shown in figure 3.4 (a). After annealing at 600ºC, a broad diffraction peak ranging between 26º to 28º (2θ), marked in the figure by an open circle, was found. According to the literature [1, 2], this intermediate phase is an oxycarbonate with the composition $(Ba,Sr)_2Ti_2O_5CO_3$, which was also observed at 600ºC and disappeared at 650ºC. No perovskite phase was detected at 600ºC. The beginning of the formation of the perovskite phase is only detected at 650ºC. As the temperature increases, the perovskite phase grows quickly and the intermediate phase disappears at 700ºC.

After addition of 1 mol% of BST seeds to the precursor sol, the presence of the perovskite is already detected by XRD at 600ºC together with a second phase located at $2\theta \approx 24.1º$ (marked in figure 3.4 (b)). This phase identified as $BaCO_3$ was also observed in other works [3, 4]. The perovskite phase is dominant in the film at temperatures as low as 650ºC.

XRD patterns of 5 mol% seeded BST thin films annealed at various temperatures (600ºC, 650ºC, 700ºC and 750ºC) for one hour in air are depicted in figure 3.4 (c). After addition of 5 mol% BST seeds to the precursor sol, pure perovskite phase was obtained at a temperature as low as 600ºC. The intensity of the perovskite peaks increases with the increasing annealing temperature.

Comparing figures 3.4 (a), (b) and (c), the temperature at which the pure perovskite phase is obtained decreases from 700ºC for the unseeded BST thin films to 600ºC for the 5 mol% seeded BST thin films.

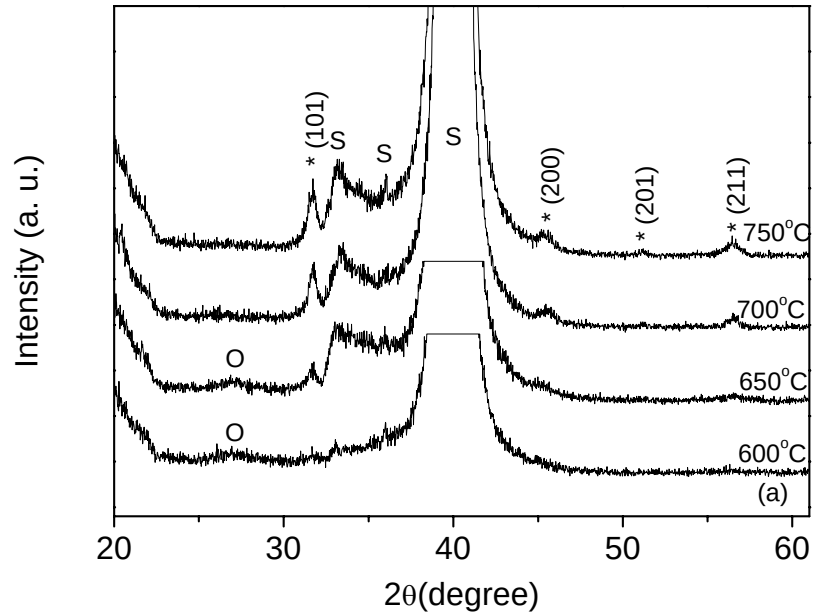
Intensity (a. u.)
* (101)
S
S
S
* (200)
* (201)
* (211)
* 750°C
700°C
O
650°C
O
600°C
(a)
20
30
40
50
60
2θ(degree)

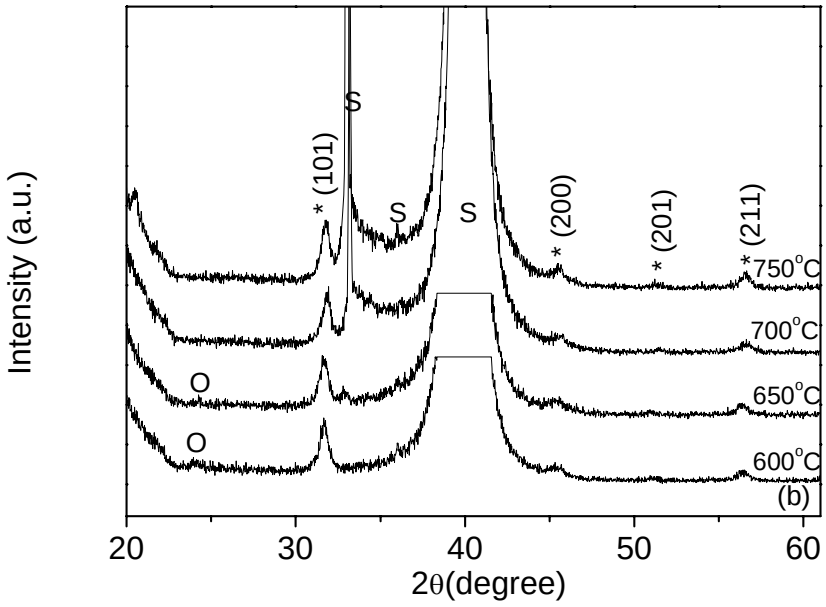
Intensity (a.u.)
S
* (101)
S
S
* (200)
* (201)
* (211)
*750°C
700°C
O
650°C
O
600°C
(b)
20
30
40
50
60
2θ(degree)

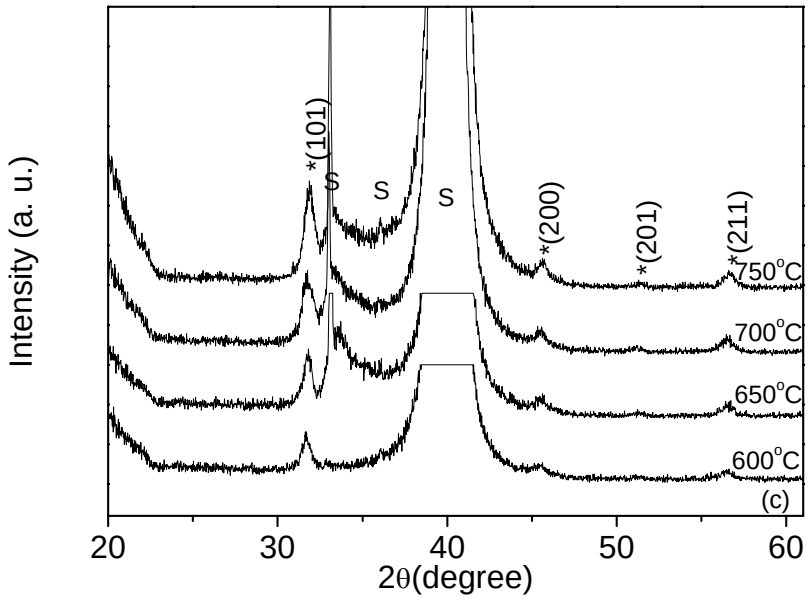

Figure 3.4. XRD patterns of (a) unseeded, (b) 1 mol% seeded and (c) 5 mol% seeded $(Ba_{0.8}Sr_{0.2})TiO_3$ thin films annealed at 600ºC, 650ºC, 700ºC and 750ºC for 1 hour in air (O-intermediate phase, *-perovskite phase, S-substrate).

The effect of the nano sized particles in the perovskite phase formation is noticeably seen in figure 3.5 when compares XRD patterns of unseeded, 1 mol%, 5 mol%, and 10 mol% seeded BST thin films annealed at 650ºC for one hour in air. The intermediate oxycarbonate phase of $(Ba,Sr)_2Ti_2O_5CO_3$ (located at 2θ=26-28º) formed at 650ºC for the unseeded BST thin films. No intermediate phase is observed in the seeded films. Pure perovskite phase is only formed in seeded films annealed under these conditions. The perovskite peaks becomes more intense with the increase of seeds content.

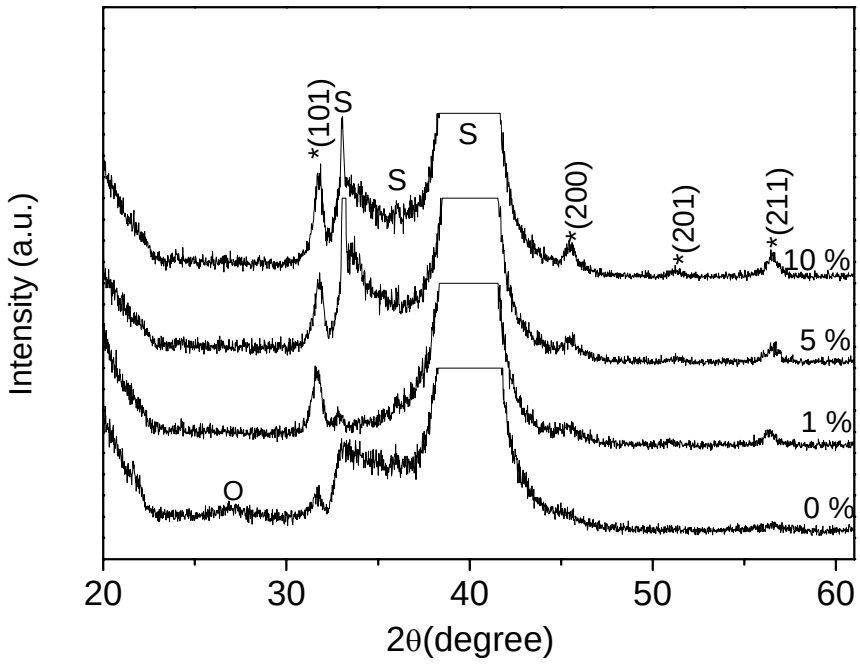

Figure 3.5. XRD patterns of unseeded, 1 mol%, 5 mol%, and 10 mol% seeded $(Ba_{0.8}Sr_{0.2})TiO_3$ thin films heat treated at 650ºC for 1 hour in air (O-Intermediate phase, *-perovskite phase, S-substrate).

It is clearly evidenced by the XRD analysis that the addition of BST seeds into the BST sol lowered the crystallization temperature of the perovskite phase and also the temperature at which monophasic perovskite phase was obtained.

The nature of the local thermodynamic conditions created during pyrolysis of sol gel films may affect the crystallization process and the defect state of the films. The combustion of the organic groups of the sol – gel precursors during pyrolysis may cause a local, temporary depletion of oxygen, causing locally reducing conditions. This is most prevalent away from the film surface near the interface with the electrode [5]. Under these conditions it is highly probable that the films will exhibit some oxygen deficiency. Annealing in oxygen will diminish these defects and will help in the perovskite

crystallization process. In order to investigate the influence of the annealing atmosphere on the crystallinity of the BST thin films, unseeded and seeded BST thin films were annealed at different temperatures in air and oxygen. It is also well known that extending annealing time is always efficient for the formation of the perovskite phase, so the unseeded and seeded BST thin films were annealed for a long period (30 hours).

In order to investigate the influence of the annealing atmosphere on the crystallinity BST thin films without seeds and with 5 mol% seeds were annealed at 600ºC for 30 hours in air and oxygen.

XRD patterns of unseeded BST films as-deposited and annealed at various temperatures (500ºC, 550ºC, 600ºC) for 30 hours in oxygen are shown in figure 3.6 (a). The BST thin films as-deposited and annealed at 500ºC have amorphous structures. The intermediate phase appeared at 550ºC. The pure perovskite BST phase was detected as the temperature increases to 600ºC. A similar phase evolution was observed for 5 mol% seeded BST films annealed under the same conditions, as depicted in figure 3.6 (b). The as-deposited BST thin films have amorphous structures. At 500ºC, no peaks of crystalline phase were found. The crystalline perovskite BST phase, identified by the peaks correspondent to the reflections (100), (101) and (211), has already appeared at 550ºC together with the intermediate phase. At 600ºC, the intermediate phase disappeared and the pure perovskite BST phase was obtained.

The effect of annealing in oxygen is clearly seen in figure 3.7 even for seeded films. Figure 3.7 compares the X-ray Diffraction (XRD) patterns of 5 mol% seeded BST thin films annealed at 600ºC in air and oxygen atmospheres for 30 hours. The patterns show that BST thin films annealed at 600ºC for 30 hours both in air and in oxygen possessed a non-textured polycrystalline perovskite structure with no evidence of intermediate phase formation. Moreover the increased intensity of the perovskite peaks of seeded BST thin films indicates the enhanced crystallinity of BST thin films annealed in oxygen.

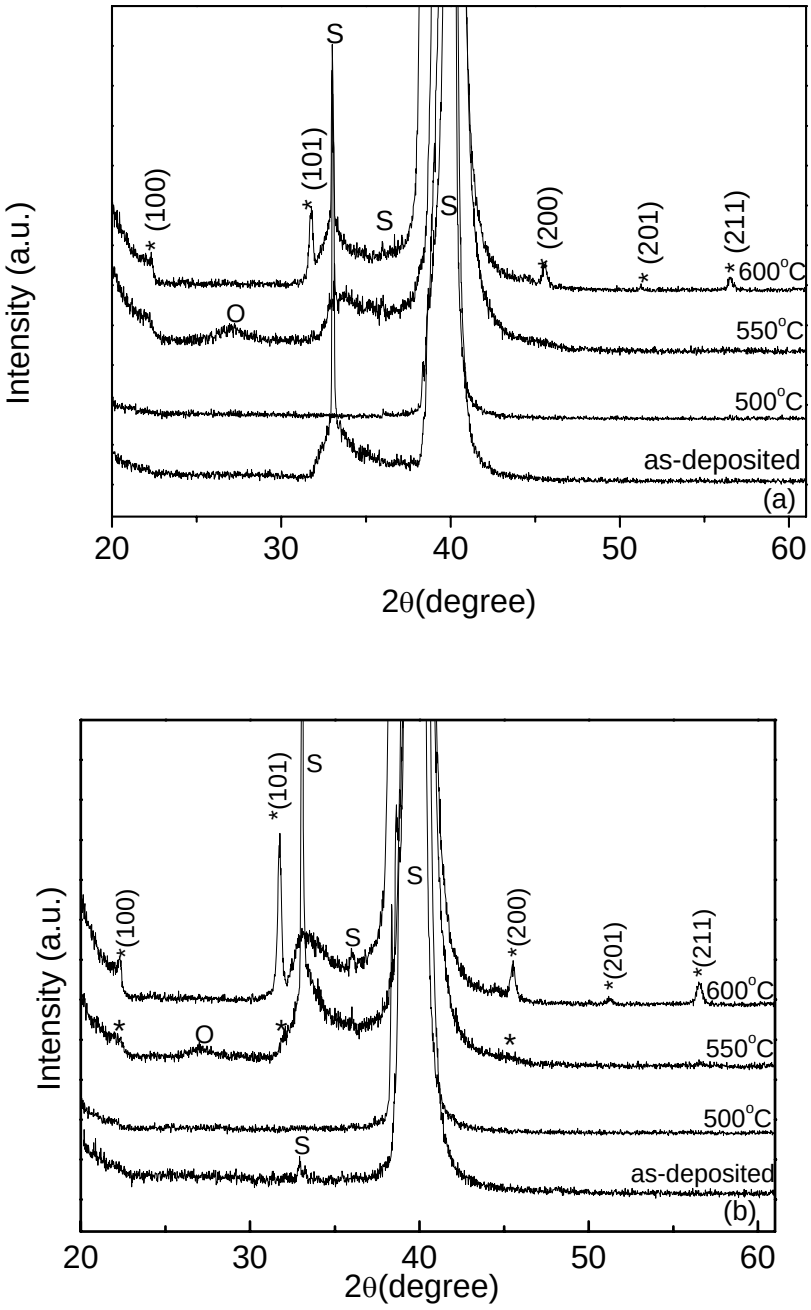

Figure 3.6. XRD patterns of (a) unseeded and (b) 5 mol% seeded $(Ba_{0.8}Sr_{0.2})TiO_3$ thin films annealed 30 hours in oxygen at various temperatures: (600ºC, 550ºC 500ºC, as deposited) (O-intermediate phase, *-perovskite phase, S-substrate).

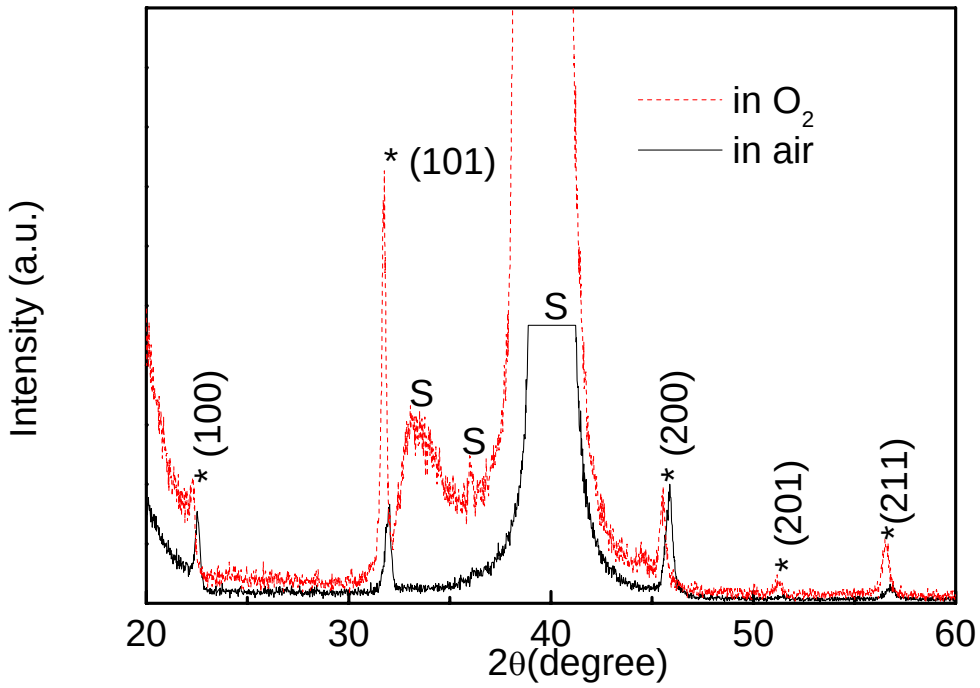

Figure 3.7. XRD pattern of 5 mol% seeded $(Ba_{0.8}Sr_{0.2})TiO_3$ thin films annealed at 600ºC in an air and in an oxygen atmosphere for 30 hours (S-substrate, *-Perovskite phase).

Table 3.1 shows the summary of the results obtained from XRD analysis of the effect of seeds on the perovskite phase formation process of BST films annealed at different temperatures and time. In spite of a similar phase evolution process the crystallization of the pure perovskite phase occurred at lower temperature in seeded films as opposed to unseeded ones. For a fixed annealing temperature, extending the annealing time is always efficient for the formation of the perovskite phase. For a fixed annealing duration, the addition of seeds in the precursor sol decreased the minimum annealing temperature required to eliminate the intermediate phases. The effect of seeds on the crystallization of the perovskite phase is obvious. The temperature at which the perovskite phase showed up was found as low as 550ºC for BST thin films with the presence of 5 mol% BST seeds in the precursor sols annealed in air for 30 hours. The

temperature at which the perovskite single phase was obtained decreased from 700ºC to 600ºC with the incorporation of 5 mol% seeds.

Table 3.1. Phase formation results obtained from XRD patterns of $(Ba_{0.8}Sr_{0.2})TiO_3$ films derived from precursors with different seeds content and heat treated at different temperatures and annealing duration. ("P" stands for single perovskite phase, "I" stands for intermediate phase and "-" stands for not measured).

Annealing time	10 Mins				30 Mins				60 Mins				90 Mins		120 Mins				240 Mins				30 hours	
seeds amount / Temperature	0%	1%	5%	10%	0%	1%	5%	10%	0%	1%	5%	10%	5%	10%	0%	1%	5%	10%	0%	1%	5%	10%	0%	5%
550ºC	-	-	-	-	-	-	-	-	-	-	-	-	-	-	-	-	-	-	-	-	-	-	I	P+I
600ºC	-	-	-	-	-	-	-	-	P+I	P+I	P	P	-	-	P+I	P+I	P	P	P+I	P	P	P	P	P
650ºC	-	-	-	-	P+I	P	P	P	P+I	P	P	P	-	-	P+I	P	P	P	P+I	P	P	P	-	-
700ºC	P	P	P	P	P	P	P	P	P	P	P	P	-	-	-	-	-	-	-	-	-	-	-	-
750ºC	-	-	-	-	-	-	-	-	P	P	-	-	P	P	-	-	-	-	-	-	-	-	-	-

It has been suggested that the kinetics of crystallization of perovskite PZT phase could be considered as controlled by a combination of nucleation and growth process [6]. Therefore, the Avrami phase transformation expression [7, 8] is used in this work to calculate the overall activation energy for the perovskite crystallization in unseeded and seeded BST thin films.

The relationship between volume fraction and time is given by the following well-known phenomenological Johnson-Mehl-Avrami (JMA) equation [9]:

$$x(t) = 1 - \exp(-kt^n) \tag{3.1}$$

where x(t) stands for the volume fraction of the transformed phase at time t, n and k stand for the Avrami coefficient and rate constant, respectively. According to the following transformation of equation (3.1):

$$\ln[-\ln(1-x)] = \ln k + n\ln t \tag{3.2}$$

the representation of ln[-ln(1-x)] as a function of lnt yields the values of n and k.

In these calculations it was assumed that a film's volume fraction of perovskite phase was proportional to the integrated area under the BST peaks determined by the XRD data [7, 8]. To eliminate the effect of the substrate, the five individual diffraction peaks for BST ((100), (101), (002), (200), (201), (211)) were selected. The calculated integrated area was normalized to that obtained from the fully crystallized perovskite film, which was BST thin films derived from 10 mol% seeded precursor sol and annealed at 650ºC for 2 hours, to generate the time t dependent fraction x(t) for a fixed annealing temperature T. When rate k was determined for each temperature, the activation energy Ea for the transformation could be determined from the Arrhenius relationship:

$$k = A \exp(Ea/RT) \tag{3.3}$$

where A stands for a constant, Ea stands for the activation energy for phase transformation, R is the ideal gas constant and T stands for temperature.

Figure 3.8 illustrates Avrami plots of ln[-ln(1-x)] as a function of lnt for unseeded, 1 mol% and 5 mol% seeded films annealed at different temperatures. The Avrami coefficients (n) and the rate constants (k) for BST thin films were obtained from the slope of the straight line at each temperature. Figure 3.9 illustrates Arrhenius plots of the crystallization rate constant versus temperature for unseeded, 1 mol% seeded and 5 mol% seeded $(Ba_{0.8}Sr_{0.2})TiO_3$ films. The activation energy (Ea) for the phase transformation was obtained from the slope of the straight line at each temperature. Table 3.2 summarizes the obtained Avrami coefficients and the rate constants for the studied BST thin films.

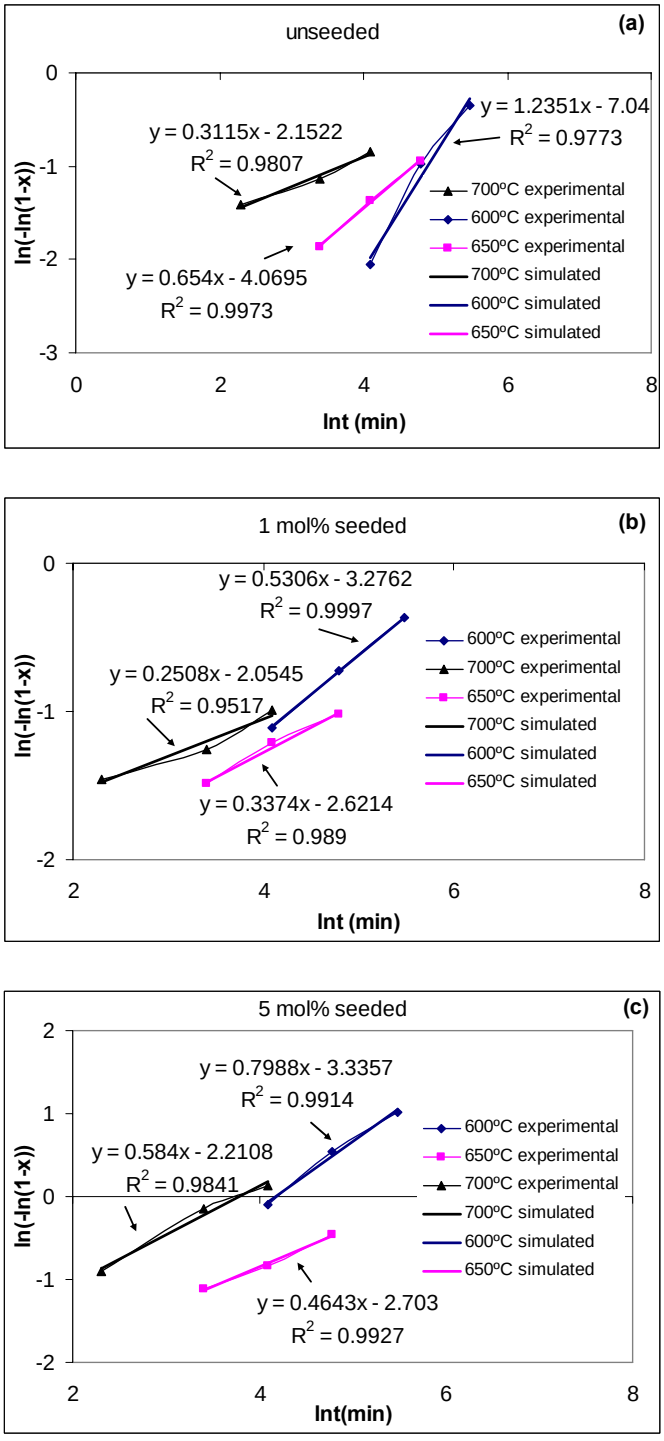

Figure 3.8. Avrami plots of perovskite $(Ba_{0.8}Sr_{0.2})TiO_3$ formation as a function of the natural logarithm of annealing times for different annealing temperatures and for (a) unseeded , (b) 1 mol% and (c) 5 mol% seeded BST films. The slope lines of y=ax+b are indicated in the figure, where y is ln(-ln(1-x)), x is lnt, a is n and b is lnk.

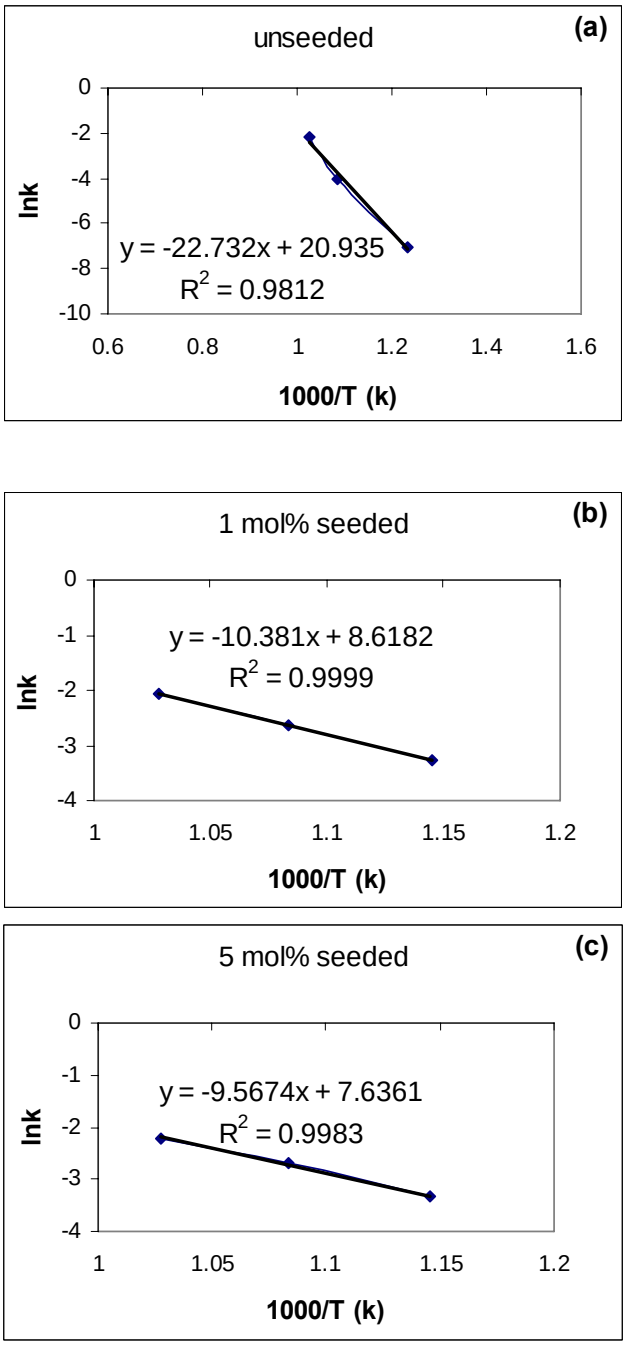

Figure 3.9. Arrhenius plots of the crystallization rate constant versus temperature for (a) unseeded, (b) 1 mol% seeded and (c) 5 mol% seeded $(Ba_{0.8}Sr_{0.2})TiO_3$ films.

The values obtained for the activation energy of perovskite crystallization in the case of unseeded BST80/20 films, 189 KJ/mol, though lower, is of the same order of magnitude, of the data reported by Bao et al [10] of 270.8 KJ/mol, for the crystallization of BST80/20 *powders*. No data for the activation energy of BST perovskite phase formation was reported in thin films. The difference between these energies might be related to the film/substrate interface. In fact BST films should have lower activation energy for the perovskite phase formation than BST powders. It is expected that the energy state associated with the film/substrate interface will decrease the total energy necessary for the phase formation process; the film/substrate interface acts as a preferential crystallization site for the perovskite phase facilitates the nucleation of the perovskite phase (heterogeneous nucleation process) with a corresponding lowering of the associated energy.

Table 3.2. Avrami coefficients n, rate constants k, and activation energies Ea for the perovskite crystallization of $(Ba_{0.8}Sr_{0.2})TiO_3$ thin films derived from unseeded and seeded precursor sols.

T (ºC)	Unseeded		1 mol% seeded		5 mol% seeded	
	n	lnk	n	lnk	n	lnk
600	1,2351	-7,04	0,5306	-3,2762	0,7988	-3,3357
650	0,654	-4,0695	0,3374	-2,6214	0,4643	-2,703
700	0,3115	-2,1522	0,2508	-2,0545	0,584	-2,2108
Ea(kJ/mol)	189		86		80	

For seeded films, the obtained Ea values are much lower (one order of magnitude lower) than those obtained for unseeded films. These results support the XRD results (figures 3.4 - 3.6) and the statement that the presence of nano sized BST seeds reduces the activation energy needed to reach the critical nuclei size and, consequently, reduces the activation energy of the crystallization processes.

To our knowledge, the actication energy for the perovskite formation of BST80/20 thin films deposited by sol-gel has not been published yet.

In summary, BST80/20 thin films were prepared by sol-gel on $Pt/TiO_2/SiO_2/Si$ substrates using different concentration of seeds (0 - 10 mol %) in the precursor solution. Their crystallization behaviour were evaluated and compared. It was shown that using perovskite BST nanopowders as seeds results in the crystallization of a single perovskite phase in BST films either at lower temperatures or at shorter annealing time when compared with unseeded films. The presence of nano sized BST seeds in the film lowers the barrier for BST nucleation and results in a high density of small crystallites in the film. The seeded BST films exhibit enhanced crystallization kinetics and the overall activation energy for the perovskite crystallization was reduced from 189 kJ/mol for the unseeded film to 86 kJ/mol for 1 mol% seeded BST film and to 80 kJ/mol for 5 mol% seeded film.

3.3 Microstructure of BST thin films

Figure 3.10 presents the SEM cross section image of unseeded BST thin films annealed at 650ºC for 2 hours in air. The thickness of this film is 240 nm. Similar thicknesses were observed for the other BST films under study in this work.

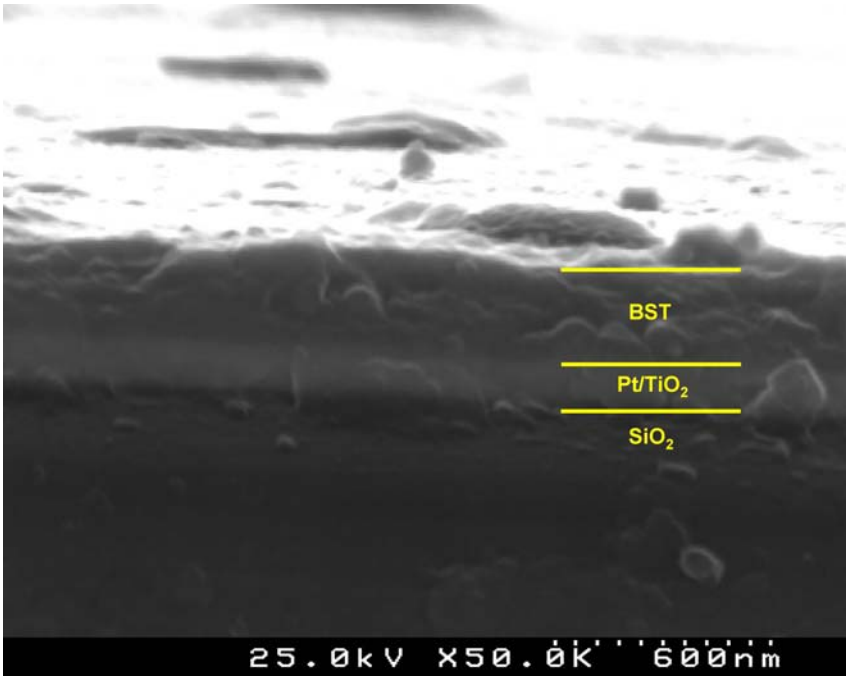

Figure 3.10. SEM cross section micrographs of unseeded $(Ba_{0.8}Sr_{0.2})TiO_3$ thin films annealed at 650ºC for 2 hours in air.

Figure 3.11 depicts the SEM surface morphology of unseeded BST films annealed at various temperatures. The SEM images reveal that all the films are dense and fine-grained. The average grain size of the obtained SEM micrographs was calculated by the linear intercept technique. As expected, a significant increase of the grain size was observed as the annealing temperature increased. Films annealed at 650ºC have grains rather fine with an average grain size of 40 nm and a homogeneous size distribution and for films annealed at 700ºC the average grain size increased being of 58 nm. When annealed at 750ºC the grains grew up to an average grain size of 100 nm and the film surface roughness increased.

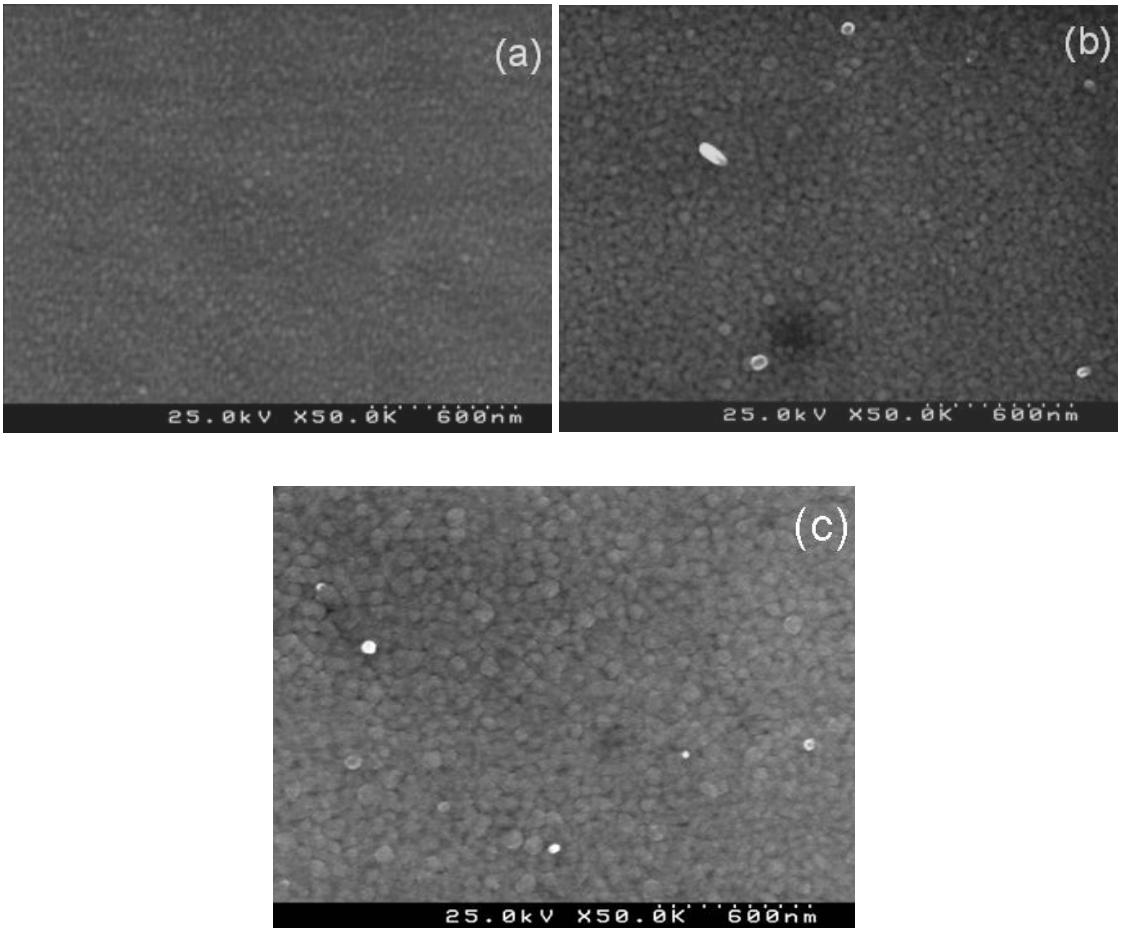

Figure 3.11. SEM micrographs of unseeded $(Ba_{0.8}Sr_{0.2})TiO_3$ thin films as a function of annealing temperature: (a) 650ºC, (b) 700ºC, and (c) 750ºC for 1 hour.

The average grain size and the surface roughness of unseeded and 5 mol% seeded BST films annealed at 650ºC for 2 hours were also determined by Atomic Force Microscopy (AFM). The topography images of unseeded and 5 mol% seeded films annealed at 650ºC for 2 hours in air are shown in figure 3.12. The differences of the surface morphologies between unseeded and seeded films are quite obvious through the observation of the 3 dimension (3D) AFM images. Seeded films clearly present a smaller grain size with a narrow grain size distribution when compared with unseeded films. The average grain size measured by linear intercept technique of seeded BST films is 45 nm. In the unseeded films the grain size is not homogeneous, with big grains around 200 nm and small grains around 60 nm. Meanwhile, the root mean square (RMS) roughness of the films was decreased from 12.85 nm for unseeded films to 5.35 nm for films with 5 mol% seeds, calculated from an area of 2×2 μm square. According to table 3.1, an intermediate phase is still detectable in unseeded BST films annealed at 650ºC for 2 hours, however pure perovskite phase was obtained in 5 mol% seeded BST thin films annealed at the same temperature for the same duration. Hence the presence of the intermediate phase might also contribute to the more inhomogeneous grain structure observed in unseeded BST thin films which is consistent with the suggestion of Chen et al [11]. These results are consistent with the crystallization kinetic study conducted in section 3.2. The presence of the nano-seeds and their action as heterogeneous nucleus sites contribute to the development of a more homogeneous microstructure with small grain size in seeded films.

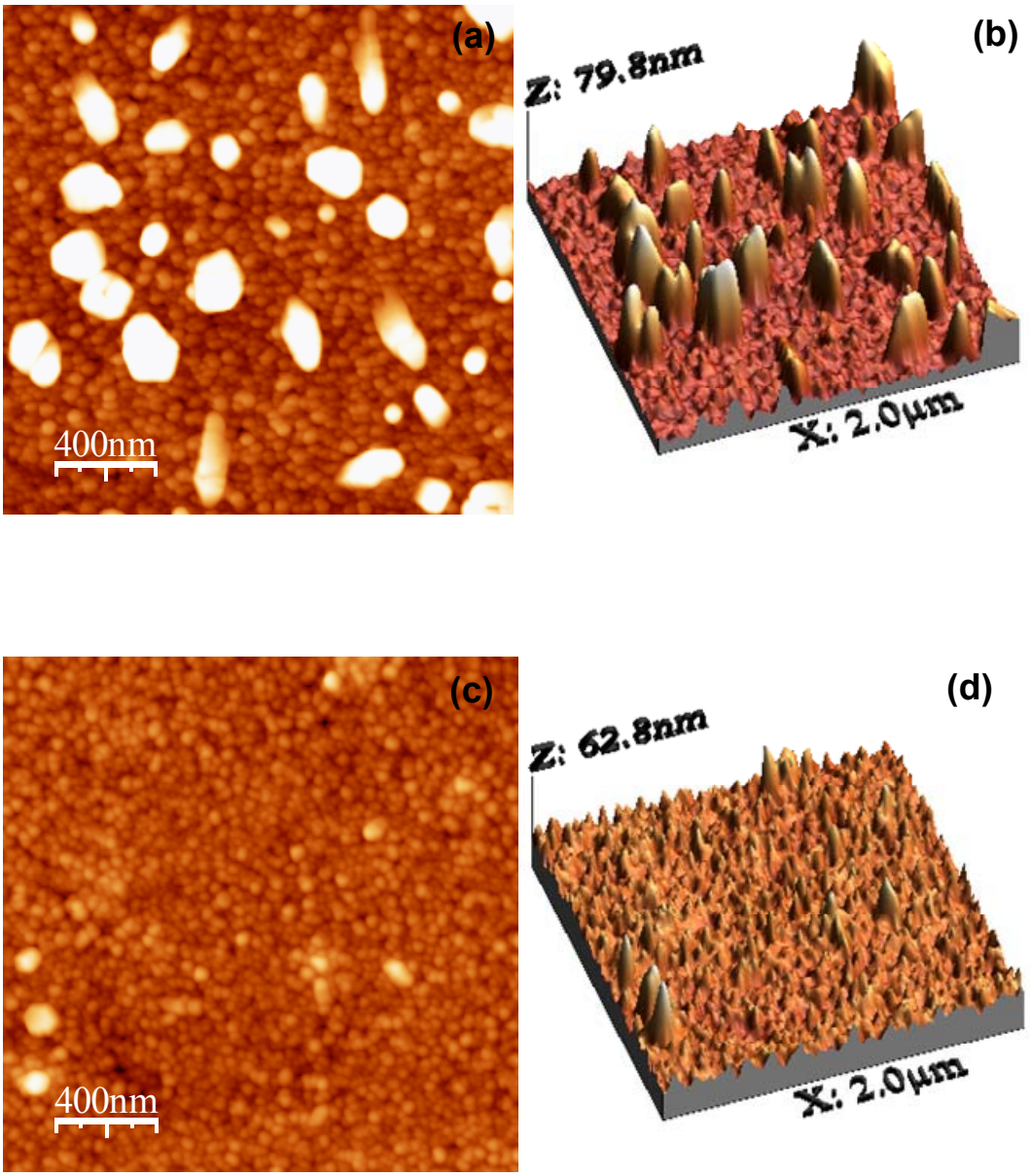

Figure 3.12. Two dimensional AFM images of $(Ba_{0.8}Sr_{0.2})TiO_3$ thin films (a) without seeds, (c) with 5 mol% seeds, three-dimensional topography AFM images of BST thin films (b) without seeds, (d) with 5 mol% seeds annealed at 650ºC for 2 hours.

Figure 3.13 (a) and (b) depict the topographic images of 5 mol% seeded BST films annealed at 600ºC for 30 hours in oxygen. The film is fully crystallized and dense. The spherical shaped grains are uniformly distributed with an average grain size of 15 nm

measured by the linear intercept technique. The root mean square (RMS) roughness is 3.53 nm. On the other hand, micro-cracks and a heterogeneous grain size distribution were found in unseeded BST80/20 thin films annealed under the same conditions as shown in figure 3.13 (c) and (d). The average grain size of unseeded films is 22 nm, and RMS surface roughness is 3.77nm, slightly higher than equivalent values of 5 mol% seeded films.

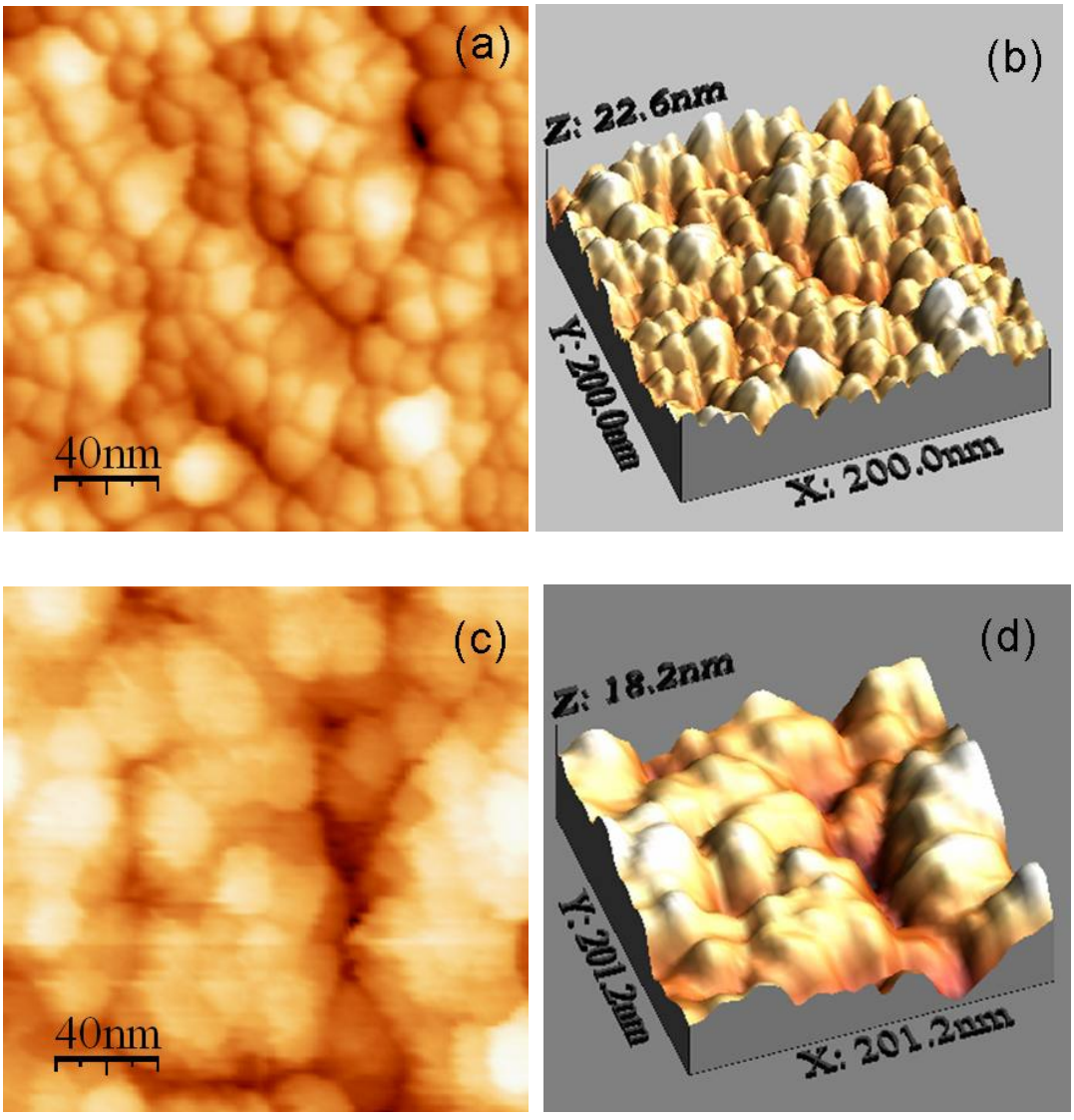

Figure 3.13. AFM topographic images of $(Ba_{0.8}Sr_{0.2})TiO_3$ thin films (a), (b) 5 mol% seeded, (c) (d) unseeded annealed at 600ºC for 30 hours in oxygen.

In order to investigate the influence of the annealing atmosphere and annealing time on the microstructure of the BST thin films, 240 nm BST thin films without seeds and with 5 mol% seeds annealed at 600ºC for 30 hours in air and oxygen were also analyzed by AFM.

The topography of 5 mol% seeded BST80/20 thin films annealed at 600ºC for 30 hours in air ambient is shown in figures 3.14 (a) and (b). The grains are quite inhomogeneous and the grain size varies between 25nm to 100nm and clusters of small grains were found. In some of these clusters, the grain boundaries are barely discernible. The root mean square (RMS) roughness is 12.944 nm. Figures 3.14 (c) and (d) depict the topographic images of 5 mol% seeded BST80/20 thin films annealed in identical conditions to the previous one. A remarkable difference between these two microstructures can be noticed. The microstructure of seeded films is more homogeneous than the previous one, the average grain size is of 15 nm and the RMS roughness is 3.53 nm.

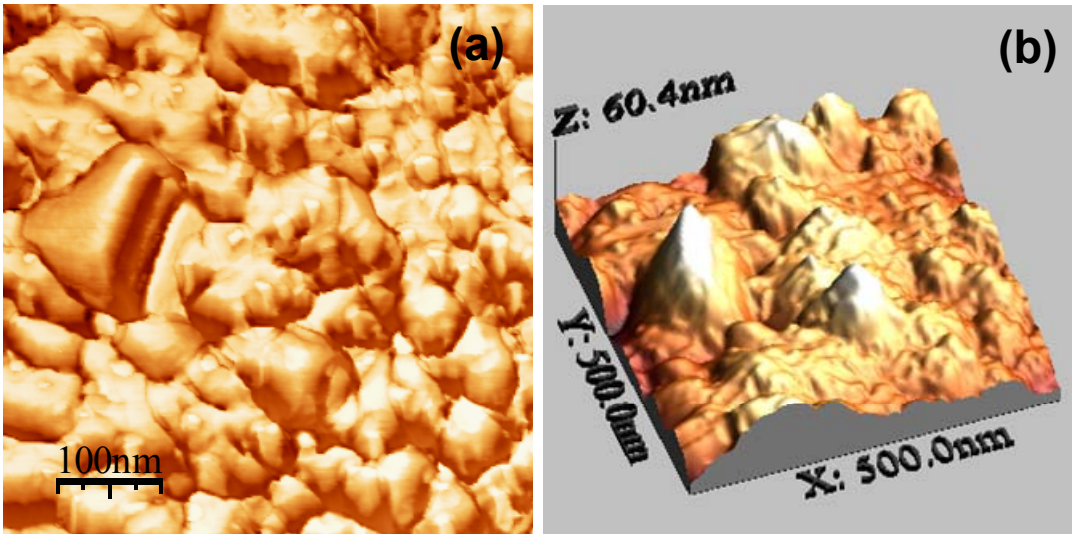

Figure 3.14. AFM topographic images of 5 mol% seeded $(Ba_{0.8}Sr_{0.2})TiO_3$ thin films annealed at 600ºC for 30 hours (a) (b) in air, (c) (d) in oxygen.

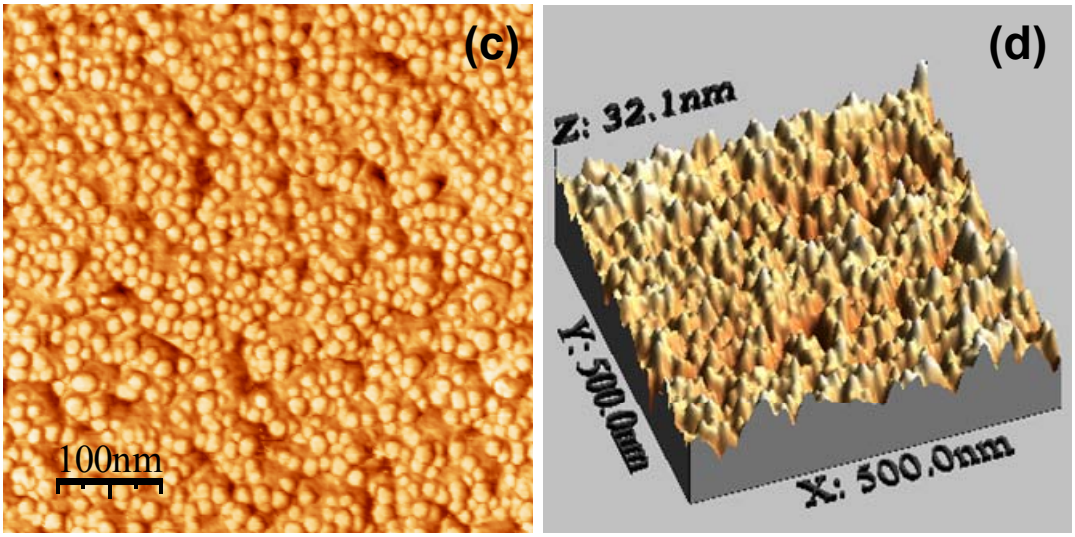

Figure 3.14. AFM topographic images of 5 mol% seeded $(Ba_{0.8}Sr_{0.2})TiO_3$ thin films annealed at 600ºC for 30 hours (a) (b) in air, (c) (d) in oxygen (continuation).

In order to further investigate the interface microstructure of the unseeded and seeded films TEM analysis was performed on cross sections of BST thin films annealed at 600ºC for 30 hours in oxygen.

Figure 3.15 (a) and (b) correspond to unseeded films and the inset is the electron diffraction (ED) pattern taken in the BST film area. Both amorphous and crystalline regions were observed in the same film as illustrated by the ED patterns. The halo ED pattern (inset of figure 3.15a) evidences the amorphous area that exists in unseeded BST films. The discrete diffraction bright spots of diffraction in ED patterns (inset of figure 3.15b) indicate the crystalline area of these BST films. A clear interface between the film and the substrate was observed.

Figure 3.15 (c) shows identical cross section of 5 mol% seeded BST films annealed under identical conditions. ED pattern (figure inset) evidences the crystalline state of these BST films. Several seeded films were analyzed by TEM and the observed microstructures are typical for seeded films in which no amorphous regions were

observed. The interface between the film and the platinum bottom electrode was very well defined.

TEM analysis of unseeded films and 5 mol% seeded BST films clearly shows that the degree of crystallinity of seeded films increase with the presence of seeds under the same processing conditions, in accordance with the XRD results already presented. Moreover TEM analysis clearly pointed to the incomplete crystallization of unseeded BST films at 600ºC even annealed under oxygen atmosphere, in spite of the crystalline XRD patterns of these films. This constitutes important supplementary information not obtained by any of the other used techniques.

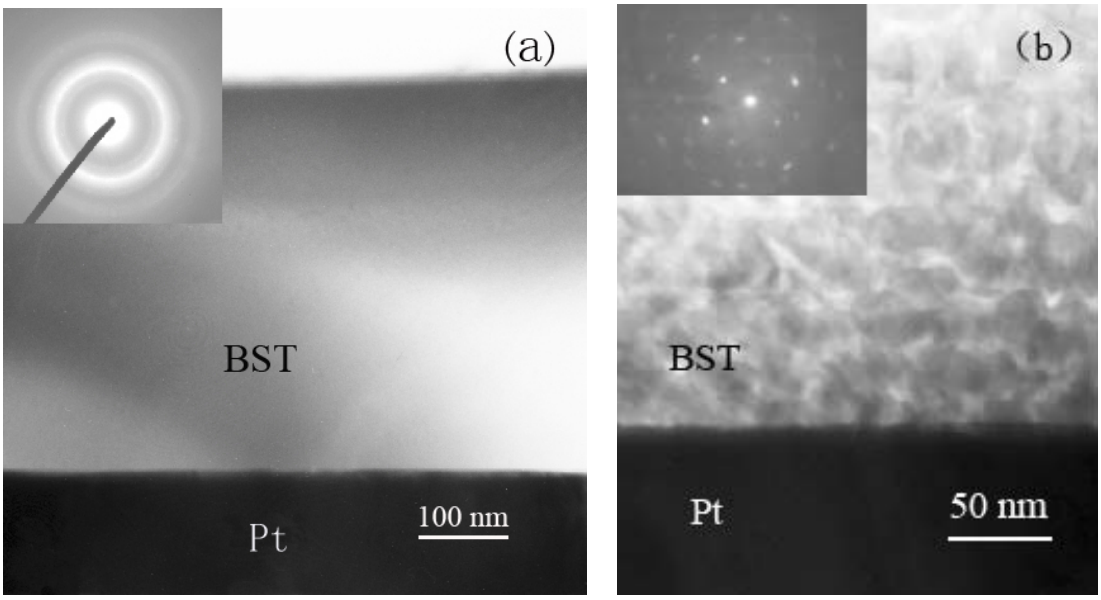

Figure 3.15. TEM cross section of $(Ba_{0.8}Sr_{0.2})TiO_3$ thin films annealed at 600ºC for 30 hours in oxygen (a) and (b)without seeds, and (c) with 5 mol% of seeds.

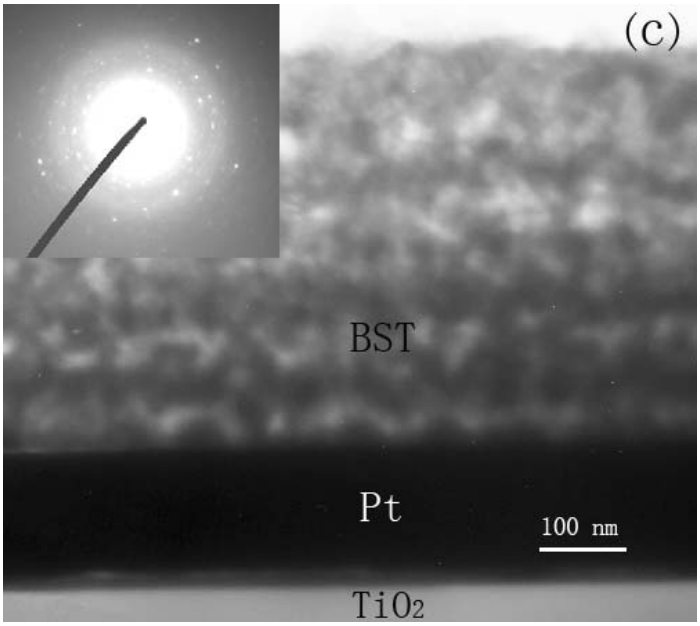

Figure 3.15. TEM cross section of $(Ba_{0.8}Sr_{0.2})TiO_3$ thin films annealed at 600ºC for 30 hours in oxygen (a) and (b) without seeds, and (c) with 5 mol% of seeds (continuation).

In summary, BST80/20 thin films prepared with seeds showed a more uniform with a smaller grain size microstructure than unseeded films prepared under identical conditions. This enhanced microstructure homogeneity of seeded films is also evidenced by lower roughness of the surface of these films when compared with unseeded ones. Even after annealing under oxygen atmosphere for a long period of time that generally benefits the perovskite phase formation as it was observed by the phase formation studies, unseeded films still show a heterogeneous microstructure in which amorphous regions were clearly observed by TEM. In opposition fully crystalline films were obtained for seeded BST films prepared under identical conditions.

Because films with dense, homogeneous, monophasic and crystalline microstructures with smooth surface and with no interfacial reactions between the film and the substrate are decisive for achieving optimal dielectric properties, improved dielectric properties are expected for the seeded films prepared in this work.

3.4 Electrical properties of BST thin films

The frequency dependence of the dielectric constant of unseeded and 5 mol% seeded BST thin films annealed at 650ºC for 2 hours is shown in figure 3.16. The dielectric constant ε_r tends to decline with the increasing frequency range up to 1 MHz. Meanwhile, the dielectric constant ε_r of BST films was enhanced with the addition of seeds from 290 to 377 at 10 kHz and from 191 to 342 at 1 MHz and the loss tangent, tanδ, was decreased with the addition of 5 mol% seeds from 0.395 to 0.057 at 10 kHz and from 0.095 to 0.078 at 1 MHz. The dielectric frequency dispersion was obviously decreased. These results suggest that seeds served indeed to improve, together with the microstructure, also the electrical response of the seeded films: low dielectric loss, high dielectric constant and good frequency dispersion characteristics were obtained for seeded films.

According to the XRD analysis shown in table 3.1, intermediate phase is detectable in unseeded BST films annealed at 650ºC for 2 hours, and pure perovskite phase is obtained for 5 mol% seeded BST thin films annealed at the same temperature for the same duration. The high loss of the unseeded film is may be due to the presence of the intermediate phase.

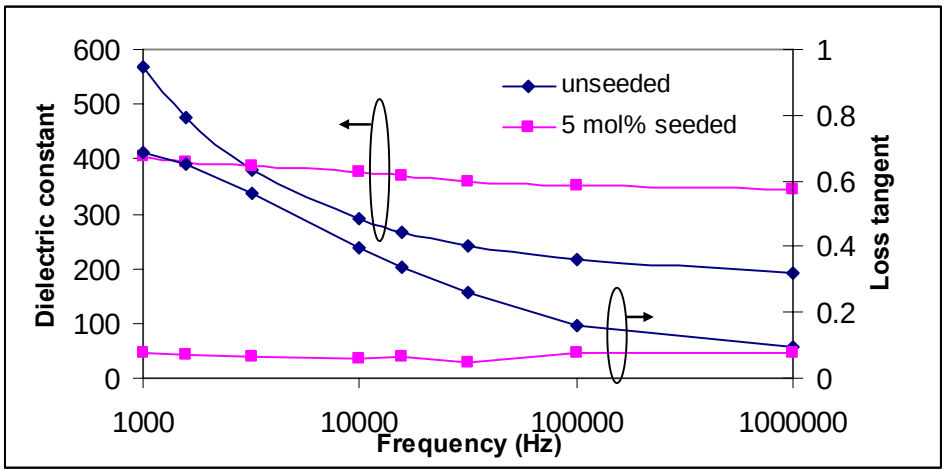

Figure 3.16. Dielectric constant and loss tangent of unseeded and 5 mol% seeded $(Ba_{0.8}Sr_{0.2})TiO_3$ films annealed at 650ºC for 2 hours in air measured at room temperature as a function of frequency.

Figure 3.17 illustrates the influence of the annealing atmosphere on the dielectric constant and loss tangent of 5 mol% seeded $(Ba_{0.8}Sr_{0.2})TiO_3$ films. It was found that annealing in oxygen enhances the dielectric response of BST films; the dielectric constant increased and in particular the loss tangent decreased. For films annealed in air loss tangent declined sharply as the frequency increases, which may be an indication of the presence of space charges and oxygen vacancies in the films. On the other hand, improved dielectric quality (dielectric losses and frequency dependence of the dielectric losses) was found in films annealed in oxygen, pointing to possible oxygen vacancies compensation.

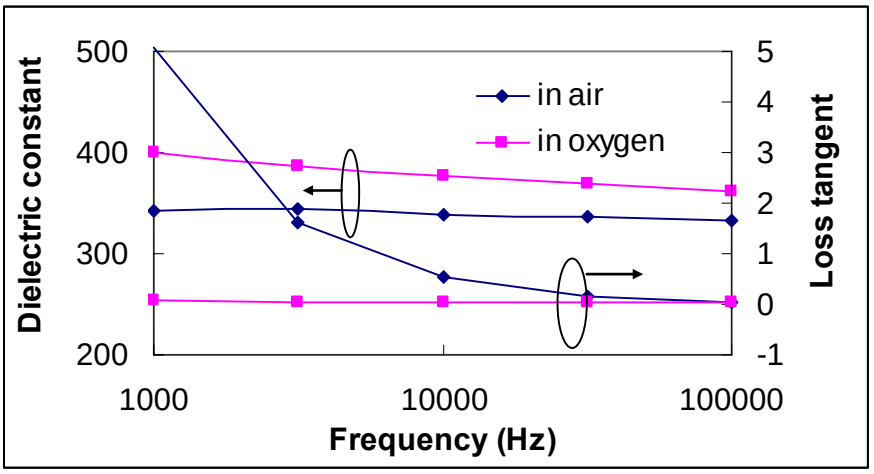

Figure 3.17. Room temperature dielectric constant and loss tangent of 5 mol% seeded $(Ba_{0.8}Sr_{0.2})TiO_3$ films annealed at 600ºC for 30 hours in air and oxygen atmosphere.

Figure 3.18 shows the dielectric constants and loss tangent of unseeded and 5 mol% seeded films annealed at 600ºC for 30 hours in oxygen as a function of frequency. As observed in previous figure the dielectric constant tends to decline with the increasing frequency. The dielectric constants of unseeded films annealed at 600ºC for 30 hours in oxygen were also improved by the addition of 5 mol% seeds from 324 to 400 at 1 kHz, from 273 to 343 at 1 MHz, respectively. Simultaneously, the dissipation factors were decreased by the presence of 5 mol% seeds from 0.0966 to 0.065 at 1 kHz, from 0.0656 to 0.0136 at 1 MHz, respectively. The results of dielectric properties of unseeded film and seeded films are in a good agreement with the microstructure studies previously presented and discussed.

These results also indicate that even annealed in oxygen atmosphere and for a long annealing time (both favourable conditions for enhanced ctrstallization and dielectric response) unseeded films due to the heterogeneous microstructure (presence of amorphous regions within the films as shown in figure 3.15) still exhibit poor dielectric properties when compared with seeded films prepared under identical conditions.

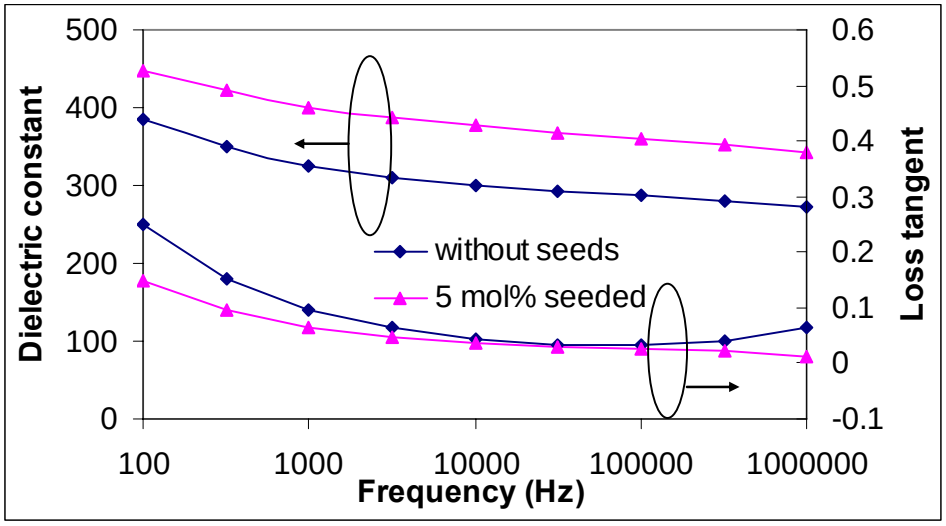

Figure 3.18. Room-temperature dielectric constant and loss tangent of $(Ba_{0.8}Sr_{0.2})TiO_3$ films without and with 5 mol% seeds annealed at 600ºC for 30 hours oxygen as a function of frequency.

Table 3.3 summarises the obtained dielectric properties of unseeded and 5 mol% seeded BST films. After heat treatment at 600ºC for 30 hours, the achieved dielectric constant of 5 mol% seeded BST films is approximately equal to the dielectric constant of unseeded BST films annealed at 750ºC for 1 hour and is higher than the unseeded BST films annealed at 700ºC for 1 hour. Loss tangent shows a minimum value for 5 mol% seeded annealed at 600ºC for 30 hours.

Table 3.3. Summary of the obtained dielectric properties of $(Ba_{0.8}Sr_{0.2})TiO_3$ films.

T_{ann} (ºC)	Annealing time (h)	Annealing atmosphere	Seeds amount	ε_r (at room temperature 1 kHz)	tanδ (at room temperature 1 kHz)	ε_r (at room temperature 100 kHz)	tanδ (at room temperature 100 kHz)
750	1	air	no seeds	419	0.06	358	0.05
700	1	air	no seeds	375	0.06	342	0.064
650	2	air	5 mol%	403	0.07	351	0.07
600	30	oxygen	5 mol%	400	0.06	360	0.027

One of the main attractions of BST materials, related to their use in voltage tunable devices, depends on the ability to change the material capacitance by means of an applied electric field. The dependence of the dielectric constant on the electric field, an indication of the tunability, for BST films at room temperature with and without seeds, is shown in figures 3.19 and 3.20.

In accordance with the dielectric permittivity results, unseeded films present a lower value of capacitance than seeded films, in spite of similar variation with the electric filed. A slight asymmetry was observed in the C-V curves of unseeded BST films, which suggests that the films contain oxygen vacancies at the interface between the film and the electrode [12]. The variation of the dielectric losses between 5 mol% seeded films annealed in air and in oxygen (figure 3.17) support the existence of such defects. Meanwhile the different material of top electrode (Au) and bottom electrode (Pt) may also contribute to this asymmetry.

The values of tunability, 37% and 47%, were calculated from figure 3.19 for unseeded and 5 mol% seeded BST thin films, respectively. The obtained tunability value for unseeded films is comparable to the recent results of 37% and 35.8% reported in references [13] and [14], with sol-gel derived BST80/20 thin films annealed at 700ºC and 750ºC, respectively.

Figure 3.20 shows the dependence of the capacitance on the applied electric field of unseeded and 5 mol% seeded BST films annealed at 600ºC for 30 hours in oxygen. Dielectric constant of the films was calculated from the capacitance measured at 100 kHz with bias voltage (from -6 V to 6 V). A slight asymmetry was also observed in the C - V curves of unseeded films as previously observed. This asymmetry is smaller than the one formely observed since these films were heat treated in O_2. This observation is in good agreement with the variation of dielectric losses for films heat treated in oxygen and also confirms the role of defects. The presence of 5 mol% seeds improved the tunability of BST films and an increment from 52% to 65% at 6V was observed. These values are higher than the recent results of 37% [13] and 35.8% [14] reported for sol-gel derived BST80/20 thin films annealed at 700ºC and 750ºC, respectively.

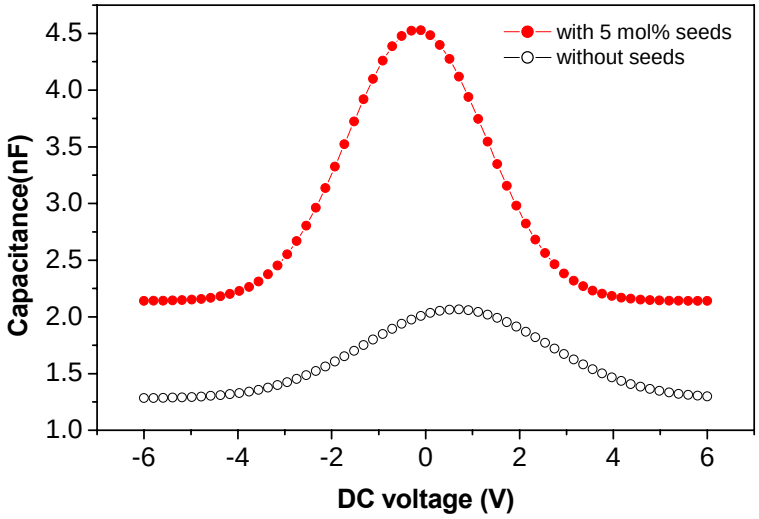

Figure 3.19. Room-temperature capacitance versus dc voltage of $(Ba_{0.8}Sr_{0.2})TiO_3$ films without and with 5 mol% seeds annealed at 650ºC for 2 hours in air.

Figure 3.21 depicts the polarization *P* versus electric field *E* dependence measured at 400 Hz and room temperature of unseeded and 5 mol% seeded BST films annealed at 600ºC for 30 hours in oxygen. Showing a similar trend as the previous dielectric characterization, under identical measurement conditions, the *P-E* hysteresis curve of BST films was improved by the introduction of seeds. The remnant polarization, *P*r of samples with 5mol% seeds was 3.55 μC/cm^2 with a coercive field of 75 kV/cm, which was considerably enhanced when compared to 1.8 μC/ cm^2 for BST films without seeds with a coercive field of 50 kV/cm. The literature claimed for $(Ba_{0.8}Sr_{0.2})TiO_3$ sol-gel films and for a well-saturated *P-E* hysteresis loop, a remnant polarization of 3.5 μC/cm^2 and a coercive field of 86 kV/cm for BST80/20 films annealed at 750ºC [15].

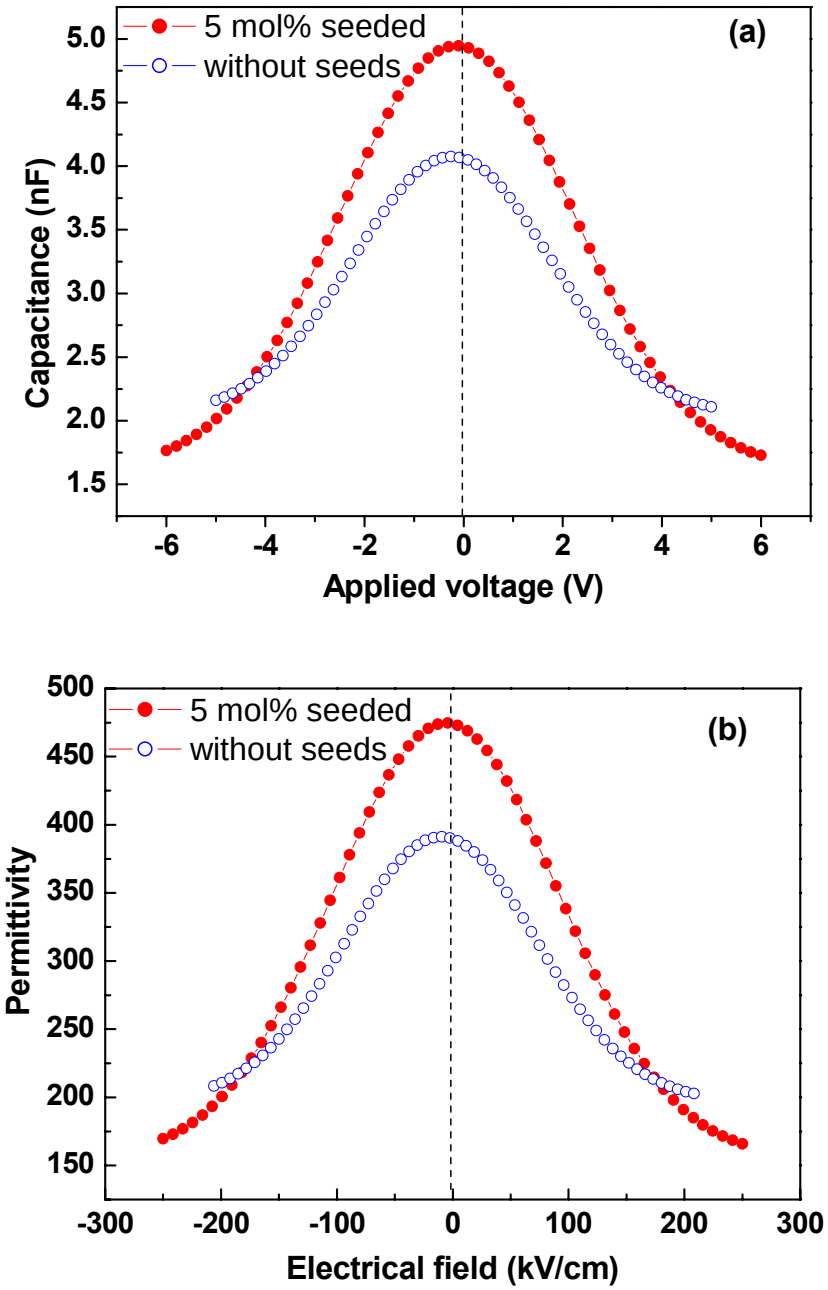

Figure 3.20. Room temperature (a) capacitance versus dc bias voltage dependence, and (b) permittivity versus electrical field dependence of unseeded and 5 mol% seeded $(Ba_{0.8}Sr_{0.2})TiO_3$ thin films annealed at 600ºC in oxygen for 30 hours at a frequency of 100 kHz (scanned voltage from negative to positive).

Sol-gel derived BST films do not usually display pronounced ferroelectric hysterisis loop [16]. Several possible reasons have been pointed that include: (i) the critical size for the existence of ferroelectricity of $BaTiO_3$ (~120 nm [17]) is much larger than that of $PbTiO_3$ (~12.6 nm [18]). D. M. Tahan et al [16] deposited BST films of various compositions by the sol-gel method with grain size ranging from 20 to 50 nm, and no ferroelectricity was present; (ii) sol-gel deposition of $BaTiO_3$ films commonly results in polycrystalline, granular films with grain diameters of lower than 70 nm due to random nucleation in the pyrolyzed gel films [19]. This is in contrast to PZT films, which can be easily grown by sol-gel into a columnar or epitaxial structure [20]; (iii) the tetragonality (c/a) of BST films decreases with the increasing of strontium content [19], and a small c/a value may not be sufficient to create the charge separation and spontaneous polarization in the films, so the fabrication of BST ferroelectric films is more difficult than that of $BaTiO_3$.

Hysteresis loop of sol gel $Ba_{0.8}Sr_{0.2}TiO_3$ thin films annealed at 750ºC were reported the Cheng´s group [15] when using a highly diluted precursor solution. It was claimed that the film with large grains, with sizes varying from 100 to 200 nm formed from a highly diluted precursor solution, resulted in measurable ferroelectric hysteresis curves. On the contrary, films with small grains size of 40 nm didn't exhibit any hysteretic response of the polarization versus field.

However, in spite of the small grains (15 nm, as revealed by AFM in figure 3.13), of the films annealed in oxygen for 30 hours well defined hysteresis curves were measured in this work. This clearly indicates that the high quality of the films with dense nano-sized microstructure, lower defect content, including a low oxygen vacancy amount, in this case induced by the presence of BST seeds and annealing in oxygen for a long period, plays a crucial role. This is also an indication that "size effects" need to be separated from "defect effects".

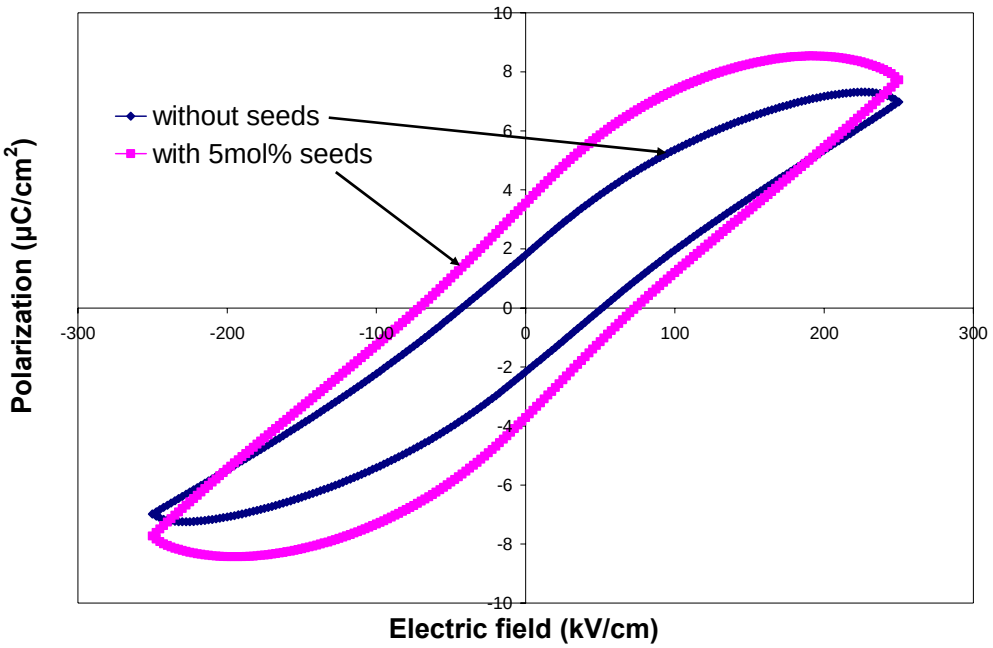

Figure 3.21. Room-temperature hysteresis loops of $(Ba_{0.8}Sr_{0.2})TiO_3$ films without and with 5 mol% seeds annealed at 600ºC for 30 hours in oxygen atmosphere.

In order to further investigate the effect of BST nanometric seeds on the nano-scale ferroelectric properties of BST thin films. PFM was performed to study the domain imaging of unseeded and seeded BST thin films. In the piezo-response image, dark regions (hereafter referred to as negative domains) correspond to domains with polarization oriented towards the substrate, and bright regions (positive domains) to domains with polarization oriented to the film surface; grains with non-ferroelectric nature or in-plane polarization will exhibit an intermediate grey contrast. Since the PFM images were obtained with the same batch of cantilever and identical scanning and acquisition conditions, comparative analysis can be made for different films. Tip artifacts were excluded by using brand new tips and calibrated samples to check the resolution.

Figure 3.22 (a-1) and (b-1) show the topography images of unseeded and 5 mol% seeded BST films annealed under the same conditions (750ºC for 1 hour in air), respectively. The surface morphology of unseeded BST films showed some big grains,

not homogeneously distributed, and with a grain size ranging from 100 nm to 200 nm (figure 3.22 (a-1)). On the contrary, seeded BST films are characterized by a more uniform distribution of fine grains with an average grain size of 100 nm (figure 3.22 (b-1)). This result is consistent with the previous microstructure study (figures 3.12 to 3.15). The presence of the nano-particles and their action as nucleus sites seems to be the reason for the uniformity and small grain growth of seeded films even for films heat treated at high annealing temperatures.

The piezoresponse images acquired simultaneously with topography for unseeded and 5 mol% seeded BST films annealed at 750ºC for 1 hour are shown in figure 3.22 (a-2) and (b-2). A large fraction of gray regions (exhibiting weak piezoresponse signal) were observed in unseeded films (figure 3.22 (a-2)). Meanwhile, strong domain contrasts (deep bright and dark areas) were found in the PFM image of the 5 mol% seeded film (figure 3.22 (b-2)), which is a sign of significant out-of-plane component of polarization (circled by solid lines). Seeded BST films exhibit higher percentage of well-defined domains than unseeded BST films. From the cross-sectional analysis or out-of-plane domain images (figure 3.22 (a-3) and (b-3)), it can be noticed that the difference of the maximum PFM amplitude was improved from 280 mV to 480 mV by the presence of 5 mol% seeds, evidencing the role of the seeds in enhancing the polarization of BST films. This result is consistent with the macroscopic P – E hysterysis response shown before (figure 3.21).

Leakage current is a limiting factor of DRAM capacitors because they are closely related to the reliability of the device. High leakage currents are undesirable because they require more frequent refreshing, use more power, and limit the maximum field that may be applied across the device [21]. The leakage current of a dielectric film is an estimate of the films electrical quality, and is directly correlated to the resistive loss mechanism of the film. The benchmark for maximum allowable leakage current varies with DRAM cell design. The target for ideal Gbit era dynamic random access memory (DRAM) dielectrics requires a maximum leakage current of 1×10^{-7} A cm^{-2} at 1.6 V [22].

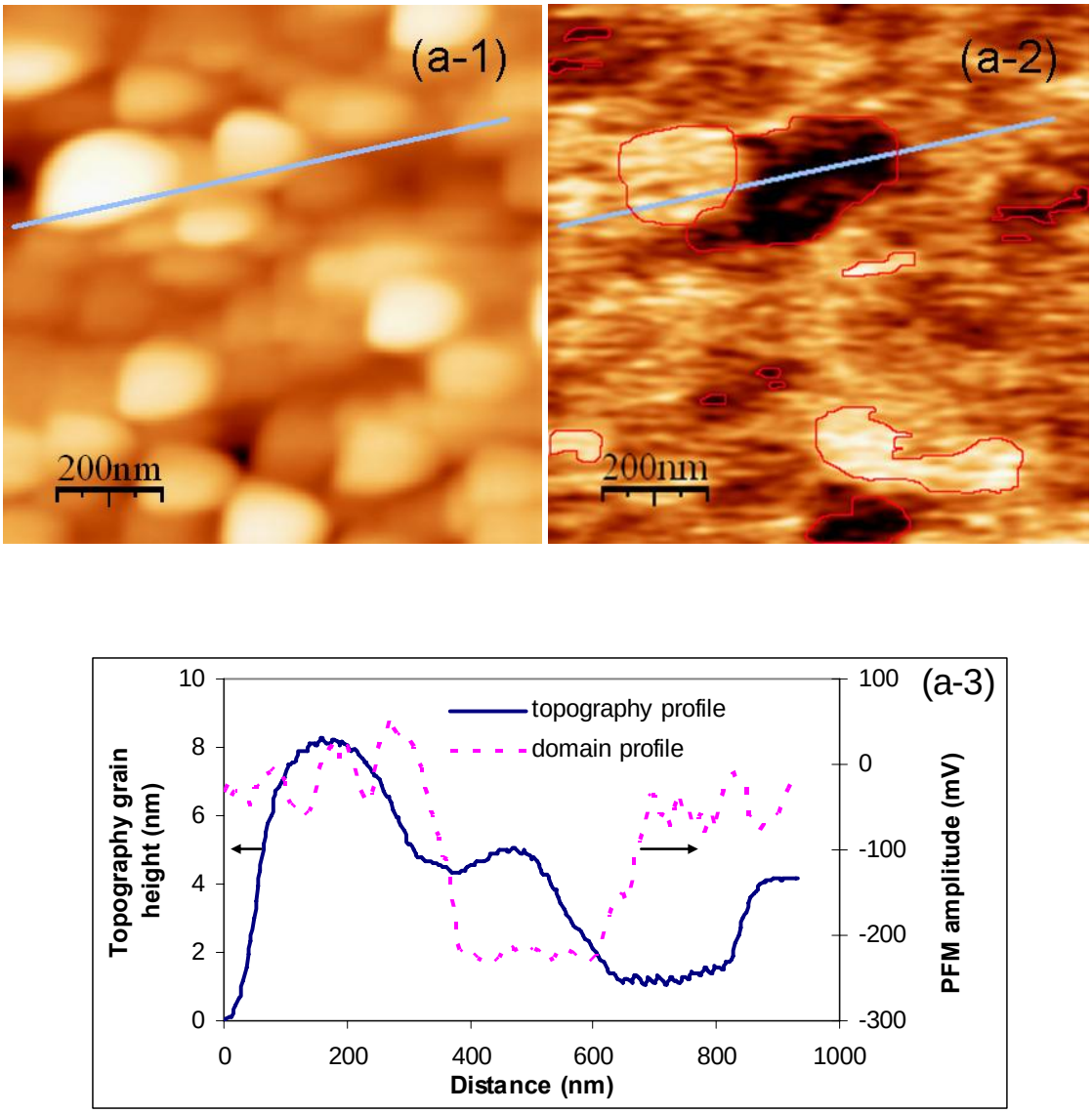

Figure 3.22. Topography (a-1), out of plane PFM signal (a-2) and simultaneous cross-sections of topography and PFM (a-3) taken on unseeded BST thin films annealed at 750ºC for 1 hour; topography (b-1), out of plane PFM signal (b-2) and simultaneous cross-sections of topography and PFM (b-3) taken on 5 mol% seeded BST thin films annealed at 750ºC for 1 hour.

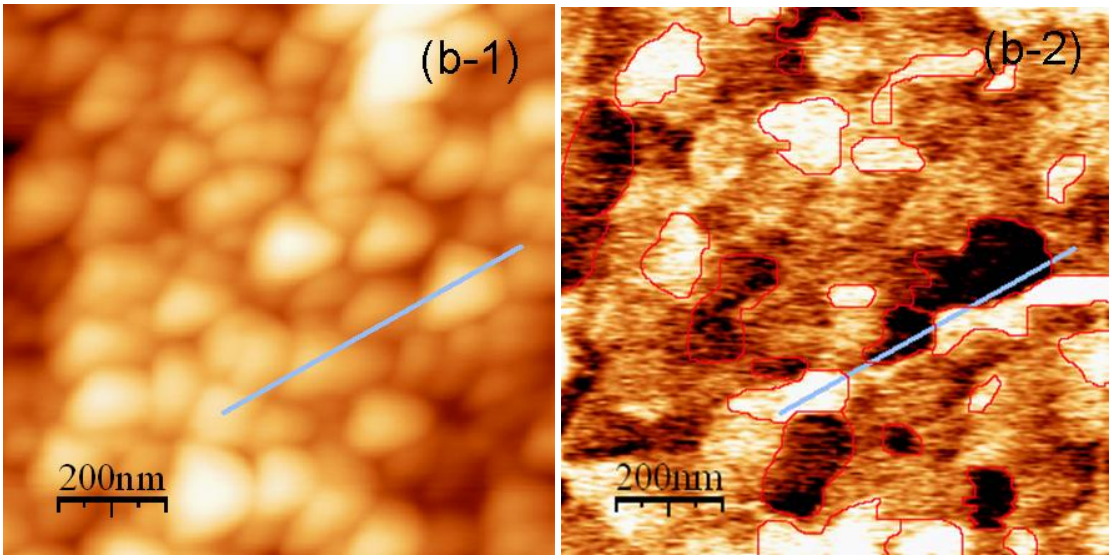

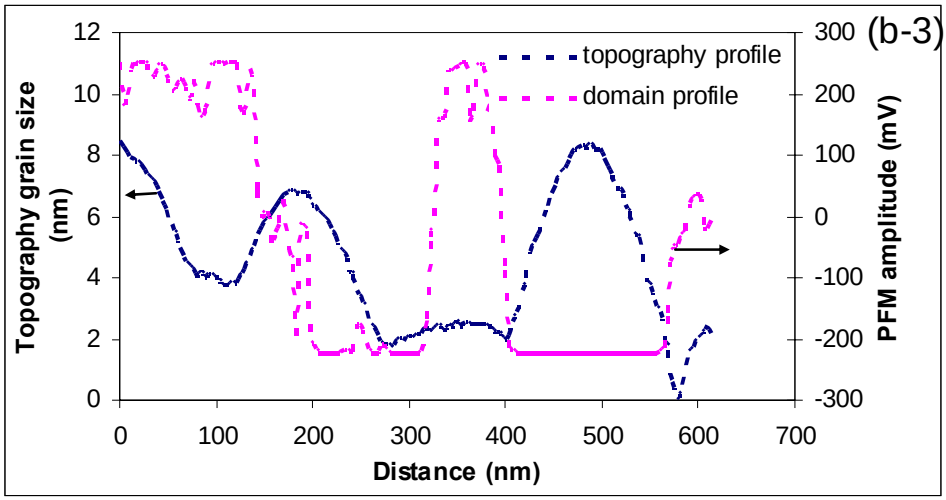

Figure 3.22. Topography (a-1), out of plane PFM signal (a-2) and simultaneous cross-sections of topography and PFM (a-3) taken on unseeded BST thin films annealed at 750ºC for 1 hour; topography (b-1), out of plane PFM signal (b-2) and simultaneous cross-sections of topography and PFM (b-3) taken on 5 mol% seeded BST thin films annealed at 750ºC for 1 hour (continuation).

The effect of seeds on the leakage current of BST films is presented in figure 3.23. As shown the leakage current density (J) of BST films with 5 mol% seeds is 0.952 $\times 10^{-7}$

A/cm^2 up to the applied voltage of 2.33 V (97 kV/cm), which was improved when compare to 0.884 × 10^{-7} A/cm^2 up to 2.02 V (84 kV/cm) measured for BST films without seeds. The values of the leakage current of both unseeded and 5 mol% seeded films meet the requirements for Gbite DRAMs.

The leakage current was found to be dependent on grain size of films [23]. Unseeded BST films with larger grain size have short conduction paths along the highly resistive grain boundaries resulting in higher leakage current compared with seeded BST films with smaller grain size.

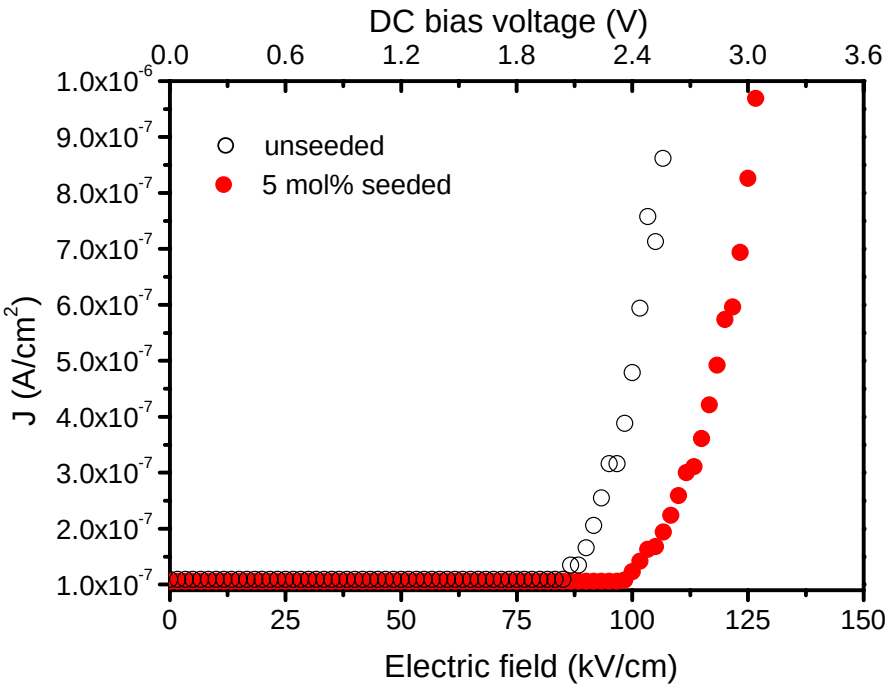

Figure 3.23 Room-temperature leakage current density of unseeded and 5 mol% seeded BST thin films annealed at 600ºC for 30 hours in oxygen as a function of applied external voltage.

Table 3.4 sum up the electrical properties of BST thin films prepared in this work. As a comparison, reported data for BST thin films fabricated by different techniques are also included.

The analysis of table 3.4 clearly evidences the importance of the results obtained in this work. In relation to tunability, the value of 65% for 5 mol% seeded BST thin films annealed at a temperature as low as 600ºC for 30 hours in oxygen prepared in this work is considerably higher than the reported values, even when compared to the value of 52% presented by PLD derived BST thin films [27] and 49.4% presented by sputtered derived BST films [28]. Regarding the remnant polarization, values of 3.55 $\mu C/cm^2$ obtained in this work for 5 mol% seeded BST films, are slightly higher when compared to the reported values of 3 and 3.5 $\mu C/cm^2$ [24, 25] for sol-gel derived BST80/20 films. A similar trend is observed for the dielectric permittivity and dielectric losses. The values for the dielectric permittivity and dielectric losses obtained in this work, 400 and 0.065 at 1 kHz, respectively, for 5 mol% seeded BST thin films annealed at a temperature as low as 600ºC for 30 hours in oxygen are comparable with the values obtained for PLD derived BST thin films of 350 for the dielectric permittivity and 0.07 for the loss tangent value at 100 kHz [27]).

BST80/20 films prepared by diphasic precursor sol gel method and heat treated at temperatures as low as 600ºC possess improved dielectric and ferroelectric properties identical to those exhibited by BST films prepared by physical vapour deposition techniques and at higher annealing temperatures.

Table 3.4. Electrical Properties of BST Films Prepared in This Work and Reported in the Literature.

Film/T_{ann}(ºC)	Deposition Technique	Seeds amount/ film thickness	Єr(at room temperature)	tanδ	Pr (μC/cm^2)	J (A/cm^2)	tunability in room	Ref.
BST(80/20), 650ºC	sol-gel	no seeds / 240	290 (at 10 kHz)	0.39 (at 10 kHz)			37% at 250 kV/cm	this work
BST(80/20), 650ºC	sol-gel	5 mol% / 240	377 (at 10 kHz)	0.057 (at 10 kHz)			47% at 250 kV/cm	this work
BST(80/20), 600ºC	sol-gel	no seeds/ 240	324 (at 1 kHz)	0.1 (1 kHz)	1.8	0.88×10^{-7} at 2.02 V	52% at 250 kV/cm	this work
BST(80/20), 600ºC	sol-gel	5 mol% / 240	400 (at 1 kHz) 343 (at 1 MHz)	0.065 (at 1 kHz) 0.013 (at 1 MHz)	3.55	0.95×10^{-7} at 2.33 V	65% at 250 kV/cm	this work
BST(80/20), 700ºC	sol-gel	400 (with 30 nm seed layer)	830 (at 1kHz)	0.05 (at 1 kHz)	1.6	8.0×10^{-7} at 6.7 V	37% at 150 kV/cm	11
BST(50/50), 600ºC	sol-gel	4.9 mol% / 300	303 (at 1kHz)	0.151 (at 1 kHz)	-	-	-	23
BST(50/50), 600ºC	sol-gel	17.0 mol% / 300	244 (at 1kHz)	0.209 (at 1 kHz)	-	-	-	24
BST(80/20), 750ºC	sol-gel	no seeds/300	400 (at 10 kHz)	0.014 (at 10 k Hz)	3	1×10^{-6} at 10 V		24
BST(80/20), 750ºC	sol-gel	no seeds/260	520 (at 100 kHz)	0.03 (at 100 kHz)	3.5	-	40% at 230 kV/cm	25
BST(50/50), 800ºC	sol-gel	no seeds/350	459 (at 1kHz)	0.07 (at 1 kHz)	-	-	19.5% at 140 kV/cm	26
BST(60/40), 700ºC	PLD	no seeds/200	350 (at 100 kHz)	0.07 (at 100 kHz)	-	-	52% at 300 kV/cm	27
BST(60/40), 600ºC	Sputtering	no seeds/220	682 (at 100 kHz)	0.015 (at 100 kHz)	-	3.9×10^{-8} at 10 V	49.4% at 455 kV/cm	28

Based on the above data, the utilization of nanometric crystalline perovskite particles dispersed in the precursor solution results in improved dielectric and ferroelectric properties of BST thin films prepared at low temperatures. The possible way how seeds may affect film properties deserves some remarks.

It is well-known that the perovskite phase formation in BST is a nucleation-controlled process where the perovskite nucleation is the rate-controlling step. The kinetics of this process in sol-gel derived films depends on many experimental factors such as solution chemistry, drying and pyrolysis cycles, and lattice matching with the substrate. In this work nanometric perovskite BST powders dispersed in the stock sol that act as perovskite nucleus decreased the activation energy for the perovskite formation (heterogeneous nucleation). Consequently, a pure perovskite phase is obtained at lower temperatures.

Besides the kinetic aspects, the nanometric BST powders affect markedly the structural and microstructural development of the films. Perovskite seeds, serving as heterogeneous nucleation sites, favored the perovskite formation throughout the bulk of the film, as proved by TEM. Besides the nucleation induced by Pt bottom electrode that promotes the crystallization front from bottom to top, the nucleation and growth of perovskite in seeded BST films occur also in the bulk and near the top surface. As a result, the degree of crystallinity of BST films at low annealing temperature increases markedly in spite of a random growth. The perovskite phase does not grow preferentially along any of the crystallographic directions of the under layers (in this case Pt) and any preferred orientation is lost, as experimentally observed by XRD and TEM. This type of nucleation and growth also affects the interface between the film and electrode in seeded films. As observed by TEM there are no interfacial reactions between the film and the underlying layers. The effect of seeds was also noticeable even after annealing in oxygen for a long period of time. Seeded films demonstrate a higher degree of crystallinity visible by the increased intensity of XRD peaks and proved by TEM analysis when compared with unseeded films.

It is reasonable to assume that dielectric and ferroelectric properties are directly affected by film microstructure details such as defects, electrode/film interface and preferred orientation. The enhanced crystallization induced by the crystalline seeds results in pure perovskite phase formation at low temperatures in seeded films. Simultaneously, dense films with uniform microstructure and small surface roughness were obtained for seeded films. The high quality microstructure, film/electrode interface and, as a consequence, a low content of defects of seeded films are the reason for the enhancement of the final electrical properties of seeded films.

In summary seeded BST80/20 thin films prepared by sol-gel on $Pt/TiO_2/SiO_2/Si$ substrates and with optimised microstructure features showed a clear improvement in dielectric and ferroelectric properties compared with unseeded films.

3.5 References

[1] S.-Y. Chen, H.-W. Wang, L.-C. Huang, Role of an Intermediate Phase $(Ba,Sr)_2Ti_2O_5CO_3$ in Doped $(Ba_{0.7}Sr_{0.3})TiO_3$ Thin Films, Materials Chemistry and Physics, **7**(2002) 632

[2] H. Huang, W. Qiu, O. K. Tan, W. Zhu, L. M. Zhou, Effect of Excess TiO_2 on the Phase Evolution and Densification of Sol-Gel Derived $(Ba,Sr)TiO_3$ Powders, Journal of Electroceramics, **16**(2006) 337

[3] M. C. B. Lopez, G. Fourlaris, B. Rand, F. L. Riley, Characterization of Barium Titanate Powders: Barium Carbonate Identification, Journal of the American Ceramics Society, **7**(1999) 1777

[4] M. Stockenhuber, H. Mayer, J. A. Lercher, Preparation of Barium Titanates from Oxalates, Journal of the American Ceramics Society, **76**(1993) 1185

[5] A. Wu, P. M. Vilarinho, I. M. M. Salvado, J. L. Baptista, Z. Zhou, I. M. Reaney, A. R. Ramos, M. F. Silva, Effect of Lead Zirconate Titanate Seeds on Pt_xPb Formation During the Pyrolysis of Lead Zirconate Titanate Thin Films, Journal of the American Ceramic Society, **85**(2002) 641

[6] C. K. Kwok, S. B. Desu, Pyrochlore to Perovskite Phase-Transformation in Sol-Gel Derived Lead-Zirconate-Titanate Thin-Films, Applied Physics Letters, **60**(1992) 1430

[7] M. Avrami, Kinetics of Phase Change. II. Transformation-Time Relations for Random Distribution of Nuclei, Journal of Chemical Physics, **8**(1940) 212

[8] J. W. Christian, The Theory of Transformations in Metals and Alloys, Part I Equilibrium and General Kinetic Theory, Pergamon Press, 1975

[9] V. Znidarsic-Pongarac, D. Kolar, The Crystallization of Diabase Glass, Journal of Materials Science, **26**(1991) 2490

[10] D. Bao, Z. Wamg, W. Ren, L. Zhang, X. Yao, Crystallization Kinetics of $Ba_{0.8}Sr_{0.2}TiO_3$ Sols and Sol-Gel Synthesis of $Ba_{0.8}Sr_{0.2}TiO_3$ Thin Films, Ceramics International, **25**(1999) 261

[11] X. Chen, W. Lu, W. Zhu, S. Y. Lim, S. A. Akbar, Structural and Thermal Analyses on Phase Evolution of Sol-Gel $(Ba,Sr)TiO_3$ Thin Films, Surface and Coatings Technology, **167**(2003) 203

[12] S. Song, J. Zhai, X. Yao, The Study of the Microstructure and Tunability of $Ba(Sn_xTi_{1-x})O_3$ Thin films, Integrated Ferroelectrics, **78**(2006) 337

[13] Z. Fu, A. Wu, P. M. Vilarinho, Effect of Seed Layer Thickness on Texture and Electrical Properties of Sol-Gel Derived $(Ba_{0.8}Sr_{0.2})TiO_3$ Thin Films, Chemistry of Materials, **18**(2006) 3343

[14] S. U. Adikary, H. L. W. Chan, Dielectric Dispersion and Tunability of Sol-Gel Derived $(Ba_xSr_{1-x})TiO_3$ Thin Films, Journal of Materials Science, **39**(2004) 6523

[15] J.-G. Cheng, X.-J. Meng, B. Li, J. Tang, S.-L. Guo, J.-H. Chu, M. Wang, H. Wang, Z. Wang, Ferroelectricity in Sol-Gel Derived $(Ba_{0.8}Sr_{0.2})TiO_3$ Thin Films Using a Highly Diluted Precursor Solution, Applied Physics Letters, **75**(1999), 2132

[16] D. M. Tahan, A. Safari, L. C. Klein, Preparation and Characterization of $(Ba_xSr_{1-x})TiO_3$ Thin Films by a Sol-Gel Technique, Journal of the American Ceramics Society, **79**(1996) 1593

[17] K. Uchino, E. Sadanago, T. Hirose, Dependence of the Crystal Structure on Particle Size in Barium Titanate, Communications for the American Ceramic Society, **72**(1989) 1555

[18] M. C. Gust, N. Evans, L. Momoda, M. Mecartney, In-Situ Transmission Electron Microscopy Crystallization Studies of Sol-Gel Derived Barium Titanate Thin Films, Journal of the American Ceramic Society, **80**(1997) 2828

[19] B. A. Baumert, L.-H. Chang, A. Matsuda, C. Tracy, N. Cave, R. Gregory, P. Fejes, A Study of Barium Strontium Titanate Thin films for Use in Bypan Capacitors, Journal of Materials Research, **13**(1998) 197

[20] A. Siefert, F. F. Lange, J. S. Speck, Epitaxial Growth of $PbTiO_3$ Thin Films on (001) $SrTiO_3$ from Solution Precursors, Journal of Materials Research, **10**(1995) 680

[21] D. Tahan, A. Safari, L. C. Klein, Sol-Gel Preparation of Barium Strontium Titanate Thin Films, Applications of Ferroelectrics, Proceedings of the Nineth IEEE, 1995, 427

[22] S. Ezhilvalavan, T. Y. Tseng, Progress in the Development of (Ba,Sr)TiO_3 (BST) Thin Films for Gigabit Era DRAMs, Materials Chemistry and Physics, **65**(2000) 227

[23] Y. Kobayashi, Y. IIzuka, T. Tanase, M. Konno, Low-Temperature Synthesis of Single-Phase Barium Strontium Titanate Thin Film With a nm-Seeding Technique and Its Dielectric Properties, Journal of Sol-Gel Science and Technology, **33**(2005) 315

[24] J.-G. Cheng, X.-J. Meng, J. Tang, S.-L. Lou, J.-H. Chu, Fabrication and Electrical Properties of Sol-Gel-Derived $Ba_{0.8}Sr_{0.2}TiO_3$ Ferroelectric Films from a 0.05-M Spin-on Solution, Applied Physics: A, **70**(2000) 411

[25] S. U. Adikary, H. L. W. Chan, Compositionally Graded $Ba_xSr_{1-x}TiO_3$ Thin Films for Tunable Microwave Applications, Materials Chemistry and Physics, **79**(2003) 157

[26] M. B. Gonzalez, A. Wu, P. M. Vilarinho, Influence of Solvents on the Microstructure and Dielectric Properties of $Ba_{0.5}Sr_{0.5}TiO_3$ Thin Films Prepared by a Diol-Based Sol-Gel Process, Chemistry of Materials, **18** (2006) 1737

[27] D. M. Potrepka, S. Hirsch, M. W. Cole, W. D. Nothwang, S. Zhong, S. P. Alpay, Effect of Strain on Tunability in $Ba_{0.6}Sr_{0.4}TiO_3$ Thin Films on Pt-Si Substrate, Journal of Applied Physics, **99**(2006) 014108

[28] Y. Wang, B. Liu, F. Wei, Z. Yang, J. Du, Fabrication and Electrical Properties of (111) Textured $(Ba_{0.6}Sr_{0.4})TiO_3$ Film on Platinized Si Substrate, Applied Physics Letters, **90**(2007) 042905

Chapter 4 General conclusions and future work

$(Ba_{0.8}Sr_{0.2})TiO_3$ (BST80/20) thin films with improved dielectric and ferroelectric properties were prepared at low annealing temperature (600ºC). Thin films of BST80/20 on commercial platinised silicon substrates were prepared by a modified sol gel-diphasic precursor route, in which nano sized $(Ba_{0.8}Sr_{0.2})TiO_3$ (BST80/20) polycrystalline particles were dispersed in the precursor sol (diphasic precursor sols). Seeded films exhibited improved microstructure and enhanced electrical properties when compared with unseeded films. The role of the nanoparticles on the crystallinity, microstructure and electrical properties of BST thin films was investigated and presented in this work.

$(Ba_{0.8}Sr_{0.2})$ TiO_3 (BST80/20) powders were first prepared by sol-gel method. The obtained particles were very fine with a narrow particle size distribution and an average particle size of 60 nm.

The synthesised perovskite BST80/20 powders were then added as seeds to BST precursor sols in order to act as heterogeneous nucleation sites for the perovskite phase formation. BST80/20 thin films were fabricated on $Pt/TiO_2/SiO_2/Si$ substrate using the diphasic precursors prepared with 1 mol%, 5 mol% and 10 mol% of BST nano seeds and processed under different conditions (annealing temperature, annealing dwell time and annealing atmosphere).

From the phase formation study conducted by XRD, the temperature for the appearance of the perovskite BST phase was found to be as low as 550ºC for 5 mol% seeded BST thin films and the temperature for the complete formation of the perovskite BST phase was found to decrease from 700ºC for the unseeded BST thin films to 600ºC for the 5 mol% seeded BST thin films. It was shown that the addition of BST seeds results in the crystallization of a single perovskite phase in the BST film either at low

temperature or at short annealing time. Moreover the presence of nano sized BST seeds in the film lowers the energy barrier for BST nucleation. The overall activation energy for the perovskite crystallization was reduced from 189 kJ/mol for unseeded films to 86 kJ/mol for 1 mol% seeded film and to 80 kJ/mol for 5 mol% seeded film.

Scanning Electron Microscopy (SEM) and Atomic Force Microscopy (AFM) revealed that grains of seeded films are smaller, more uniform and with a more homogeneous grain size distribution than unseeded ones. The surface roughness of BST films measured by AFM was decreased by the presence of BST nano seeds. TEM analysis clearly expose that the crystallinity of BST films was enhanced with the presence of BST seeds under the same annealing conditions. Moreover BST thin film edges are very obvious at low annealing temperature.

The dielectric constant of unseeded films annealed at 600ºC for 30 hours in oxygen was improved by the addition of 5 mol% seeds from ~300 to 400 at 1kHz, from 273 to 343 at 1 MHz, respectively. Simultaneously, the dissipation factors were decreased by the presence of 5 mol% seeds from ~0.1 to 0.07 at 1 kHz, from 0.07 to 0.01 at 1 MHz, respectively.

The presence of 5 mol% seeds improved the tunability of BST films and an increment from 52% for unseeded films to 65% at 6V for 5 mol% seeded BST thin films annealed at 600ºC for 30 hours in oxygen was observed.

The leakage current density of BST films with 5 mol% seeds heat treated at 600ºC for 30 hours in oxygen is 0.95×10^{-7} A/cm^2 up to the applied voltage of 2.33 V (97 kV/cm), which was improved when compared with 0.88×10^{-7} A/cm^2 up to 2.02 V (84 kV/cm) measured for BST films without seeds. The values of the leakage current of both unseeded and 5 mol% seeded films meet the requirements for Gbit DRAM applications.

Identically to the rest of the electrical properties, the polarization versus electric field (*P-E)* hysteresis was improved by the introduction of seeds. The remnant polarization *P*r of BST films with 5 mol% seeds was 3.55 μC/cm^2 with a coercive field of

75 kV/cm, which was considerably enhanced when compared to 1.8 μC/cm^2 for BST films without seeds with a coercive field of 50 kV/cm.

Corroborating the above results, piezo force microscopy (PFM) of BST seeded and non seeded thin films demonstrated the improved ferroelectric properties of BST films at a nanoscale level when prepared from diphasic precursor sols.

Based on the results obtained in this work a few other studies should be conducted to further explore the potentialities of the diphasic precursor technique used to prepared BST thin films. Some of these are listed below:

1) To study the dependence of the phase formation process, development of microstructure and final electrical properties on seeds size and size distribution; identification of the critical seede size effect;

2) Exploitation of this process on the fabrication of BST thin films on different substrates, such as metallic or glass substrates;

3) Exploitation of the possibility of utilization of the nano seeds as “dopant carriers” (such as MgO, MnO, Nb_2O_5, among others) to improve the electric properties of BST thin films;

4) To verify the effect of seeds, different stoichiometric BST thin films will be prepared and characterized in terms of phase evolution, crystallinity, microstructure and electrical properties.